Salmonella and the oxidative burst: tales of a complicated relationship

by

Joris van der Heijden

B.Eng., Technical University of Delft, 2006

M.Sc., Leiden University, 2009

A THESIS SUBMITTED IN PARTIAL FULFILLMENT OF

THE REQUIREMENTS FOR THE DEGREE OF

DOCTOR OF PHILOSOPHY

in

THE FACULTY OF GRADUATE AND POSTDOCTORAL STUDIES
(Microbiology and Immunology)

THE UNIVERSITY OF BRITISH COLUMBIA
(Vancouver)

May 2015

Abstract

Salmonella is one of the most abundant bacterial pathogens infecting humans in developed and developing countries. It is the causative agent of disease and mortality resulting in billions of dollars in associated medical costs and lost productivity every year. In the laboratory, findings regarding the physiology of *Salmonella* infections are often used to model a wide range of bacterial infections impacting fields far beyond the scope of *Salmonella* pathogenesis alone. For these reasons, significant resources have been dedicated to gaining a better understanding of mechanisms underlying *Salmonella* infection and the interaction between the pathogen and the immune system. In this thesis, *Salmonella* is used to study the interaction between bacterial pathogens and the host's oxidative and nitrosative burst. Recently, new findings have challenged the conventional perspective of reactive oxygen and nitrogen species as merely antimicrobial agents by revealing redox-sensitive virulence mechanisms that benefit *Salmonella* infection. These new findings, together with processes that drive *Salmonella* infection, are highlighted in **Chapter 1.** To better address questions concerning redox stress inside bacteria we used redox-sensitive GFP which enabled real-time analysis of the intra-bacterial redox environment. In **Chapter 2** this redox-biosensor combined with high-throughput microscopy, was used to evaluate oxidative/nitrosative stress evasion strategies inside macrophages. In **Chapter 3**, the same method was used to explore the bacterial outer membrane permeability to hydrogen peroxide. Real-time measurements of the intra-bacterial redox potential revealed novel regulatory mechanisms that alter outer membrane permeability based on the presence or absence of reactive oxygen and nitrogen species. **Chapter 4** describes the identification and characterization of a redox-sensitive regulatory modification in *Salmonella* effector SteB. This modification was found to be crucial for

regulation of tubulin-mediated transport of the *Salmonella* containing vacuole. Cumulatively these studies describe strategies for oxidative/nitrosative stress evasion while also highlighting several mechanisms by which reactive oxygen and nitrogen species aid *Salmonella* during infection. In **Chapter 5,** these findings have been integrated in order to gain a more comprehensive understanding of the complicated relationship between *Salmonella* and oxidative/nitrosative stress which has the potential to lead to the development of novel antimicrobial therapies.

Preface

A version of Chapter 1 has been published. **Joris van der Heijden** and Brett B. Finlay. Type III effector-mediated processes in *Salmonella* infection. *Future Microbiol*. 2012 Jun;7(6):685-703. doi: 10.2217/fmb.12.49. I wrote this perspective.

A version of Chapter 2 has been published**. Joris van der Heijden**, Else S. Bosman, Lisa A. Reynolds and Brett B. Finlay. Direct measurement of oxidative and nitrosative stress dynamics in *Salmonella* inside macrophages. *Proc Natl Acad Sci U S A*. 2015 Jan 13;112(2):560-5. doi: 10.1073/pnas.1414569112. Else S. Bosman helped with experiments to determine the redox stress time line analysis of the *sifA* mutant. Lisa A. Reynolds prepared bone-marrow derived macrophages before infection experiments. I designed all experiments, completed all data analysis and wrote the manuscript.

A version of Chapter 3 has been prepared for submission. **Joris van der Heijden,** Lisa A. Reynolds, Roland Scholz, Allen T. Mills, Koshi Imami, Leonard J. Foster, Franck Duong, B. Brett Finlay. *Salmonella* rapidly regulates membrane permeability to survive oxidative stress and form persisters. Roland Scholz helped perform mass spectrometry analysis, Lisa A. Reynolds prepared bone-marrow derived macrophages before infection experiments and is currently performing mouse experiments to test persister formation *in vivo*, Koshi Imami helped analyze mass spectrometry data. I designed all experiments, performed all experiments, completed all data analysis (except the mass spectrometry data analysis) and wrote the manuscript.

A version of Chapter 4 is being prepared for submission. **Joris van der Heijden**, Roland Scholz, Lisa A. Reynolds, Else S. Bosman, Robyn J. Law, Leonard J. Foster, B. Brett Finlay. Oxidation of cysteine residue in *Salmonella* effector SteB regulates tubulin-mediated translocation to juxtanuclear position. Roland Scholz helped perform mass spectrometry analysis and data analysis, Lisa A. Reynolds prepared bone-marrow derived macrophages and helped with analysis of cytokine secretion, Else S. Bosman helped with mass spectrometry analysis to identify oxidized thiols in effectors, Robyn J. Law helped with experiments that confirmed the SteB binding partner. I designed all experiments, performed all experiments, completed all data analysis (except the mass spectrometry data analysis and part of the CBA FACS analysis) and wrote the manuscript.

The mouse work presented in this thesis was approved by the UBC Animal Care Committee, certificate number: A13-0265

Publications arising from my PhD work:

1. **Joris van der Heijden**, Else S. Bosman, Lisa A. Reynolds and Brett B. Finlay. Direct measurement of oxidative and nitrosative stress dynamics in *Salmonella* inside macrophages. *Proc Natl Acad Sci U S A*. 2015 Jan 13;112(2):560-5. doi: 10.1073/pnas.1414569112

2. **Joris van der Heijden** and Brett B. Finlay. Type III effector-mediated processes in *Salmonella* infection. *Future Microbiol*. 2012 Jun;7(6):685-703. doi: 10.2217/fmb.12.49

3. **Joris van der Heijden,** Lisa A. Reynolds, Roland Scholz, Allen T. Mills, Koshi Imami, Leonard J. Foster, Franck Duong, B. Brett Finlay. *Salmonella* rapidly regulates membrane permeability to survive oxidative stress and form persisters. *Submitted.*

4. **Joris van der Heijden**, Roland Scholz, Lisa A. Reynolds, Else S. Bosman, Robyn J. Law, Leonard J. Foster, B. Brett Finlay. Oxidation of cysteine residue in *Salmonella* effector SteB regulates tubulin-mediated translocation to juxtanuclear position. *In preparation.*

Table of Contents

List of Tables

List of Figures

List of Abbreviations

5-IAF	5-iodoacetamidofluorescein
ADP	adenosine diphosphate
ATP	adenosine triphosphate
BMDM	bone marrow derived macrophages
CFU	colony forming unit
DNA	deoxyribonucleic acid
DTT	dithiotreitol
EDTA	ethylenediaminetetraacetic acid
EEA1	early endosome antigen 1
EGFR	epidermal growth factor
ER	endoplasmic reticulum
GAP	GTPase activating protein
GEF	G-nucleotide exchange factor
GFP	green fluorescent protein
HECT	homologous to the E6-AP carboxyl terminus
HPLC	high-performance liquid chromatography
IL	interleukin
iNOS	inducible nitric oxide synthase
LAMP1	lysosomal-associated membrane protein 1
LPM	low phosphate medium

LPS	lipopolysaccharide
MAPK	Mitogen activated protein kinase
M-cells	microfold cells
mRNA	messenger ribonucleic acid
NAD^+	nicotinamide adenine dinucleotide
$NADP^+$	nicotinamide adenine dinucleotide phosphate
NEM	N-ethyl maleimide
NLRP	Nod-like receptor family
OM	outer membrane
OMP	outer membrane protein
OSBP	oxysterol binding protein
PAMP	pathogen associated molecular pattern
PBS	phosphate buffered saline
PFA	paraformaldehyde
PMA	phorbol myristate acetate
PMN	polymorphonuclear leukocytes
PTM	post translational modification
RNS	reactive nitrogen species
ROS	reactive oxygen species
SCAMP	secretory carrier membrane protein
SCV	*Salmonella* containing vacuole
SDS-PAGE	SDS-polyacrylamide gel

SIF	*Salmonella* induced filament
SILAC	stable isotope labeling by amino acids in cell culture
SKIP	kinesin binding protein
SNX1	sorting nexin 1
SOD	superoxide dismutase
SPI	*Salmonella* pathogenicity island
T3SS	type-3 secretion system
TrxA	thioredoxin
VAMP8	Vesicle-associated membrane protein 8
VAP	vacuole associated actin polymerization
VSP	valosin containing protein
WT	wild type

Acknowledgements

I don't think anyone can get through a PhD without the help and support from people that surround them. In this section I would like to mention some people that have supported me over the past couple of years.

First of all, I would like to thank Brett for offering me a position in his lab. Thanks for creating an environment in which I had the freedom to choose my own research project. I thoroughly believe that only if researchers can choose their own projects they are motivated enough to finish them with excellence.

Secondly, I would like to thank Deng. You have been my mentor since the beginning of my PhD and without your advice I would never have been able to write this thesis. Thanks so much!

Thanks to all present and past members of the Finlay lab. Many PhD students and postdocs have been my colleagues over the years and thanks to your shared kindness, patience and knowledge I always had the luxury of having someone to ask for help or "talk science" with. Especially Roland, Eric, Lisa, Shannon and Robyn have been great friends and co-workers. I can only hope that my future colleagues will appreciate "witty banter", cheesy pranks and dry ice bombs ;-). I am really going to miss working with you guys.

What is a PhD without copious amounts of coffee? Fortunately, throughout my PhD I had access to the perfect place for blowing off some steam. The coffee room was really the best place to get inspired and to discuss science among many other things. Thanks to everyone that shared some quality coffee-time with me!

I had the pleasure to work with three great students. Thanks to Else, Dylan and Grant for their work and input. I am sure that all of you will be very successful in your future careers.

Thanks to my great committee members for your advice and suggestions of the last 4.5 years! Thanks to my parents for supporting me throughout my studies and thanks to Chris and Lucy for helping me find this PhD position.

And last but (definitely) not least, thanks to my wonderful wife-to-be! Jo, thanks for the countless evenings on which you had to listen to me talk about my work. Thanks for proof-reading my written words. This thesis wouldn't be here in its current shape if it wasn't for you.

Thanks everyone!

Chapter 1: Introduction

1.1 *Salmonella* infection

Salmonella infections are a significant source of human morbidity and mortality. There are an estimated 1.3 billion *Salmonella* related infections per year, ranging from gastroenteritis to typhoid fever, a potentially fatal systemic infection (1, 2). One of the most common *Salmonella* species to infect humans is *Salmonella enterica* which is typically acquired through ingestion of contaminated food or water (3). *Salmonella enterica* has many serovars, including *Salmonella enterica* Typhimurium which is often used in the laboratory and most of our current understanding of *Salmonella* infections is derived from research using this serovar. *S.* Typhimurium can infect a wide variety of hosts and can cause a self-limiting gastroenteritis in healthy humans and a fatal typhoid-like disease in mice. Once *S.* Typhimurium enters the gastrointestinal tract, it can either invade microfold cells (M-cells) or it can be phagocytosed by dendritic cells (4). After reaching the epithelial layer, it induces an inflammatory response resulting in IL-8 secretion and stimulation of a polymorphonuclear leukocyte (PMN) migration across the intestinal epithelium (5, 6). Both, the ability to invade non-phagocytic cells and the ability to survive and replicate inside the host cell are essential aspects of *S.* Typhimurium infection.

1.1.1 Formation of the *Salmonella* containing vacuole

S. Typhimurium can enter epithelial cells by "active" remodeling of the actin cytoskeleton leading to the formation of membrane ruffles or through "passive" uptake by immune cells with phagocytic properties (1, 7). The mechanisms by which uptake is facilitated has a dramatic impact on the further development of infection in the specific host cell (7). After bacterial internalization,

S. Typhimurium resides in the *Salmonella* Containing Vacuole (SCV) where it creates a niche for survival and replication (8). The SCV goes through different stages of maturation, all of which are associated with the presence of different sets of markers on the vacuole (9).

Early SCV biogenesis (< 30 minutes) is a process similar to maturation of nascent phagosomes with *S.* Typhimurium controlling the abundance of various markers on the SCV (9). Between 30 minutes and 5 hours post-infection the SCV moves to the perinuclear region of the host cell where it positions itself in the juxtanuclear position in close proximity to the Golgi apparatus. The late stage of SCV development (>5 hours) is characterized by the formation of *Salmonella* Induced Filaments (SIFs) (10) which are long tubules enriched in LAMP1. At approximately 8 hours post-infection these SIFs form stable networks that fuse with endocytic vesicles. This fusion presumably facilitates nutrient aquisition and is required for bacterial intracellular replication (11). Throughout SCV biogenesis, the SCV membrane is enriched with cholesterol. Cholesterol is important for bacterial replication as blocking cholesterol biosynthesis inhibits bacterial growth inside host cells (12). The late stage of SCV maturation is also marked by vacuole-associated actin polymerization (VAP), a process involving the formation of F-actin around the SCV (13, 14). Inhibition of this process causes the release of bacteria into the cytosol (14).

1.1.2 Type III secretion systems and effectors

All of these events result from the orchestrated activities of greater than 35 effectors secreted by two T3SS (1). Both T3SS-1 and T3SS-2 are associated with a set of effectors and are located in clusters on two *Salmonella* Pathogenicity Islands (SPI-1 and SPI-2 respectively) (15). It is believed that SPI-1 and SPI-2 are acquired by horizontal gene transfer and it is clear that both pathogenicity islands play a major role in the infection process (15, 16). Generally SPI-1 effectors are secreted

early in infection and are associated with bacterial internalization and early SCV biogenesis. T3SS-2 is induced in the lumen of the ileum and after bacterial internalization, secreted SPI-2 effectors are mostly involved in late SCV maturation and intracellular survival (17-19). Despite differences in temporal activation of the two T3SS it has become clear that both systems have a much closer relationship than previously thought. This is highlighted by the finding that T3SS-2 is induced even before *S.* Typhimurium enters the cell (19), the existence of several effectors that are secreted by both T3SS (20), the requirement of both T3SS for intestinal inflammation *in vivo* (21) and by SPI-1 effectors that are present and active at late time points post-infection (22). To summarize the current understanding of effector-mediated infection the process will be explained in chronologically ordered events starting with the induction of SPI-1 secretion. Many effectors have multiple functions and therefore will appear in several sub-sections in this introduction.

1.1.3 SPI-1 secretion

Changes in osmolarity, growth density, pH and aeration have all been proposed to induce T3SS-1 expression (23). Several transcriptional regulators have been identified that activate HilA, which is the master regulator that drives transcription of T3SS-1 components and effectors (24). The T3SS consists of an inner and outer membrane ring, a needle complex and the translocon pore, through which effectors are translocated from the bacterial cytosol into the host cell. After assembly of the secretion system, intimate contact between bacteria and the host cell is required for the activation of T3SS-1 (25). The formation of the translocon pore is required for intimate contact and effective secretion of T3SS-1 effectors. T3SS-1 effectors SipB, SipC and SipD, also known as translocases, are involved in establishment of the bacterial-host cell connection. Each translocase is essential to facilitate injection of effector proteins since *S.* Typhimurium mutant

strains lacking any of the translocases are defective for intimate attachment and for translocation of all effector proteins (25). SipD is present at the tip of the needle complex before contact with host cells (25). The binding of SipB to cholesterol is essential for the formation of the translocon, as cholesterol depletion has been shown to block effector translocation (26). SipC binds Exo70, a component of the exocyst complex, which mediates docking and fusion of exocytic vesicles with the plasma membrane. Exo70 is enriched at sites of bacterial attachment, suggesting that exocytic vesicles are targeted to sites of *S.* Typhimurium invasion (27).

1.1.4 Non-phagocytic cellular invasion

After the successful activation of T3SS-1, eleven effectors are known to be secreted into the host (28). One of the most extensively studied processes in *S.* Typhimurium infection is its ability to invade non-phagocytic cells of which the most studied examples are intestinal epithelial cells (29-31). The combined action of five effectors (SipA, SipC, SopB, SopE and SopE2) is important for the induction of membrane ruffles and actin rearrangements leading to bacterial internalization (32). SopE and SopE2 mimic the function of G-nucleotide exchange factors (GEFs) thereby activating Rho GTPases Rac-1 and Cdc42 and stimulating pathways that drive actin cytoskeletal assembly via Arp2/3 (32, 33). Another effector, SopB, an inositol phosphatase, activates the exchange factor RhoG through activation of the SH3-containing GEF which contributes to extensive actin remodeling (34). A certain degree of redundancy of these three effectors is clearly shown by the fact that a single mutant is still invasive while mutants lacking all three effectors are defective in non-phagocytic invasion (35). The two effectors SipA and SipC are involved in actin remodeling through direct binding of F-actin (36). After binding, SipA bundles actin and promotes actin polymerization by decreasing the critical concentration of actin needed for actin assembly

(1, 6). It also stabilizes actin filaments by enhancing the localized actin-bundling activity of T-plastin (32, 37). SipA works in concert with SipC which also binds and bundles F-actin to facilitate the formation of actin filaments at the site of bacterial adhesion. Additionally SipA and SipC work together to nucleate actin and SipC prevents filament disassembly by host factors (20, 38). After bacterial engulfment, the host cytoskeleton returns to its resting state by activity of effector SptP. This effector deactivates the Rho GTPases Rac and Cdc42 by mimicking GTPase-activating proteins (GAP) thereby reversing the cytoskeletal rearrangements induced by SopE, SopE2 and SopB effectors (39).

1.1.5 Effectors induce an inflammatory response

Many effectors that are responsible for non-phagocytic cellular invasion, also induce an inflammatory response. SopE activates Rac-1 and together SopE, SopB and SopE2 activate Cdc42 (33, 40, 41). Activation of Rac-1 and Cdc42 induces MAPK signaling pathways which lead to the activation of Activator protein-1 (AP-1) and NF-κB. The activation of these pathways results in the transcription and translation of pro-inflammatory cytokines (34, 42). The effectors SipA and SopA induce inflammation by triggering signal transduction cascades that stimulate PMN migration across the intestinal epithelium (5, 6, 43, 44). SipB induces inflammation by binding and activation of caspase-1. Binding of casapase-1 leads to an increased production of IL-1β and IL-18 (20, 45).

1.1.6 Cell death regulation

After induction of inflammation *Salmonella* employs effectors that control and prevent the host cell from undergoing apoptosis (46). Suppression of apoptosis may allow for the establishment of

a stable intracellular niche inside the SCV. All effectors involved in cell death regulation inhibit NF-κB dependent gene expression in a variety of ways. Effector SspH1 binds protein kinase N1 (PKN1) to inhibit NF-κB dependent gene expression (47) and AvrA contributes to host cell survival by inhibition of JNK signaling (48). In addition to reversing effects on actin rearrangements through its GAP activity, SptP works as a protein tyrosine phosphatase (PTPase) inactivating Raf1 which in turn down-regulates MAPK signaling (49). Effector SopB also activates Akt and thereby contributes to anti-apoptotic signaling (50, 51). The phosphothreonine lyase SpvC is secreted by both T3SS and is found to inactivate MAPK through β-elimination. It also dephosphorylates ERK leading to reduced mRNA levels of pro-inflammatory cytokines (52). Finally, SPI-2 effector SseL prevents the degradation of NF-κB inhibitor, IκBα, through its deubiquitinase activity resulting in a decreased host inflammatory response (53).

In contrast, the E3 ubiquitin ligase SlrP promotes cell death by facilitating ubiquitination of mammalian thioredoxin thereby depleting thioredoxin levels in the host cell (54). Depletion of thioredoxin makes a cell vulnerable for oxidative damage and can lead to apoptosis. SlrP also binds the human chaperone ERdj3 which is a protein that binds unfolded proteins in the endoplasmatic reticulum (ER) and targets them for proteosomal degradation. It has been postulated that by preventing the binding of unfolded proteins SlrP may lead to the accumulation of unfolded proteins in the ER which may eventually induce apoptosis (55). SPI-2 effector SpvB exhibits a cytotoxic effect on infected cells and is required for delayed apoptosis following intracellular infection (56). SpvB is an ADP ribosyl transferase and deletion of SpvB results in attenuated virulence in the systemic mouse model (57).

1.1.7 Effectors induce SCV formation

Immediately after bacterial internalization, the SCV is formed in which *S.* Typhimurium resides during infection. The SCV is thought to protect bacteria from degradation and facilitates survival and replication in macrophages (9). The SCV undergoes different stages of maturation associated with the presence of different host cell markers. The early stage is mediated by SopB which associates with vesicular membranes where it recruits and activates Rab5 (1, 9). Rab5 in turn recruits the PI3-kinase Vps34 which phosphorylates PI into PI(3)P. Generation of PI(3)P is necessary for the recruitment of EEA1, VAMP8 and LAMP1 (9). The early SCV fuses with vesicles containing VAMP8 and PI(3)P. These vesicles most likely contain nutrients required for growth and replication of the bacteria within the SVC (58, 59). In addition SopB enhances invasion by cleaving PI(4,5)P2 to promote membrane elasticity and vacuole formation. SopB recruits sorting nexin-1 (SNX-1) which contributes to the disappearance of late lysosomal markers on the SCV and inhibits the degradation of epidermal growth factor receptors (EGFR) by lysosomes (1, 60). SopD and SipC act in concert with SopB during initial formation of the phagosome (9, 61). SopD plays a role in membrane fission and macropinosome formation (61) while SipC causes enhanced invasion through clustering of PI(4,5)P2 at the plasma membrane (60). Other effectors associated with SCV biogenesis and maturation are SopA and SptP (62). The HECT E3 ubiquitin ligase SopA, is associated with an increase in escape from the SCV but the significance of this activity is unclear (43). After formation of the SCV the effector SptP associates with the SCV where its PTPase activity increases pathogen replication (39). Direct SptP binding and specific dephosphorylation of host valosin-containing protein, a facilitator of cellular membrane fusion and protein degradation, enhances bacterial replication in the SCV (39).

1.1.8 SPI-2 secretion

After establishment of the early SCV, the T3SS-2 is induced and secretion of SPI-2 effectors is facilitated. Recently, it was shown that the acidification of the SCV through the actions of Toll-like Receptors is essential for *Salmonella* virulence since defective acidification results in the lack of expression and secretion of SPI-2 effectors (63). After acidification, several regulators activate the kinase SsrA which is part of a two-component system with the transcriptional regulator SsrB. The transcription factor SsrB can bind and activate all promoters of the SPI-2 operons leading to expression of SPI-2 effectors (64). Similar to the T3SS-1, the T3SS-2 also requires the formation of a translocon which is composed of SseB, SseC and SseD. All three translocases are required for the secretion of SPI2 effector proteins (65). The contributions of individual SPI-2 effectors are not yet as well characterized as those of SPI-1 effectors. The absence of obvious phenotypes associated with single deletions of SPI-2 effectors (presumably due to redundancy) complicates further research efforts (57). However, phenotypes showing reduced bacterial survival/replication in tissue culture models and the inability to cause systemic infection in a mouse model which are associated with disruption of the entire T3SS-2, clearly indicate the importance of the collective set of SPI-2 effectors on virulence (57, 62).

1.1.9 Positioning and maturation of the SCV

After formation of the SCV, the vacuole moves to the juxtanuclear position inside the host cell in close proximity to the Golgi apparatus. This position appears to be important for supply of nutrients and cellular components through fusion of the SCV with vesicles. These vesicles travel along microtubules and movement of vesicles is facilitated by dynein motors (14). Juxtanuclear positioning of the SCV is also dynein-dependent and this process is facilitated by the recruitment

of Rab7 together with the host protein RILP. Both, Rab7 and RILP recruit the microtubule motor dynein. The effector(s) driving initial transport of the SCV to the juxtanuclear position are currently unknown. After reaching the proper localization, this position is maintained by activity of effectors SseF and SseG which interact and inhibit further movement of the SCV by manipulating dynein activity (66). Also SifA plays a role in maintaining the perinuclear position by binding Rab7 and thereby blocking interaction between Rab7 and RILP which leads to inhibition of dynein recruitment (8). Finally SpiC is found to control SCV trafficking through interactions with host proteins TassC and Hook3 (67).

Studies in cell cultures reveal that after proper localization of the SCV, tubular structures extending from the SCV form SIFs (14). SIFs are enriched in LAMP1 and form stable networks that fuse with endocytic vesicles. This fusion is thought to occur to acquire nutrients for bacterial replication (11). The effector SifA is required for the formation of SIFs. This formation involves interactions with host cell proteins kinesin-1 and kinesin-binding protein (SKIP) (68). Effector PipB2 is responsible for recruitment of kinesin-1 to the SCV and in absence of SifA or SKIP, the SCV accumulates excess amounts of kinesin-1 (14). Excessive amounts of kinesin-1 result in the release of bacteria into the cytoplasm which points towards a regulatory/controlling function of SifA for kinesin-1 recruitment. The interaction between SifA and SKIP also blocks SKIP from interacting with activated Rab9 which is essential for recruitment of LAMP1 to the SCV (69). Both effectors SifA and SseJ bind host Rho GTPase RhoA. Transfection of cells with SifA is sufficient to induce SIF formation (70). Moreover, transfection with effector SseJ can induce SIF formation but only when it is co-expressed with RhoA, B or C (69). Complementation of this phenotype by combined activity of SseJ and RhoA, B or C indicates that it is likely that SifA mimics Rho GTPase activity (69). Effector SseJ is a cholesterol acyltransferase that esterifies cholesterol during infection (71).

SCVs and SIFs are enriched in cholesterol and the function of SseJ is dependent on the interaction with RhoA (72). SseJ is thought to control SIF formation, since SseJ expression inhibits SIF formation in WT *S.* Typhimurium and deletion of SseJ in the *sifA* background restores stability of the SCV and the formation of membrane tubular structures (73). A similar function is assigned to effector SopD2 since deletion of SopD2 in a *sifA* strain also restores formation of SIFs and SCV stability (74). The SPI-1 effector SipA is found to cooperate with SifA to modulate SCV morphology and ensure juxtanuclear positioning (22). A subpopulation of tubular filaments is enriched in SCAMP2 and SCAMP3 (75). These proteins are mainly found on post-Golgi endocytic and exocytic membranes and perhaps function in recycling of endocytosed receptors (14). Currently, all SIFs and other *Salmonella* induced tubules have been found in *in vitro* studies and their existence *in vivo* has not been confirmed.

After proper localization to the juxtanuclear region, an F-actin meshwork is created around the SCV. Inhibition of the VAP-network leads to decreased bacterial replication (8). SPI-2 effector SteC is a kinase and essential for VAP network formation (76). Other effectors involved in VAP are SspH2 and SseI. Both effectors co-localize to the actin cytoskeleton and bind the actin-binding protein filamin (77). SspH2 also binds profilin and profilin interacts with G-actin and enhances actin polymerization (8). *S.* Typhimurium strains mutated in both SspH2 and SseI still show normal actin polymerization indicating that there might be redundancy of effector functions (78). SpvB reverses the formation of the meshwork by ribosylating actin monomers and preventing polymerization (56).

1.1.10 Effectors impact lipid metabolism

Effectors SseJ and SseL are involved in host cell lipid and cholesterol regulation (79, 80). Cholesterol plays an important role during *Salmonella* infection. Before cellular internalization, the binding of cholesterol to SipB is already required for efficient cellular entry and after bacterial internalization high levels of cholesterol are present around the SCV. The acyltransferase activity of SseJ esterifies cholesterol during infection and deletion of *sseJ* leads to decreased levels of lipid droplets and impaired bacterial replication (79). In contrast, work from our lab showed that deletion of *sseL* leads to accumulation of lipid droplets (80, 81). This phenotype was linked to the deubiquitinase activity of SseL since infection with a strain carrying a catalytic mutant, does also result in accumulation of lipid droplets (81). In addition to its deubiquitinase activity, SseL binds oxysterol-binding protein (OSBP) inside the host cell thereby affecting its localization (81). OSBP has been associated with non-vesicular cholesterol transport, signaling, lipid metabolism and vesicular trafficking and is required for efficient replication of intracellular *S.* Typhimurium. The binding of SseL to OSBP presumably affects OSBP-dependent pathways to benefit intracellular *S.* Typhimurium by affecting OSBP mediated lipid metabolism (81). Lipids are not the only small molecules that are important for virulence of *S.* Typhimurium. The metals copper, iron, zinc, manganese, nickel, and cobalt have all been found to play an important role during infection (82, 83). A schematic representation of effector-mediated infection is shown in Figure 1-1 and Figure 1-2.

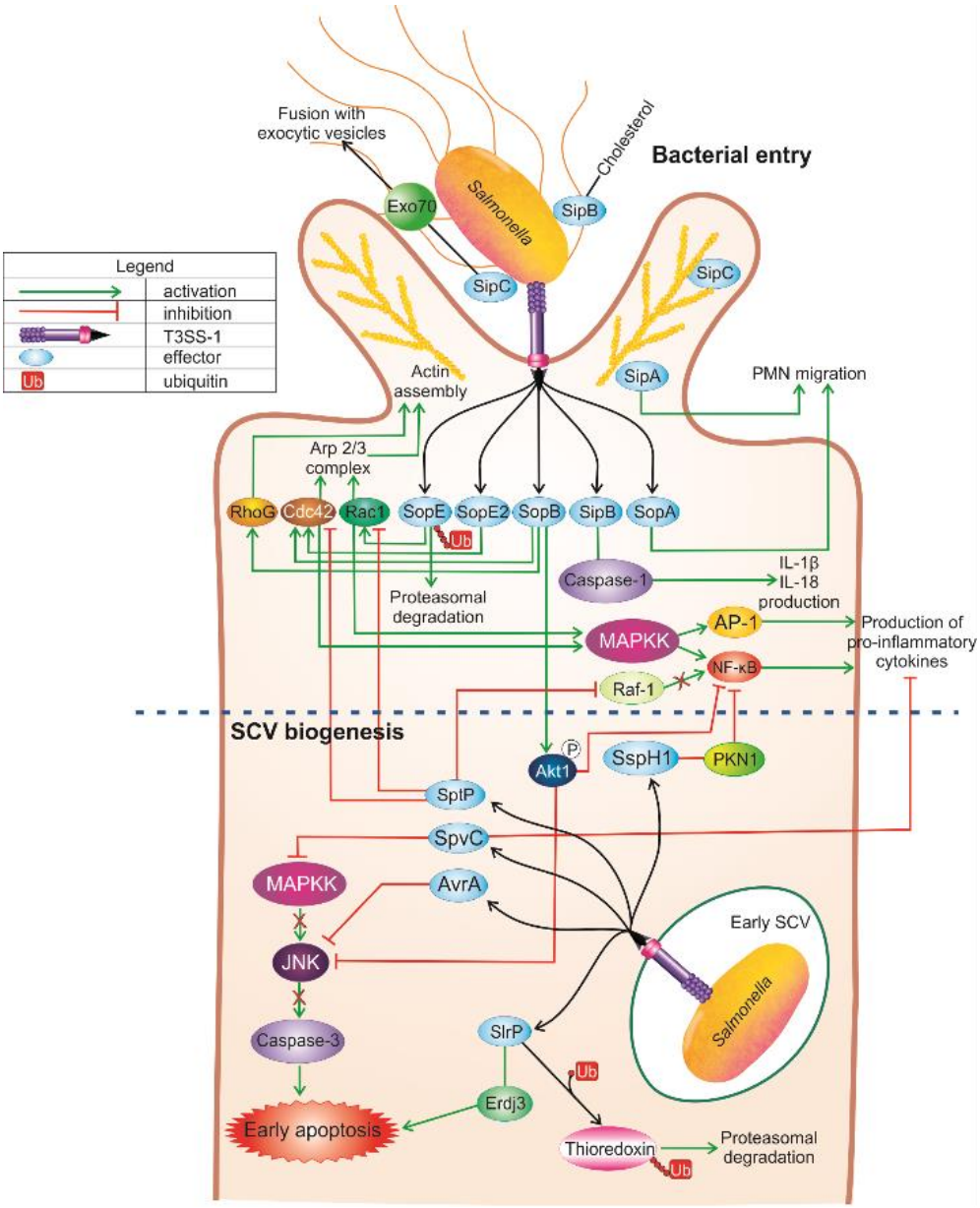

Figure 1-1: Salmonella entry and early SCV biogenesis

Upper part: T3SS-1 mediated entry of Salmonella into the host cell. Effectors mediate actin rearrangements and induce a pro-inflammatory response. Lower part: SCV biogenesis during which effectors dampen the inflammatory response and either induce or inhibit apoptosis. See text for details.

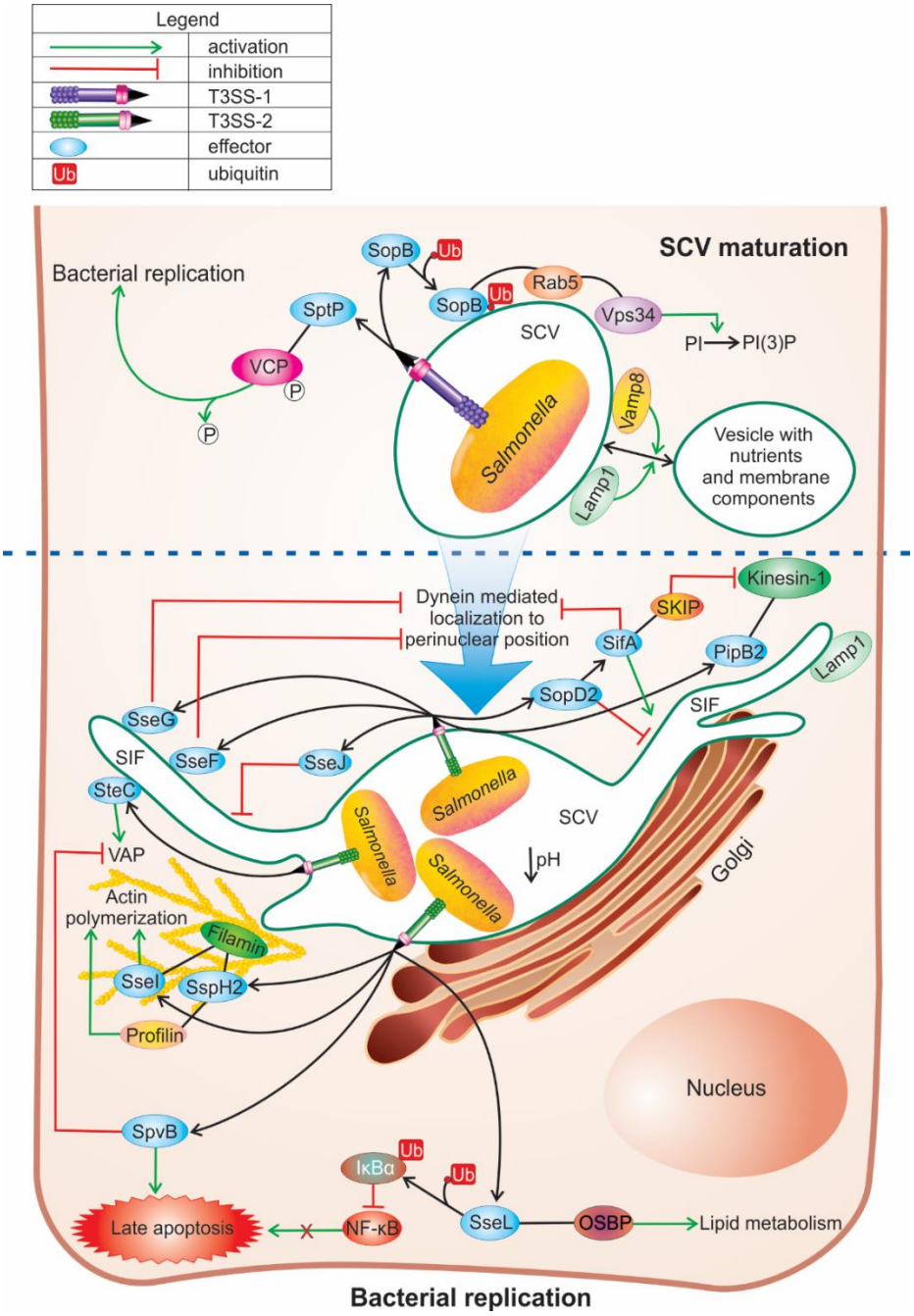

Figure 1-2: SCV maturation and bacterial replication

Upper part: The effector-induced recruitment of several markers on the SCV membrane facilitates fusion with nutrient-rich vesicles and maturation of the SCV. Dynein-mediated processes move the SCV towards the perinuclear region. Lower part: Final stages of SCV maturation and start of rapid bacterial replication. T3SS-2 secreted effectors mediate SIF formation and induce formation of the VAP network to stabilize the SCV. Effectors either induce or inhibit late apoptosis. See text for details.

1.2 The hosts oxidative and nitrosative burst

The host's immune system does not stay idle during infection with *S.* Typhimurium and the immune system of a healthy individual typically clears the body of infection within 4 to 7 days. Antimicrobial immune responses include; cell death activation, production of antimicrobial peptides, neutrophil recruitment, inflammasome activation and the oxidative and nitrosative burst. For the interpretation of results presented in this thesis, the generation of reactive oxygen species (ROS) and reactive nitrogen species (RNS) is of particular importance. At various points during infection, *S.* Typhimurium encounters ROS and RNS however, especially during the intracellular life-cycle in macrophages, bacteria experience oxidative and nitrosative stress. During infection, *S.* Typhimurium is often found within macrophages. Macrophages are specialized immune cells with phagocytic properties that yield an innate immune response after contact with bacterial invaders. During normal phagocytosis a macrophage ingests a pathogen, the pathogen becomes trapped within a phagosome, which then fuses with a lysosome to create the phagolysosome. Within this phagolysosome, antimicrobial enzymes, ROS and RNS attack, kill and digest the pathogen. During infection, ROS are mostly generated by NADPH-oxidase and RNS are produced by inducible nitric oxide synthase (iNOS) (84).

NADPH-oxidase consists of at least five subunits, two membrane proteins (p22, gp91) and three cytosolic proteins (p40, p47, p67) and is associated with the plasma membrane or phagosomal vesicles (85). Immediately after contact with bacterial products or immune stimulants (e.g. lipopolysaccharides, pro-inflammatory cytokines or phorbol myristate acetate) NADPH-oxidase is activated through Rac proteins. Activation leads to electrons transferring from NADPH to FAD and then via the haem centres of the gp91 subunit to oxygen for generation of the oxygen radical O^{2-} (85). Oxygen radicals can be converted into H_2O_2 or a variety of other ROS.

Contrary to the strict membrane association of NADPH-oxidase, iNOS seems to be present in both, cytosolic and vesicle-associated forms. This inducible enzyme catalyzes the transfer of electrons from L-arginine and oxygen for the formation of NO• and citrulline and is activated at later time points post infection (86).

The clinical significance of NADPH-oxidase is illustrated by a decreased life expectancy and recurrent bacterial and fungal infections in patients with chronic granulomatous disease (CGD) which results from mutated or missing genes that encode NADPH-oxidase subunits (84). In contrast, iNOS deficiency in humans has not been demonstrated as a clinically significant entity. Both, ROS and RNS, are generally perceived as antimicrobial agents.

1.2.1 Bacterial detoxifying enzymes

In order to cope with antimicrobial ROS and RNS inside macrophages and neutrophils during infection, *Salmonella* expresses an arsenal of detoxifying enzymes. These enzymes protect and defend intra-bacterial targets such as proteins, lipids and DNA. In *Salmonella* these enzymes include; three catalases (KatE, KatN and KatG) and two peroxidases (AhpC, TsaA) that are involved in H_2O_2 degradation within the bacterial cytoplasm. A *S.* Typhimurium HpxF(-) mutant which is devoid of catalases and peroxidases, is highly susceptible to antimicrobial ROS during infection (87). In addition to the catalases and peroxidases, *S.* Typhimurium expresses two cytosolic and two periplasmic superoxide dismutases (SOD). The cytosolic SodA and SodB bind manganese and iron respectively and catalyze the reaction of superoxide into oxygen and hydrogen peroxide. The two periplasmic superoxide dismutases, SodCI and SodCII bind copper or zinc and have been found to detoxify O^{2-} radicals within the bacterial periplasm (88). Out of the two periplasmic superoxide dismutases, only SodCI was found to play a role during infection of mice.

This is due to its resistance to protease activity and therefore it is non-covalently tethered within the periplasm (88). Mutations that offer SodCII either protease resistance or the ability to tether to the periplasm confer protection during infection (88). These results support the model that during infection, the outer membrane of *Salmonella* is partially disrupted by antimicrobial peptides. SodCII is released after disruption of the membrane while the protease resistance and the non-covalent linkage to the periplasm of SodCI enable it to detoxify O_2^- in the periplasm (88). Together, these detoxifying proteins represent a crucial aspect of *Salmonella* defense against the host oxidative and nitrosative burst.

1.3 Regulation of virulence

Host-pathogen interactions have been studied for many years however, the intricacies of these interactions are only just beginning to be appreciated. One key concept is the regulation of virulence by the pathogen. Initial activation of SPI-1 and SPI-2 expression by their respective transcriptional regulators HilA and SsrB, has been discussed earlier. However, the host-pathogen interaction is a two-way street and after *Salmonella* encounters antimicrobials generated by the immune system, it has been found to alter expression of virulence genes to accommodate for these attacks.

1.3.1 Regulation of SPI-2 secretion during infection

In particular inside macrophages, SPI-2 effectors drive bacterial replication and survival (89). The transcriptional regulator SsrB regulates more than hundred loci and is the main transcriptional regulator for the SPI-2 type III secretion system and its effectors. This transcriptional regulator is part of a two component system consisting of the integral membrane sensor kinase protein SsrA

and the cytoplasmic DNA-binding response regulator SsrB (90). Recently this transcriptional regulator has been found to directly interact with RNS that are encountered during infection. Upon encountering RNS, a cysteine residue in the dimerization domain of SsrB (CYS203) gets S-nitrosylated (91). This S-Nitrosylation prevents homo-dimerization, DNA binding and thereby inhibits activation of SPI-2 transcription. *S.* Typhimurium expressing the $SsrB^{C203S}$ mutant is attenuated in an Nramp+ murine model of oral infection in which *Salmonella* encounter substantial levels of RNS (91). Additionally, RNAseq transcriptome analysis shows that under SPI-2 inducing conditions, ROS and RNS significantly reduce transcription levels of all SPI-2 effectors and elements (92).

Another example of regulation of SPI-2 transcription is the increased expression of SPI-2 genes after *Salmonella* encounters an acidified environment. The reason for induction of SPI-2 transcription after acidification lies in the periplasmic sensor domain of SsrA which is enriched in histidine residues (93). Five histidines in the C-terminal end of the periplasmic sensor domain activate transcription with input from additional histidines in the N-terminal end of SsrA. A mutant lacking critical pH-responsive histidines was defective for acidification-based induction of SPI-2 genes.

These findings highlight that transcriptional activators can directly "sense" environmental changes after which they alter virulence programs to accommodate for acidification or oxidative and nitrosative stress.

1.3.2 Regulation of effectors by post translational modifications

Another regulatory mechanisms that is exploited by *Salmonella* is the direct modification of effectors by host proteins and components after translocation into the host cell. These post-

translational modifications (PTMs) impact effector activity, temporal dynamics, localization and interaction partners. The use of PTMs for regulatory purposes is mostly restricted to eukaryotic cells. However, bacterial effector proteins have found ways to utilize the host cell machinery to regulate their own properties and characteristics. Thus far, *Salmonella* effectors have been found to be lipidated, phosphorylated, ubiquitinated and cleaved by caspase-3. The following section outlines what is currently known about PTMs of effectors and how this impacts effector activity, stability and localization.

1.3.3 Ubiquitination

Ubiquitination is exclusively used in eukaryotic cells and regulates protein degradation by the proteasome and endocytosis from the plasma membrane. The process involves the attachment of a small peptide to lysine residues in the target protein. Poly-ubiquitination is mostly associated with proteosomal degradation whereas mono-ubiquitination can affect activity of enzymes and localization of proteins. Effector SopB is mono-ubiquitinated on one of six lysine residues since substitution of these residues almost completely eradicates SopB ubiquitination (94). Ubiquitination of SopB affects its localization since non-ubiquitinated SopB localizes to the plasma membrane where it stimulates actin rearrangements and activates Akt. After ubiquitination SopB localizes to the SCV where it activates Rab5. Impairment of ubiquitination leads to impaired bacterial replication that is similar to that of a *sopB* mutant (94).

Another example of how ubiquitination affects *Salmonella* infection is shown in the case of SopE and SptP. Both effectors (SopE and SptP) are delivered in equal amounts early in infection. However, SopE is quickly ubiquitinated and degraded through a proteasome-mediated pathway, while SptP is present and active long after translocation into the host cell (95). These results are in

line with the primary functions assigned to these effectors as SipA and SopE have shown to be involved in actin rearrangements and cellular entry while SptP restores actin rearrangements after bacterial internalization (32).

1.3.4 Caspase-3 proteolysis

Another PTM that affect activity of effectors is cleavage by host protease caspase-3. Effector SipA has two different domains that perform two different activities during the infection process. These domains are separated by a functional caspase-3 cleavage site (43). SipA is involved in induction of caspase-3 activity within the host cell and mutation of the caspase-3 cleavage site leads to attenuation of *S.* Typhimurium virulence in mice. SopA is another effector that has been shown to be cleaved by caspase-3. Mutation of the cleavage site of SopA leads to a significant reduction in the capacity to induce PMN trans-epithelial migration compared to wild-type *S.* Typhimurium (43). Many *Salmonella* effectors have a predicted caspase-3 cleavage site suggesting a major role for caspase-3 cleavage as a common mechanism to regulate effector function in host cells (43).

1.3.5 Lipidation

PTMs often contribute to proper effector localization in the host cell. For example, effector SifA was found to be lipidated on its C-terminal CAAX prenylation motif, which is required to target SifA to host cell membranes (96). This CAAX box mediates the covalent attachment of a lipid isoprenyl group to a cysteine residue. Prenylation is often followed by palmitoylation or myristoylation but this has not been confirmed for SifA. While it was first shown that removal of the CAAX box from SifA lead to abolishment of virulence (96) another group found that strains

containing a point mutation in SifA, resulting in deficient S-acylation or prenylation, were comparable to the wild-type strain (97). Although this is still a debated topic within the scientific community, it is likely that lipidation promotes activity of bacterial effectors by facilitating co-localization and interaction with host targets.

Another example of lipidation involves the SPI-2 effectors SspH2 and SseI which undergo a form of lipidation inside the host cell (98). After translocation, these proteins are *S*-palmitoylated by host-cell palmitoyltransferases resulting in their co-localization to specific domains of the plasma membrane. While SspH2 localizes to the apical membrane, SseI is found mainly in the basolateral membrane of polarized epithelial cells. The difference in localization indicates that S-palmitoylation is not the only factor that regulates localization of these effectors. SseI has been found to regulate cell migration and this activity has been found to be dependent on palmitoylation and plasma membrane targeting.

1.3.6 Many PTMs have most likely not been discovered yet

Many of the regulatory modifications that alter transcriptional regulators and bacterial effectors directly, are crucial for *Salmonella* virulence. Many more effectors contain amino acids that can undergo modifications however their existence and significance have not been confirmed yet. Table 1-1 shows an overview of *Salmonella* effectors, effector function and our current understanding of PTMs on effectors.

Table 1-1: *Salmonella* effectors and their role during infection				
Effector	**Effector modification**	**Enzymatic activity and domains**	**Binding partner**	**Role in infection**
GogB	-	N-terminal leucine-rich repeat	-	Unknown [7]
PibB	-	contains lipid rafts	-	Unknown [7]
PibB2	-	contains lipid rafts	Kinesin-1	Involved in SIF formation (14)
SifA	Prenylated, putative caspase-3 cleavage site	putative RhoA GTPase	Rab7, SKIP, RhoA	Required for SIF formation, controls SCV membrane stability (8),(68)
SifB	-	-	-	Unknown
SlrP	-	E3 ubiquitin ligase	thioredoxin, ERdj3	Promotes cell death (54, 55)
SopB	Ubiquitinated, putative caspase-3 cleavage site	inositol phosphatase	Cdc42, Rab5	Induce inflammation, control of *Salmonella*-induced inflammation (33, 40, 41), (50, 51)
SopD	putative caspase-3 cleavage site	-	-	Involved in membrane fission and macropinosome formation (9, 61)
SopD2	-	-	-	Involved in SIF formation and SCV stability (74)
SpvC	-	phosphothreonine lyase activity	-	Reduces pro-inflammatory cytokines (52)
SpiC	-	-	TassC, Hook3	Controls SCV localization (67)
SseF	-	-	SseG, junction plakoglobin	Controls SCV positioning (66)
SseG	-	-	SseF, desmoplakin, Caprin1	Controls SCV positioning (66)
SseI	Palmitoylated	Similarity to a family that possess deamidase activity	filamin, IQGAP1, TRIP6	Involved in VAP formation, promotes macrophage motility (77)
SseJ	-	cholesterol acyltransferase activity	RhoA, RhoC, cholesterol	Promotes perinuclear localization of SCV, controls SIF formation (69) (71), (79)
SseK1	-	-	-	Unknown
SseK2	-	-	-	Unknown
SseL	-	Deubiquitinase, cysteine protease	OSBP, Talin, IκBα	Downregulates inflammatory response (53), (80, 81)
SspH1	-	E3 ubiquitin ligase	PKN1	Control of *Salmonella*-induced inflammation (47)

Effector	Effector modification	Enzymatic activity and domains	Binding partner	Role in infection
SspH2	Palmitoylated	C-terminal NEL E3 ubiquitin ligase domain	filamin, profilin, Sgt1, AIP, Bub3, 14-3-3y, BAG regulator2	Involved in VAP formation (77), (78)
SpvB	putative caspase-3 cleavage site	ADP ribosyl transferase	actin	Required for delayed apoptosis, controls VAP formation (56)
SteC	-	serine/threonine kinase	F-actin	Promotes VAP formation (76)
SteA	-	-	-	Unknown
AvrA	Phosphorylated, putative caspase-3 cleavage site	acetyltransferase, deubiquitinase	MKK4/7, IκBα, β-catenin	Inhibition of JNK signalling, control of *Salmonella*-induced inflammation (48)
SipA	Caspase-3 cleavage	-	actin, T-plastin	Mediates bacterial entry, promotes SCV biogenesis, induces PMN migration (32, 37)
SipB	-	Activation of Caspase-1	caspase-1, cholesterol	SPI-1 translocase, induce inflammation (26)
SipC	-	Actin nucleation	Exo70, actin	SPI-1 translocase, mediates actin bundling (25), (27, 36), (60)
SipD	-	-	-	SPI-1 translocase (25)
SopA	Caspase-3 cleavage, Ubiquitinated	Mitochondrial MTS, E3 ubiquitin ligase	HsRMA1	Promotes bacterial escape from SCV, promotes PMN migration (43)
SopE	Ubiquitinated	G-nucleotide exchange factors	Rac-1, Cdc42	Promotes membrane ruffling and bacterial entry, induce inflammation (33, 40, 41)
SopE2	-	G-nucleotide exchange factors	Cdc42	Promotes membrane ruffling and bacterial entry, induce inflammation (33, 40, 41)
SptP	Ubiquitinated, putative caspase-3 cleavage site	Tyrosine phosphatase and GTPase activating protein	VCP, Cdc42, Rac-1, vimentin	Control of Salmonella-induced inflammation, restores cytoskeleton after bacterial internalization (49)
SteB	-	Putative picolinate reductase	-	Required for *Salmonella* biofilm formation (99)

1.4 Host-pathogen interplay; exploitation of immune responses

A generally accepted concept is that the immune response is beneficial to the host because it limits the replication and dissemination of *Salmonella* (100). Direct modification of virulence regulators and effectors by products of immune responses, highlight a more convoluted side of host-pathogen interplay. It is now clear that the host's antimicrobial immune responses not only kill bacteria but also aid *Salmonella* pathogenesis during infection. The intricacies of this relationship are often not black and white which has led to difficulties interpreting results. In particular exploitation of oxidative/nitrosative stress by *Salmonella* has been underappreciated. Powerful examples include the finding that *S.* Typhimurium utilizes the host's oxidative/nitrosative stress response to outcompete commensal microbiota in the gut (101). The growth advantage in the gut is caused by induction of reactive oxygen species by *S.* Typhimurium that actively induces inflammation. Subsequently, ROS that are generated by the immune system react with thiosulfate to form tetrathionate. A specific gene cluster in the *Salmonella* genome enables *S.* Typhimurium to use tetrathionate as a respiratory electron acceptor. The ability to use tetrathionate as an electron acceptor supports anaerobic growth on ethanolamine which is an alternative carbon source in the gut (102). Since most commensal bacteria are sensitive to oxidative stress and unable to utilize tetrathionate and ethanolamine, *S.* Typhimurium bacteria can outgrow their contenders in this highly competitive environment.

1.5 Paradox

The recent findings that show exploitation of ROS and RNS by *Salmonella* to aid pathogenesis have challenged the conventional dogma that regarded oxidative/nitrosative stress as merely an antimicrobial immune response. Additionally these results emphasize that we are still far away

from truly understanding host-pathogen relationships. This thesis focuses on beneficial aspects of ROS and RNS to the pathogen alongside their antimicrobial activities. **The overarching hypothesis is that *Salmonella* evades oxidative and nitrosative stress while also utilizing the potential of ROS and RNS as signaling moieties for regulating stress responses and virulence.** In the next three chapters research findings that outline the paradoxical relationship between *Salmonella* and oxidative/nitrosative stress are discussed.

Chapter 2: Direct measurement of oxidative and nitrosative stress dynamics in *Salmonella* inside macrophages

2.1 Summary

Many significant bacterial pathogens have evolved virulence mechanisms to evade degradation and exposure to reactive oxygen (ROS) and reactive nitrogen species (RNS), allowing them to survive and replicate inside their hosts. Due to the highly reactive and short-lived nature of ROS and RNS, combined with limitations of conventional detection agents, the mechanisms underlying these evasion strategies remain poorly understood. In Chapter 2 we describe the use of redox-sensitive GFP to non-disruptively measure real-time fluctuations in the intra-bacterial redox environment. Using this system coupled with high throughput microscopy, we report the intra-bacterial redox dynamics of *Salmonella enterica* Typhimurium (*S.* Typhimurium) residing inside macrophages. We found that the bacterial SPI-2 type III secretion system is required for ROS evasion strategies and this evasion relies on an intact *Salmonella* containing vacuole (SCV) within which the bacteria reside during infection. Additionally we found that cytosolic bacteria that escape the SCV experience increased redox stress in human and murine macrophages. These results highlight the existence of specialized evasion strategies used by intracellular pathogens that either reside inside a vacuole or "escape" into the cytosol. Taken together, the use of redox-sensitive GFP inside *Salmonella* significantly advances our understanding of ROS and RNS evasion strategies during infection. This technology can also be applied to measuring bacterial oxidative and nitrosative stress dynamics under different conditions in a wide variety of bacteria.

2.2 Introduction

A central mechanism of the innate immune response to defend against pathogens is the production of reactive oxygen species (ROS) and reactive nitrogen species (RNS) by specialized phagocytic immune cells (103). Macrophages and neutrophils generate ROS after detection of pathogen associated molecular patterns (PAMPs) through the NADPH oxidase complex while RNS is produced by inducible nitric oxide synthase (iNOS) which generates NO• through the conversion of L-arginine and oxygen (103-105).

In order to survive, replicate, and disseminate throughout the body, bacterial pathogens -especially those that reside in intracellular niches- must overcome the antimicrobial oxidative and nitrosative burst (103). General ROS and RNS enzymes such as catalases, peroxidases, superoxide dismutases and DNA repair enzymes are utilized by most bacteria to survive exposure to ROS and RNS (106). In addition to these general defenses, many intracellular pathogens have evolved specific evasion strategies that allow them to live inside their host cells. For example, the intracellular pathogens *Shigella flexneri* and *Listeria monocytogenes,* which cause shigellosis and listeriosis respectively, "escape" the phagolysosome to proliferate within the cytosol of macrophages. In contrast, the Gram-negative pathogen *Salmonella enterica* subsp. Typhimurium (*S.* Typhimurium), which is a major cause of gastroenteritis and some systemic diseases, remains inside a specific *Salmonella* containing vacuole (SCV), where it injects bacterial effector proteins directly into the host cell through a type III secretion system (T3SS). A specific set of type III effectors associated with a *Salmonella* pathogenicity island (SPI), known as SPI-2 effectors, have been implicated in ROS and RNS evasion strategies (107, 108); however the relationship between SPI-2 and oxidative stress evasion is a contentious topic after a recent study concluded that the contribution of SPI-2 to *Salmonella* pathogenesis is unrelated to its interaction with oxidative stress (87). Inadequate

analytic tools for directly measuring ROS/RNS and rapid fluctuations due to the short-lived nature of ROS/RNS have also contributed to poor reproducibility in the studies of ROS and RNS evasion strategies (103, 109-111).

Herein we describe the use of redox-sensitive GFP (roGFP2) that has previously been engineered by the group of Dr. James Remington at the University of Oregon to form a reversible disulfide bond upon oxidation or S-nitrosylation of specific cysteines (112). Formation of this disulfide bond leads to a slight shift in its conformation (Fig. 2-1A) resulting in two isoforms ($roGFP2_{ox}$ and $roGFP2_{red}$) of roGFP2. These isoforms have distinct excitation spectra with specific fluorescence signals after excitation at 405 nm and 480 nm respectively (113). Consequently, the 405/480 nm ratio can be used as a measure for the $roGFP2_{ox}/roGFP2_{red}$ ratio which essentially reports the redox balance (112). Because roGFP2 reports the redox potential by ratio-metric analysis, this system excludes variations due to differences in roGFP2 concentrations. Redox-sensitive GFP can be targeted to several intracellular compartments and has been used extensively in eukaryotic cells to measure the redox balance in the mitochondria and the cytosol (112, 114). Other variants of redox-sensitive GFP, which were developed for more oxidizing environments, were used for characterization of the endoplasmic reticulum (115). The initial response time of roGFP2 was reported to be slow (116) and oxidation by a wide variety of different oxidizing agents resulted in an unspecific redox-biosensor (117). Eukaryotic cells express the glutathione redox couple (GSH/GSSG) to buffer their intra-bacterial redox potential which is generally defined by the GSH/GSSG ratio (117, 118). To increase specificity and to fasten response time, fusions of roGFP2 with human glutaredoxin 1 (Grx1) or yeast peroxidase (Orp1) have previously been developed to measure the balance in the glutathione redox couple or intracellular levels of

hydrogen peroxide respectively (117, 119). Currently, roGFP2 or roGFP2-fusions have been used to measure the redox balance in tissue culture cells (112, 117, 120), *Arabidopsis thaliana* (121), *Saccharomyces cerevisiae* (113), *Caenorhabditis elegans* (122) and it has even been used to explore the redox balance in living mice (123).

In contrast to the extensive use of roGFP2 in eukaryotes, few studies have been published that describe the use of redox-sensitive GFP in living bacteria. The original publication by Hanson *et al*. (112) describes the expression and purification of roGFP2 in *E. coli* but in the original publication no measurements are reported of redox dynamics in living bacteria. Not all bacteria use the glutathione redox couple (GSH/GSSG) to buffer their intra-bacterial redox environment. For example, in *Mycobacterium tuberculosis,* the mycothiol redox couple (MSH/MSSM) parallels the functions of glutathione in eukaryotes. Recently, a fusion of roGFP2 to MSH-dependent oxidoreductase (Mrx1) of *Mycobacterium tuberculosis* was described (124). With this roGFP2 fusion, the authors effectively measure the intra-bacterial mycothiol balance in *M. tuberculosis* during macrophage infection making it (to our best knowledge) the first report of the use of redox-sensitive GFP to measure redox dynamics in life bacteria (124). In this Chapter we have used roGFP2 to measure the intra-bacterial redox potential in *Salmonella* Typhimurium after challenges with exogenous oxidative agents and during infection of HeLa cells (epithelial), THP-1 cells (monocytic) and bone marrow derived macrophages (BMDM) from mice. Finally, with the use of high throughput microscopy, we demonstrated the involvement of the SPI-2 T3SS in ROS evasion strategies, as well as the requirement for an intact SCV in order to evade ROS and RNS inside macrophages.

2.3 Results

2.3.1 Real-time measurement of intra-bacterial redox potential.

For our experiments we used unaltered roGFP2 that was kindly provide to us by Dr. James Remington from the University of Oregon (112). We first determined the excitation wavelength spectra of roGFP2$_{ox}$ and roGFP2$_{red}$. Purified HIS-tagged roGFP2 was exposed to 100 mM hydrogen peroxide (H_2O_2) and 10 mM dithiothreitol (DTT) respectively and fluorescent signal was measured in a fluorescence plate reader (Fig. 2-1B). Consistent with previous studies, we found specific peaks in fluorescence signals after excitation at 405 nm and 480 nm (113, 125). For the duration of this study, these excitation wavelengths were used to measure the intra-bacterial redox potential. For constitutive expression of roGFP2 in *S.* Typhimurium, we cloned the *rogfp2* gene in the pfpv25.1 vector (126) and transformed this vector into *Salmonella*. Using roGFP2 expressing *S.* Typhimurium, we measured the stability of the roGFP2 signal under different pH conditions. As *S.* Typhimurium encounters acidified environments during infection of macrophages, it is crucial that the roGFP2 ratio signal is unaffected by pH. None of the physiologically relevant pH values tested (pH 5-8) affected the maximum or minimum ratio-metric signals of roGFP2-expressing *S.* Typhimurium (Fig. 2-1C). Throughout this study each ratio-metric signal of roGFP2 was normalized to a scale of 0.1 (most reduced) and 1.0 (most oxidized). Internal reduced and oxidized controls are therefore obtained within each experiment.

S. Typhimurium, like most Gram-negative bacteria, uses the glutathione redox couple as its major low molecular weight thiol for buffering of its intra-bacterial redox environment (127). To test whether the system was able to monitor real-time fluctuations in the intra-bacterial redox potential, *S.* Typhimurium was challenged with 2.5 mM H_2O_2 and subsequently with 10 mM DTT (Fig. 2-1D). After these challenges, the roGFP2 405/480 nm ratio directly reported real-time changes to

the redox potential. The signal was entirely reversible and allowed for measurement of oxidation as well as reduction of the intra-bacterial environment. The fast response time of roGFP2 in *S.* Typhimurium benefits real-time measurements, however certain experiments require analysis at later time points. In order to "freeze" the ratio of roGFP2, addition of the alkylating compound N-ethyl maleimide (NEM) and subsequent fixation by paraformaldehyde (PFA) has been used previously (128). NEM covalently interacts with thiol groups and blocks formation of disulfide bonds. Addition of 20 mM NEM five minutes prior to H_2O_2 challenge effectively blocked oxidation of roGFP2 (Fig. 2-1D).

The response time of roGFP2 inside *Salmonella* was >50-fold faster than that of purified roGFP2 protein alone (Fig. 2-1E and 2-1F). This is most likely due to bacterial enzymes catalyzing the formation and disruption of the reversible disulfide bond. Thus, H_2O_2 stress triggers formation of a disulfide bond in roGFP2, but the mechanism is uncertain and apparently indirect. Nitric oxide reacts with thiols to form S-nitrosylated cysteines and oxidation following S-nitrosylation leads to subsequent disulfide bond formation (129). In this work, we did not create fusions of roGFP2 with Grx1 or Orp1 to ensure sensitivity to different sources of redox stress (117, 130). Since the intra-bacterial roGFP2 response to exogenous oxidants was immediate without the addition of glutaredoxins or peroxidases we used unaltered roGFP2 for our analyses.

Using the Nernst equation, the 405/480 nm ratio-metric signal can be converted into a quantitative value for the redox potential (E_{roGFP2}) inside *S.* Typhimurium (more information in the Materials and Methods section of this Chapter). The E_{roGFP2} for *S.* Typhimurium can be calculated for each of the different conditions. Many *in vitro* measurements in this study were done in low phosphate medium (LPM) at pH 5.8. This medium mimics intracellular conditions and induces expression of the SPI-2 T3SS and secretion of SPI-2 effectors by *S.* Typhimurium. Under these conditions the

resting E_{roGFP2} for *S.* Typhimurium was calculated to be -311±4 mV while the E_{roGFP2} in *Escherichia coli* (DH10B) under similar conditions was slightly higher at -302±4 mV.

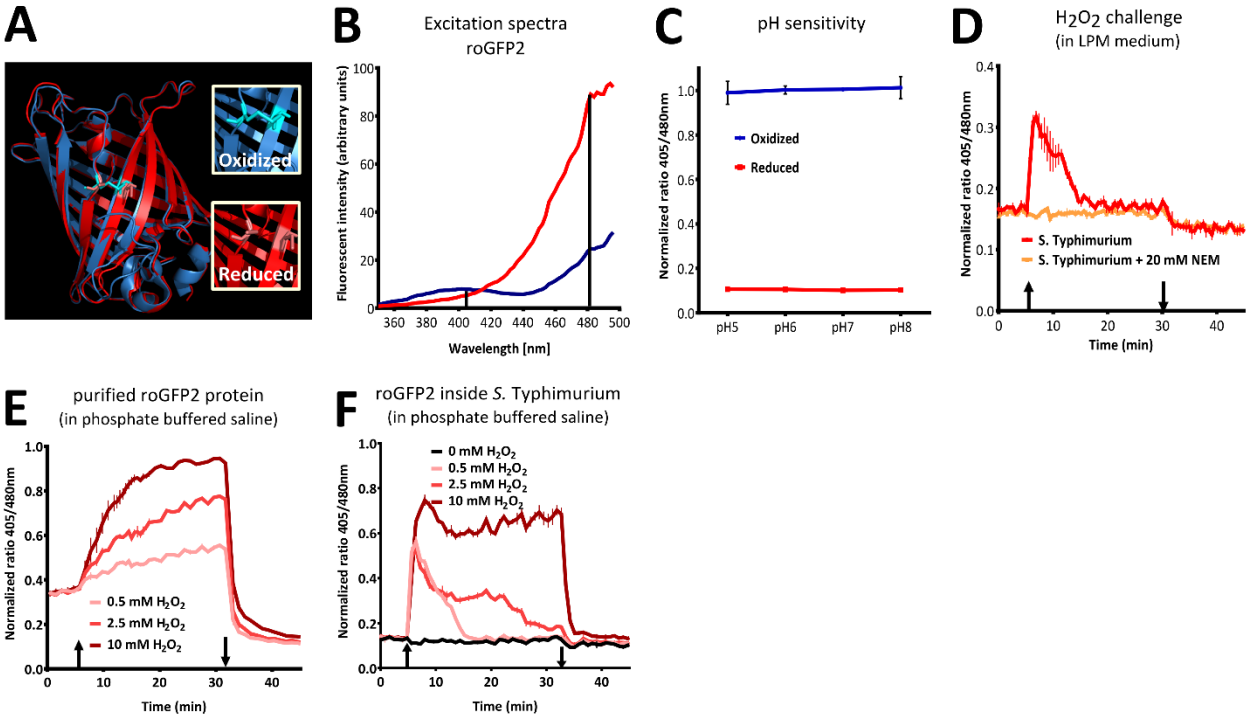

Figure 2-1: Characterization of roGFP2.

(A) Structure of roGFP2 obtained from pdb.org after processing in PyMOL in oxidized and reduced conformation. (B) Oxidized and reduced fluorescent excitation spectra with purified roGFP2 after addition of 100 mM H_2O_2 for maximum oxidation or 10mM DTT for maximum reduction (C) The maximum and minimum ratio value of roGFP2 in *S.* Typhimurium at different pH. Each value was normalized to the maximum and minimum ratio obtained in phosphate buffered saline at pH 7.4. (D) Real-time intra-bacterial redox potential after a challenge with 2.5 mM H_2O_2 (upwards arrow) and subsequent challenge with 10 mM DTT (downwards arrow) in LPM pH 5.8. *S.* Typhimurium is resuspended in phosphate buffered saline (PBS) and 20 mM NEM is added 5 minutes prior to the challenge to block oxidation of roGFP2 (see description in text). (E) Challenge of purified roGFP2 protein with varying concentrations of H_2O_2 (upwards arrow) and subsequent challenge with 10 mM DTT (downwards arrow). (F) Challenge of intra-bacterial roGFP2 protein with varying concentrations of H_2O_2 (upwards arrow) and subsequent challenge with 10 mM DTT (downwards arrow).

To further analyze the sensitivity and responsiveness of roGFP2 in *S.* Typhimurium after challenges with different oxidative agents, the intra-bacterial redox potential was measured in real time with a fluorescence plate reader. Following the addition of different concentrations of H_2O_2 (Fig. 1A) or SpermineNONOate (Fig. 1B) a dose-dependent increase in the 405/480 nm ratio was

observed. A one-time addition of H_2O_2 led to a sudden increase in the redox potential after which the bacteria detoxified H_2O_2 and restored a more reduced redox environment (Fig. 2-2A). After addition of SpermineNONOate (decay into NO•) a continuous generation of RNS resulted in a sustained increase in the redox potential (Fig. 2-2B).

Models predict that ROS concentrations inside macrophages are in the micromolar range (109, 131, 132). To test if intra-bacterial roGFP2 was able to measure low concentrations of H_2O_2, a *Salmonella* mutant without three catalases (KatE, KatG, and KatN) and two alkyl hydroperoxide reductases (AhpC and TsaA) was used to calibrate the system (133). This HpxF(-) strain was almost deprived of detoxifying power and using roGFP2 we were able to show micromolar sensitivity to H_2O_2. This demonstrates that roGFP2 is able to detect biologically relevant concentrations of ROS inside macrophages (Fig. 2-2C).

Intra-bacterial redox dynamics can also be analyzed by fluorescent microscopy. After addition of 2.5 mM H_2O_2, images were taken by fluorescence microscopy and the ratio values of these images were obtained (Fig. 2-2D). Individual images were analyzed by ImageJ to create pseudo-colored images for better visualization (Fig. 2-2E). These images confirm our results from the fluorescence plate reader and allow for visualization of redox differences between individual bacteria.

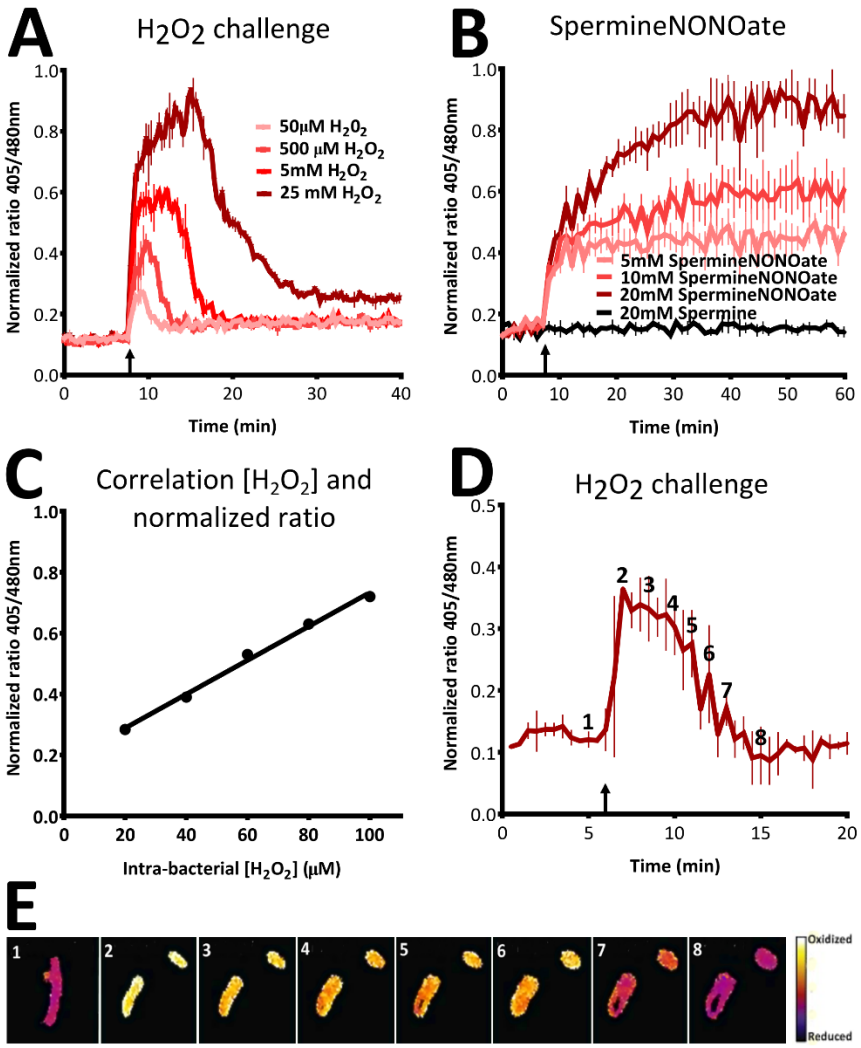

Figure 2-2: Real time measurement of roGFP2 in *S.* Typhimurium.
(A, B) Dose-dependent response of intra-bacterial redox potential after a challenge with H_2O_2 (A) or SpermineNONOate (B), respectively. The upward arrow indicates injection of the oxidative compound. These experiments are done in low phosphate medium at pH 5.8. (C) Correlation between the intra-bacterial H_2O_2 concentration and the normalized 405/480 ratio in HpxF(-) *Salmonella*. (D and E) Microscopic analysis of real-time response to challenge with 2.5 mM H_2O_2 in phosphate buffered saline. The false-colored ratio images are obtained after analysis by ImageJ. The numbers in the images in (E) correspond to the time points indicated in (D).

2.3.2 Intra-bacterial redox potential during infection of cells.

Following the verification of roGFP2 in *S.* Typhimurium, the system was used to analyze redox dynamics during infection of cultured cells. Both epithelial-like HeLa cells and macrophage-like THP-1 cells were infected with *S.* Typhimurium. HeLa cells are permissive for intracellular *S.* Typhimurium, in contrast to THP-1 cells, which kill the majority of *S.* Typhimurium (134). Images of infected cells were taken at 30 minutes post infection (p.i.) with fluorescence microscopy. Extracellular bacteria were labeled with a red fluorescent antibody to distinguish them from intracellular bacteria (Fig. 2-3A).

In HeLa cells, no significant overall H_2O_2 production was measured by the Amplex red assay at 2 hours p.i. (data not shown), and no oxidative stress was observed in intracellular bacteria compared to extracellular bacteria. For THP-1 cells we measured a significant efflux of H_2O_2 at 2 hours p.i. but analysis of roGFP2 did not show increased oxidative stress inside intracellular *S.* Typhimurium by fluorescence microscopy.

In order to increase sampling size and ensure an unbiased approach, consecutive measurements of the redox potential in intracellular *S.* Typhimurium were done using an AMNIS ImageStream system. This system integrates flow cytometry and fluorescence microscopy, enabling very high throughput fluorescence microscopy by acquiring at least 15,000 images of individual cells per time point and condition tested. A minimum of three individual experiments were done. Infected cells were fixed with NEM and PFA at various time points p.i. after which the cells were passed through a flow cytometry system. The ImageStream recorded each individual cell and all images were processed automatically. The results of the AMNIS ImageStream confirmed our previous findings with conventional fluorescence microscopy and enabled the visualization of infected cells during the first 90 minutes of infection (Fig. 2-3B). The average 405/480 ratio was obtained for

each experiment and together these results created a "redox stress" time line for intracellular *S.* Typhimurium in HeLa cells and THP-1 cells (Fig. 2-3C). In HeLa cells, intracellular bacteria did not experience significant redox stress, whereas inside THP-1 cells *S.* Typhimurium experienced gradually increasing redox stress. Collectively these results generate, for the first time, an accurate portrayal of the redox stress dynamics experienced by wild type *Salmonella* inside host cells during the first 10 hours of infection.

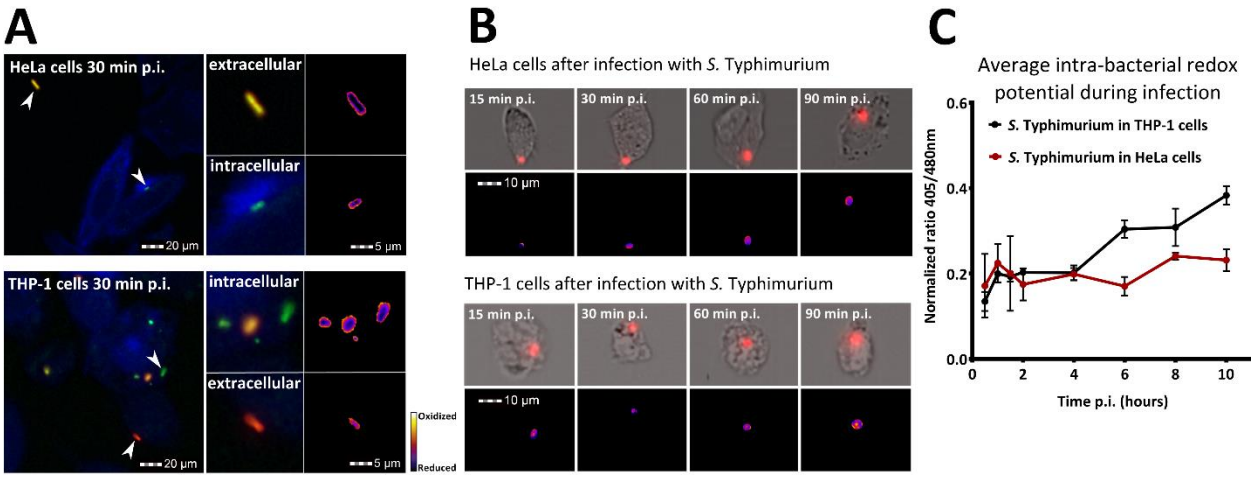

Figure 2-3: Intra-bacterial redox potential after infection of HeLa and THP-1 cells.
(A) Infected HeLa cells and THP-1 cells at 30 minutes post infection (p.i.) with fluorescence microscopy. All *S.* Typhimurium bacteria are shown in green, extracellular bacteria are shown in red and actin is shown in blue. The upward arrows indicate extracellular bacteria and the downward arrows indicate intracellular bacteria. Images were analyzed by ImageJ and pseudo-colored ratio images of individual bacteria are shown in the right panels. (B) For each time point an image from the AMNIS ImageStream was selected and analyzed by ImageJ. In the upper panels, a bright field image of individual infected cells is shown. Intracellular *S.* Typhimurium is shown in red. In the lower panels pseudo-colored ratio images of the corresponding bright field images are shown. The pseudo-colored legend is similar to the legend for panel A. (C) "Redox stress" time line showing the average normalized 405/480 ratio value of intracellular *S.* Typhimurium in HeLa and THP-1 cells for the first 10 hours p.i.. Each value represents analysis of more than 15,000 pictures of individual cells over three separate experiments.

2.3.3 *Salmonella* SPI-2 evasion of the oxidative burst.

After determining redox stress dynamics during regular *Salmonella* infection, we used the roGFP2 system to investigate specific *Salmonella* ROS and RNS evasion mechanisms. From within the SCV, *S.* Typhimurium injects SPI-2 effectors into the cell via a T3SS. The SPI-2 system has been

linked to ROS and RNS evasion strategies by interfering with proper co-localization of NADPH-oxidase and iNOS with the SCV (107, 108, 135). However a recent study was unable to find a correlation between SPI-2 involvement and oxidative stress evasion (87) which has contributed the ongoing controversy regarding SPI-2 involvement in ROS evasion (109, 110). These inconsistencies emphasize the need for better analytical tools to analyze redox stress of pathogens. To investigate the involvement of the SPI-2 system in ROS and RNS evasion, redox dynamics in the *ssaR* mutant, which is deficient in the assembly of a functional SPI-2 T3SS (136), were compared to infection with WT *S.* Typhimurium. By plating colony forming units (CFU), it was confirmed that *ssaR* is attenuated for survival in THP-1 cells but not for survival in HeLa cells (Fig. 2-5A). Next, the redox potential of intracellular WT or *ssaR S.* Typhimurium during infection of HeLa and THP-1 cells was obtained with the AMNIS ImageStream. Infected THP-1 cells were harvested at 2 hours and 16 hours p.i. and redox stress was measured. HeLa cells were harvested at 2 hours and 10 hours p.i. because many HeLa cells did not survive past 10 hours p.i.. No significant redox stress was observed after infection of HeLa cells with the *ssaR* mutant (Fig 2-4A). In THP-1 cells however, a significant increase in redox stress at 2 hours and 16 hours p.i. was observed in *ssaR S.* Typhimurium (Fig. 2-4B). To demonstrate the distribution of redox stress per cell, ratio values for all infected THP-1 cells were plotted in histograms (Fig. 2-4C). A random selection of images from each time point was processed by ImageJ to create pseudo-colored ratio images (Fig. 2-4D).

To determine the source of bacterial redox stress, we infected THP-1 cells with inhibitors of NADPH oxidase (DPI) or iNOS (L-NMMA) (Fig 2-5B and 2-5C). These measurements revealed that under the conditions that we used, increased redox stress in *ssaR S.* Typhimurium resulted from phagosomal ROS.

Because inhibitors can also alter other cellular processes, we next wanted to confirm our results in macrophages lacking phagosomal ROS and RNS production. In infected BMDM from C57BL/6J mice no redox stress was observed at 2 hours p.i. indicating a difference in timing of the oxidative burst. At 16 hours p.i. however, we measured increased redox stress in *ssaR* similar to that in THP-1 cells (Fig 2-5D). Infection of *gp91phox-/-* and *iNOS-/-* BMDM (which are unable to generate phagosomal ROS or RNS respectively) also showed that under our conditions, the source of redox stress ROS rather than RNS (Fig 2-5E).

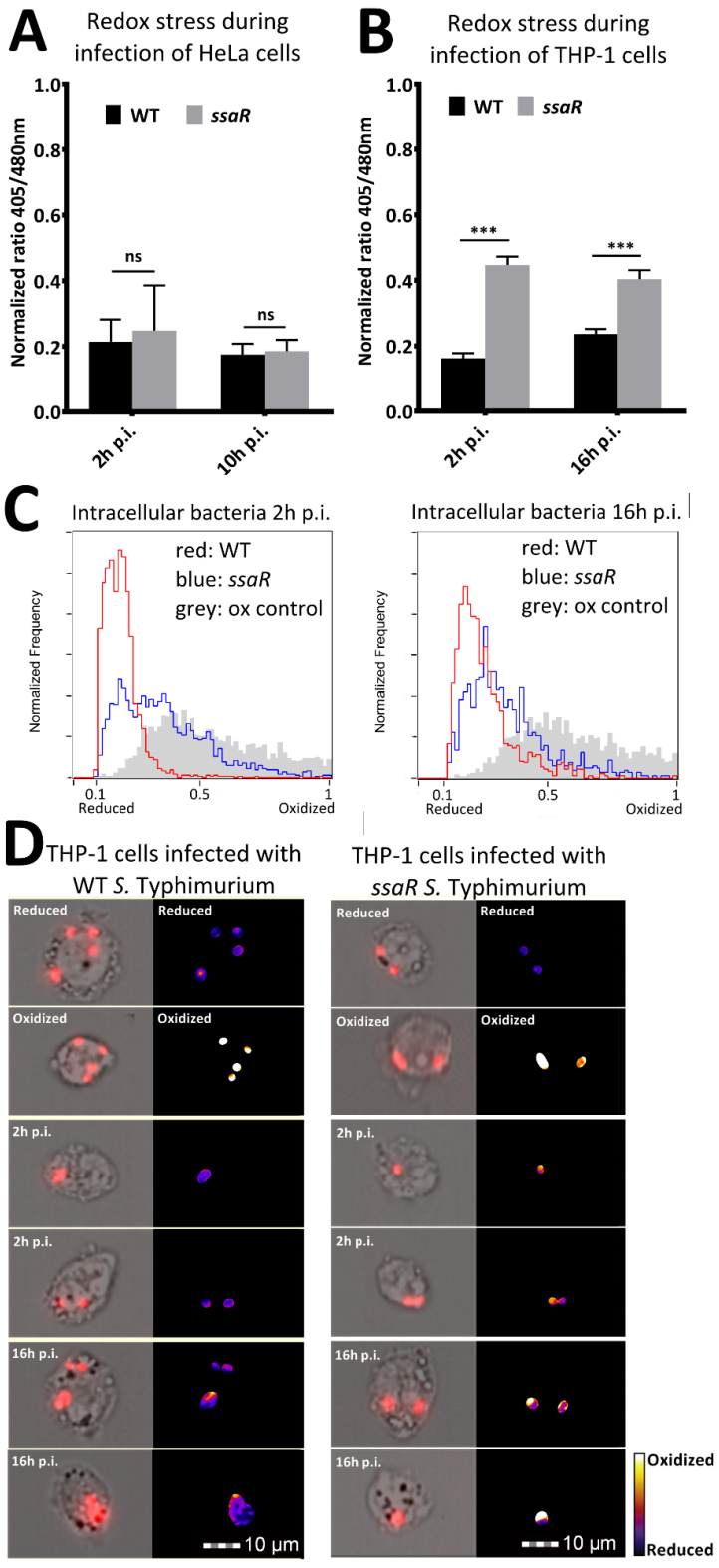

Figure 2-4: Involvement of SPI-2 system in ROS and RNS evasion.
(A) Average intra-bacterial redox potential of WT and *ssaR S.* Typhimurium in HeLa cells at 2 h and 10 h p.i. (B) Average intra-bacterial redox potential of WT and *ssaR S.* Typhimurium in THP-1 cells at 2 h and 16 h p.i. over three separate experiments. Error bars indicate the standard deviation. Each value represents analysis of at least 15,000 pictures. Significance was analyzed by a student's t-test (*** p <0.001). (C) Representative pictures of infected THP-1 cells at 2 h p.i. and 16 p.i.. Images on the right are pseudo-colored ratio images after analysis with ImageJ. (D) 405/480 nm ratio histograms of intra-bacterial redox potential after infection of THP-1 cells with WT and *ssaR* at 2 h p.i. and 16 h p.i. The grey histogram represents the oxidized control, the red line represents WT ratio values and the blue line represents *ssaR* ratio values.

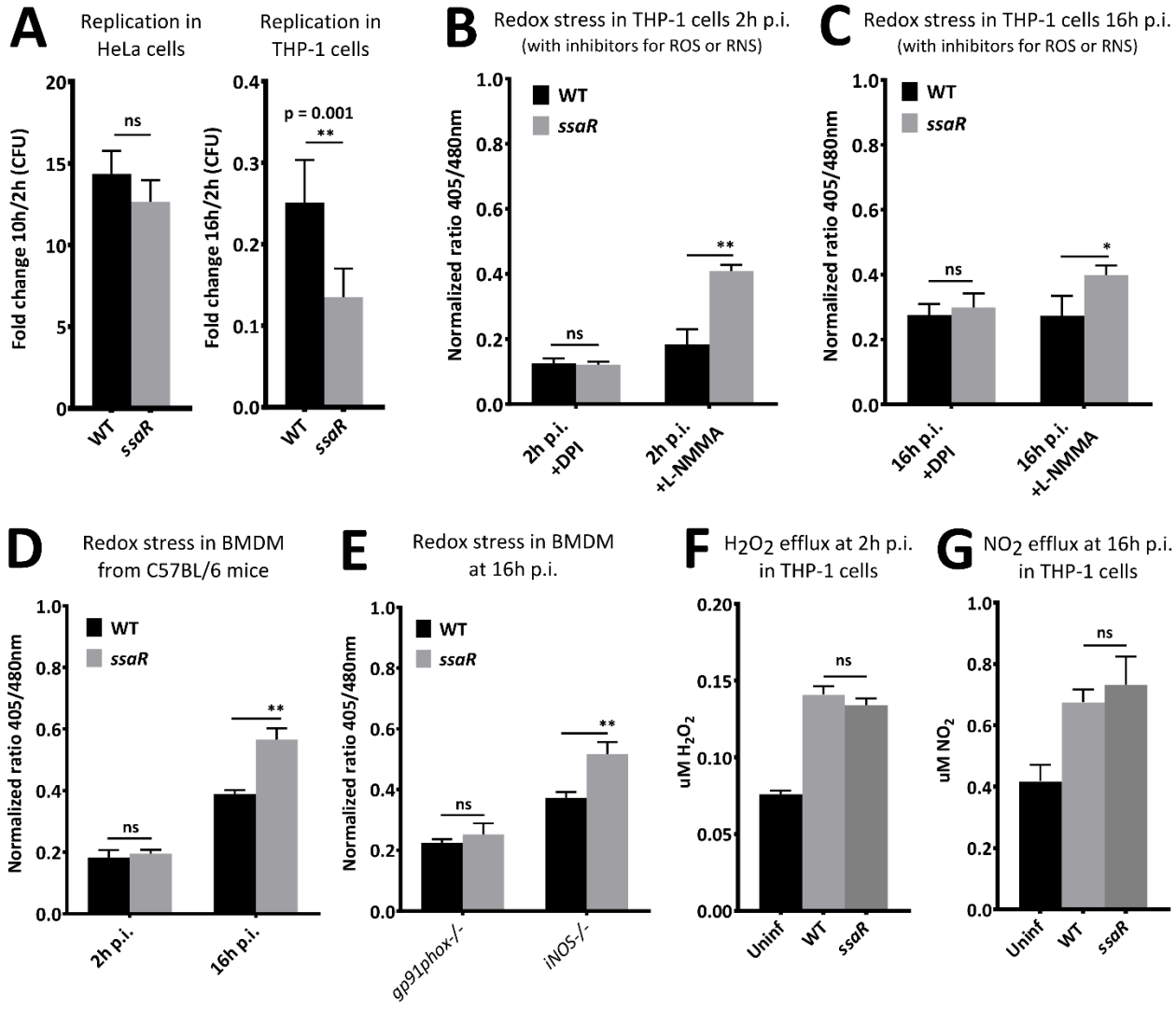

Figure 2-5: Infection dynamics of WT and *ssaR S.* Typhimurium.
(A) Intracellular survival of intracellular WT and *ssaR S.* Typhimurium in HeLa cells and THP-1 cells determined by CFU counts taken at 10/16 hours and 2 hours p.i.. Error bars indicate the standard deviation. Each experiment was repeated at least 12 times. (B and C) Intra-bacterial redox stress in WT and *ssaR S.* Typhimurium in THP-1 cells with the addition of inhibitors for oxidative stress (DPI) or nitrosative stress (L-NMMA) at 2 hours and 16 hours p.i. Error bars indicate the standard deviation. (D) Intra-bacterial redox stress in WT and *ssaR S.* Typhimurium in BMDM. (E) Intra-bacterial redox stress in WT and *ssaR* S. Typhimurium in gp91phox-/- and iNOS-/- BMDM. Each value represents analysis of at least 15,000 pictures. Error bars indicate the standard deviation over three separate experiments. (F) Overall H_2O_2 production of THP-1 cells after 2 hours p.i. with WT and *ssaR S.* Typhimurium as measured by the Amplex red assay. (G) Overall NO_2 efflux of THP-1 cells after 16 hours p.i. with WT and *ssaR S.* Typhimurium as measured by the Griess assay. The NO_2 concentration corresponds with the NO• production. Significance was obtained by a student's t-test (* $p<0.5$; ** $p<0.01$).

To further demonstrate that increased bacterial redox stress in *ssaR S.* Typhimurium was not caused by an increase in overall H_2O_2 and NO• generation, the H_2O_2 and NO• production of infected THP-1 cells was measured using the Amplex red assay and the Griess assay (Fig. 2-5F and 2-5G). THP-1 cells were infected with WT and *ssaR S.* Typhimurium, and the SPI-2 system was not found to inhibit overall H_2O_2 or NO• production. These results are consistent with previous studies that show SPI-2 mediated exclusion of NADPH-oxidase from the SCV, but no inhibition of overall H_2O_2 or NO• production in the host cells (108, 137). Interestingly, when examining individual infected THP-1 cells that contained many intracellular bacteria, the majority of bacteria in the cell experienced similar levels of oxidative stress (2 hours p.i.); however, we observed heterogeneity in redox stress between intracellular bacteria at 16 hours p.i. (Fig. 2-6).

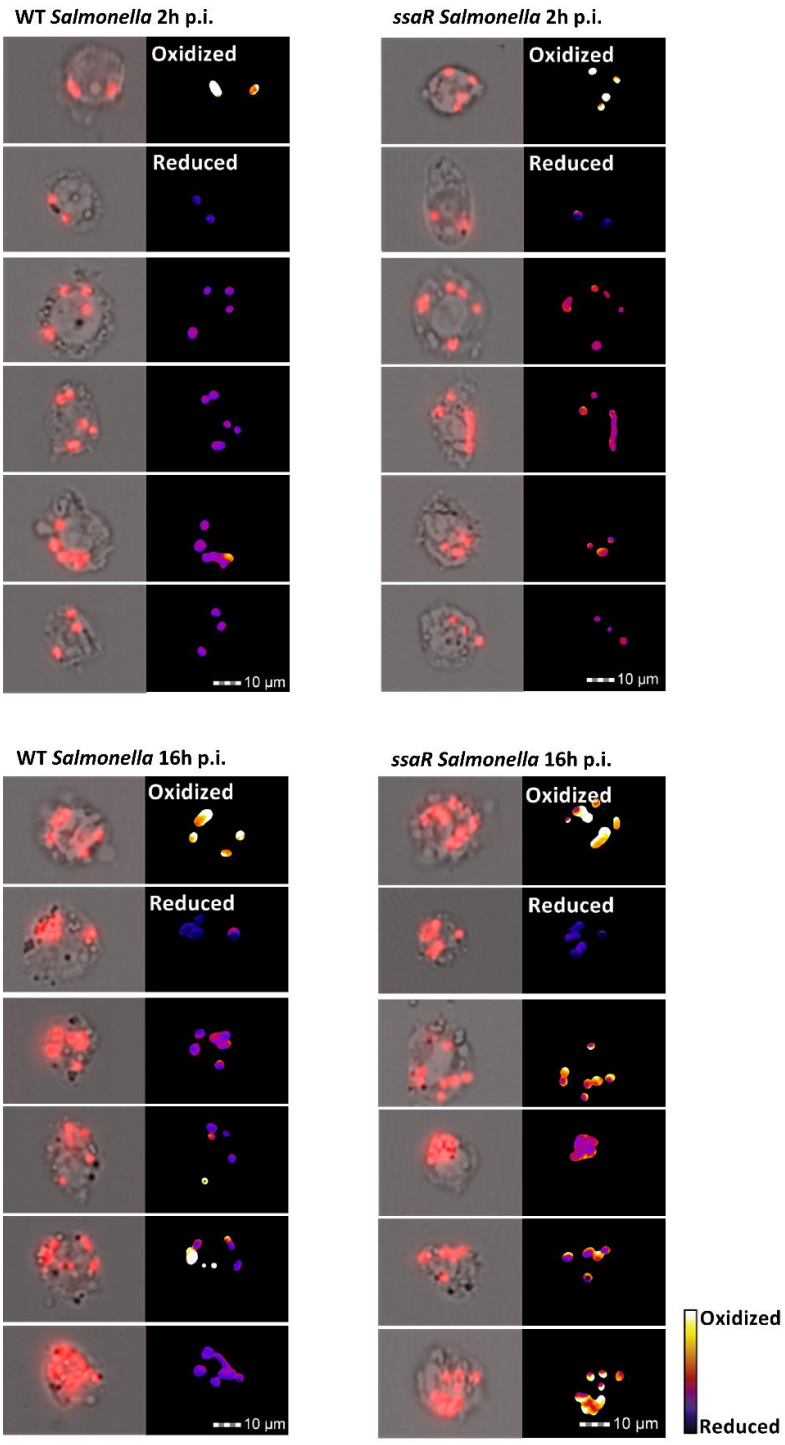

Figure 2-6: Representative images of infected THP-1 cells with WT and *ssaR Salmonella*.
Representative images of infected THP-1 cells that contain multiple intracellular bacteria from the AMNIS ImageStream. Images were taken at 2 hours and 16 hours p.i.. The corresponding pseudo-colored ratio images were obtained after analysis with ImageJ. Heterogeneity between intracellular bacteria is observed at 16 hours p.i..

2.3.4 An intact *Salmonella* containing vacuole is required for evasion.

The above experiments demonstrate that *S.* Typhimurium utilizes the SPI-2 system to evade ROS and that these evasion strategies are most likely the result of SPI-2 mediated prevention of effective ROS co-localization with the SCV. We hypothesized that, for *Salmonella* to control ROS co-localization, it is essential to reside within the SCV. It is known that from inside the SCV, *S.* Typhimurium regulates fusion with vesicles through the actions of SPI-2 effectors. For example, SPI-2 effector SifA directs trafficking of mannose-6-phospate receptors and thereby inhibits lysosome function (138). Additionally, SifA is implicated in maintaining the integrity of the SCV and it is well documented that infection with the *sifA* mutant leads to loss of SCV integrity (139). In contrast to *S. flexneri* and *L. monocytogenes*, *S.* Typhimurium is unable to survive in the cytosol of macrophages which results in severe attenuation of the *sifA* mutant (136).

To investigate whether the SCV is important for ROS or RNS evasion, THP-1 cells were infected with WT or *sifA S.* Typhimurium. A redox stress timeline from 2 hours p.i. until 10 hours p.i. was created that showed increased redox stress at 10 hours p.i. for *sifA S.* Typhimurium (Fig. 2-7A). In order to determine if this redox stress was caused by vacuole disruption or inhibition of lysosome fusion, a *sifAsseJ* double mutant was constructed. This mutant maintains SCV integrity but is unable to inhibit lysosome fusion (138, 139). To determine the contribution of SseJ to redox stress in *sifAsseJ*, the double mutant was complemented by integration of *sifA2HA* in the chromosome effectively creating a *sseJ* single deletion mutant. THP-1 cells were infected by all four strains and both the *sifA* mutant as well as the *sifAsseJ* double mutant were similarly attenuated for intracellular survival in THP-1 cells (Fig. 2-7B). Complementation with *sifA2HA* reversed replication to levels of WT infection indicating that deletion of *sifA* is the major reason for attenuated virulence.

Analysis of WT and *sifA* infected THP-1 cells at 2 hours and 16 hours p.i. using the AMNIS ImageStream demonstrated that only the *sifA* single mutant experienced significantly more redox stress than WT *S.* Typhimurium (Fig. 2-7C). Both the *sifA* single mutant and the *sifAsseJ* double mutant are deficient in the inhibition of lysosome fusion but only the *sifA* single mutant "escapes" the SCV and resides in the cytosol (138). Therefore, these results clearly suggest that cytosolic bacteria experience more redox stress than bacteria that reside inside the SVC.

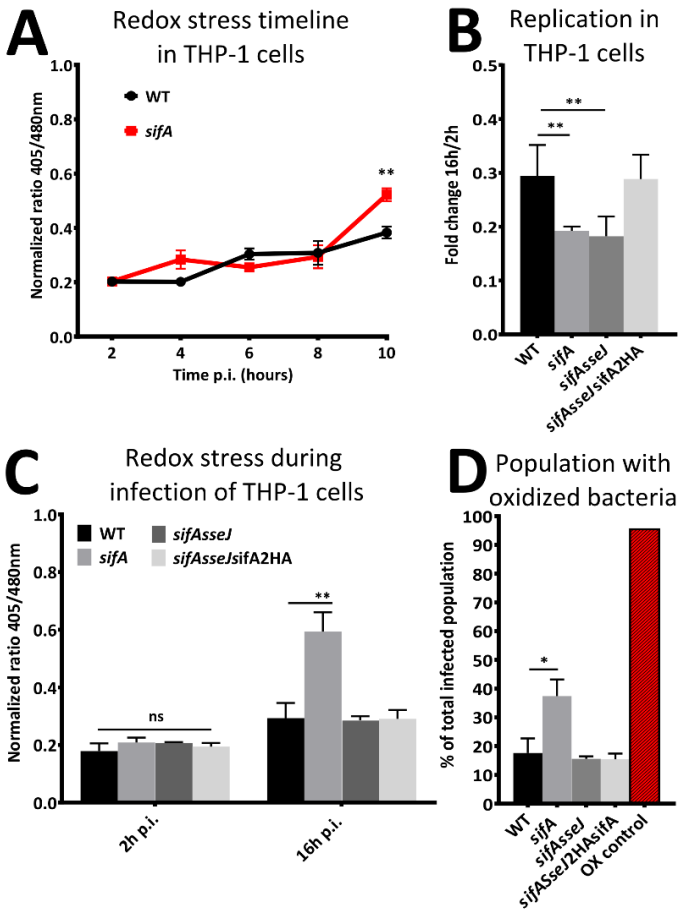

Figure 2-7: *Salmonella* containing vacuole is crucial for RNS evasion.
(A) "Redox stress" time line showing the average normalized 405/480 ratio value of intracellular WT and *sifA* S. Typhimurium in THP-1 cells for the first 10 hours p.i.. (B) Intracellular survival of intracellular WT, *sifA*, *sifAsseJ* and *sifAsseJ*2HAsifA *S.* Typhimurium in THP-1 cells determined by CFU counts fold change between 2 hours p.i. and 16 hours p.i.. Each experiment was repeated at least 12 times. (C) The average intra-bacterial redox potential in THP-1 cells at 2 h p.i. and 16 h p.i. Each value represents analysis of more than 15,000 individual cells over three separate experiments. (D) Subset of infected THP-1 cells that contain highly oxidized bacteria. Error bars indicate the standard deviation. Significance was analyzed by a student's t-test (* $p<0.5$; ** $p<0.01$).

In order to confirm that the increase in redox stress observed in *sifA S.* Typhimurium was not caused by increased generation of H_2O_2 or NO•, the total production was measured with the Amplex red and Griess assay (Fig. 2-8A and 2-8B). No significant increase in H_2O_2 or NO• production was observed. Further in depth analysis of redox stress in *sifA S.* Typhimurium in infected THP-1 cells revealed a significantly larger subset of cells containing "stressed" bacteria than WT infected cells (Fig. 2-7D). Furthermore, for THP-1 cells that contained higher numbers of intracellular bacteria were examined, more heterogeneity was observed in *sifA* infected cells than for any of the other mutants (Fig. 2-95).

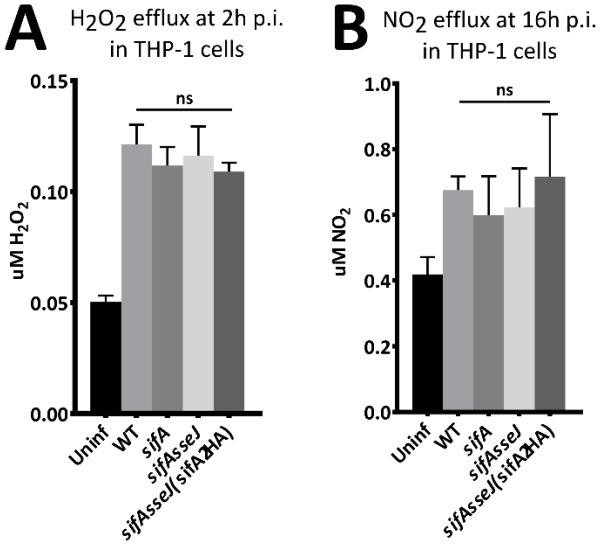

Figure 2-8: Measurement of overall H_2O_2 and NO efflux.
(A) H2O2 production at 2h p.i. with WT *sifA, sifAsseJ* and *sifAsseJ*2HAsifA S. Typhimurium in THP-1 cells as obtained by the Amplex red assay. (B) NO2 concentration at 16h p.i. with WT *sifA, sifAsseJ* and *sifAsseJ*2HAsifA *S.* Typhimurium in THP-1 cells as obtained by the Griess assay. The NO2 concentration corresponds with the NO• production. Error bars indicate the standard deviation. Significance was obtained by a student's t-test.

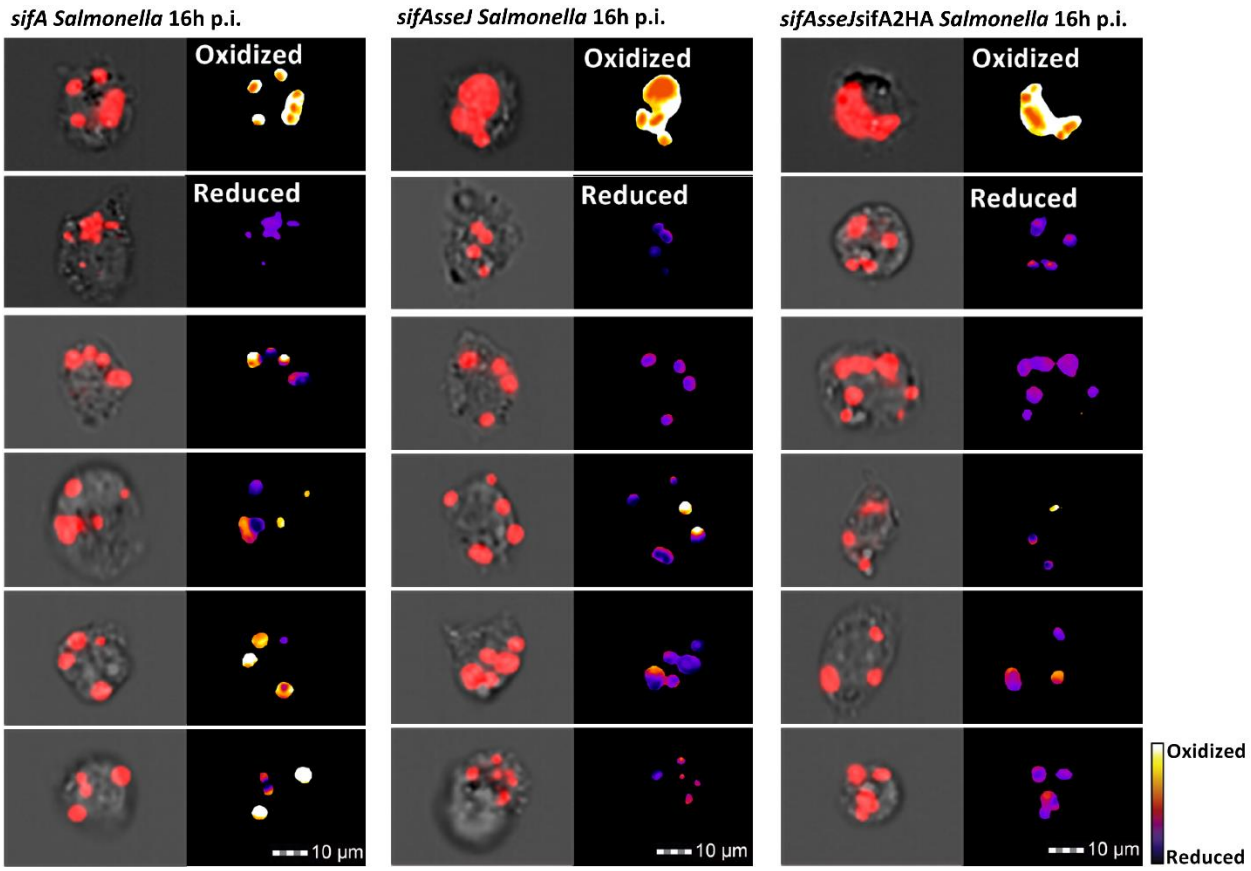

Figure 2-9: Representative images of infected THP-1 cells.
Similar to our analysis in Figure 2-6, we selected representative images of infected THP-1 cells that contain multiple intracellular bacteria from the AMNIS ImageStream. Images were taken at 16 hours p.i.. The corresponding pseudo-colored ratio images were obtained after analysis with ImageJ. More pronounced heterogeneity between intracellular *sifA* bacteria is observed at 16 hours p.i..

To test whether the redox stress of cytosolic bacteria was caused by ROS or RNS, we infected THP-1 cells with WT or *sifA* and added DPI and L-NMMA. In human THP-1 cells we found increased redox stress in *sifA* resulting from RNS (Fig 2-10A). Infection of murine BMDM with *sifA* did also result in increased redox stress (Fig 2-10B) but infection of *gp91phox-/-* and *iNOS-/-* BMDM revealed that the source was phagosomal ROS rather than RNS (Fig 2-10C).

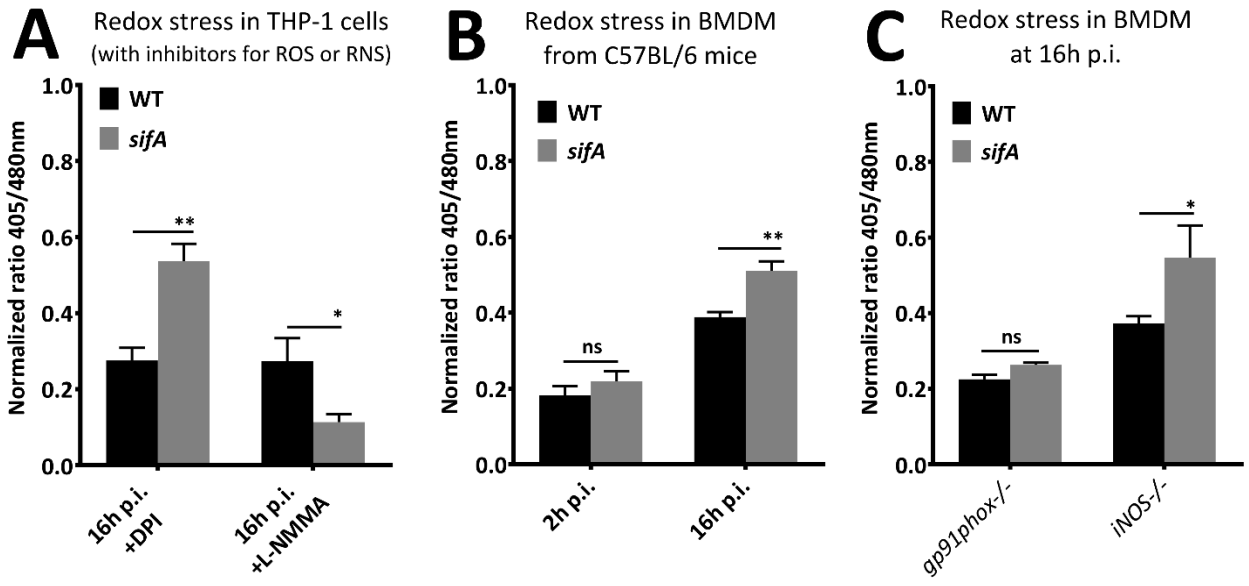

Figure 2-10: Redox stress in cytosolic *S.* Typhimurium in THP-1 cells and mouse BMDM.
(A) Intra-bacterial redox stress in WT and *sifA S.* Typhimurium in THP-1 cells with the addition of inhibitors for oxidative stress (DPI) or nitrosative stress (L-NMMA) at 16 hours p.i. Error bars indicate the standard deviation. (B) Intra-bacterial redox stress in WT and *sifA S.* Typhimurium in BMDM. (C) Intra-bacterial redox stress in WT and *sifA S.* Typhimurium in gp91phox-/- and iNOS-/- BMDM. Each value represents analysis of at least 15,000 pictures. Error bars indicate the standard deviation over three separate experiments. Significance was determined by a student's t-test (* $p<0.5$; ** $p<0.01$).

Collectively, these results highlight that *Salmonella* uses specific oxidative stress evasion strategies that rely on SPI-2 mediated processes to prevent co-localization of ROS with the SCV. *S.* Typhimurium that escape the SCV into the cytosol experience more redox stress. The source and intensity of redox stress may be dependent on the host donor and the stimulation of macrophages by different cytokines and stimuli.

2.4 Discussion

Despite the successful use of roGFP2 in eukaryotic systems, this biosensor had yet to be extensively applied in bacterial systems. Here we showed that roGFP2 can be used as a robust and direct redox biosensor in *S.* Typhimurium. Moreover, this provides a novel non-disruptive measure

of real-time fluctuations in the intra-bacterial redox potential. All these properties make roGFP2 a superior biosensor for the study of redox dynamics in bacteria compared to other systems that are currently being used.

Using this novel approach, we studied *Salmonella* redox dynamics during infection of human cultured cells and BMDM. By measuring roGFP2 fluorescence, "redox stress" was measured inside *S.* Typhimurium from within the infected cells. Significantly more redox stress was observed inside antimicrobial macrophages than in permissive HeLa cells. For the study of infected cells, we used the AMNIS ImageStream to ensure an unbiased and highly sampled approach. High throughput acquisition of images by this machine made it possible to detect sub-populations of THP-1 cells whereas the processing of individual images allowed for analysis of individual bacteria. Because of the large sampling size and high image resolution, we observed heterogeneity between cells and even between bacteria within one cell. Recently, several studies showed that not all *S.* Typhimurium bacteria within one cell replicate at similar rates and not all bacteria are equally affected by antimicrobial immune responses (132, 140, 141). Our observations clearly show variance in redox stress among bacteria within one cell. What determines the level of redox stress that intracellular bacteria undergo is still unclear; however, we speculate that diversity of expression profiles and variation in effector secretion play important roles. It is crucial to better understand heterogeneity since this is thought to be the core of bacterial persistence and resistance to current antimicrobial therapies (141).

The role of the SPI-2 system in evasion of oxidative stress by *S.* Typhimurium has been discussed for many years and continues to be a hotly debated topic. Earlier studies found that abrogation of the oxidative burst rescued attenuation of SPI-2 deficient *S.* Typhimurium and concluded involvement of SPI-2 effectors in ROS evasion (108, 137). Additionally the authors showed

ineffective SPI-2 mediated co-localization of NADPH-oxidase with the SCV (108, 137). Although neither of these studies were able to directly measure oxidative stress inside *S.* Typhimurium during infection, these results implicate SPI-2 involvement in ROS evasion.

A more recent attempt to indirectly measure oxidative stress inside *S.* Typhimurium used induction of an oxidation sensitive *ahpCp*-GFP transcriptional fusion (87). Unable to measure differences in oxidative stress between WT and SPI-2 deficient *S.* Typhimurium during infection of macrophages and mice, the authors concluded that *Salmonella* detoxifying enzymes are sufficient to cope with the host oxidative burst and there is no role for the SPI-2 system in evasion strategies (87). These seemingly conflicting results created some confusion about the role of SPI-2 in ROS evasion strategies (109, 110). Recently, researchers using a similar approach had to substitute the *ahpC* promotor for the *katGp* promoter because of lower baseline activity and a larger dynamic range. (132). It is therefore possible that the original *ahpC* promotor did not offer enough sensitivity to measure subtle but important differences in oxidative stress. With the roGFP2 biosensor we clearly demonstrate the involvement of the SPI-2 system in ROS evasion strategies by directly measuring redox stress inside *S.* Typhimurium in human and murine macrophages. Furthermore our results show that SPI-2 mediated evasion relies on discordant localization of ROS with the SCV.

In human and murine macrophages we found that cytosolic *S.* Typhimurium experience increased redox stress compared to vacuolar bacteria. Interestingly, we found that the source of redox stress varied between human and murine macrophages. Macrophages are highly heterogeneous cells that can quickly alter their function in response to local signals and stimuli (142). It is most likely that both ROS and RNS can play a role in the antimicrobial response but the intensity and nature of redox stress is dependent on the host and how the macrophages are stimulated. Specifically the differences in the source of redox stress for cytosolic bacteria in human macrophages compared to

murine macrophages may be explained by differences in cytosolic PAMP recognition. In murine macrophages for example, it was found that caspase-11 protects against cytosolic bacteria (143) whereas human macrophages do not express caspase-11 but instead express caspase-4. Although caspase-4 and caspase-11 shares some similarities there may be differences with regard to the immune response towards cytosolic bacteria. Another difference is the expression of TLR-11 in murine macrophages which recognizes *Salmonella* flagellin. Human macrophages do not express TLR-11 which has already be shown to have a dramatic impact on *Salmonella* infection (144).

From these results, one can speculate that intracellular pathogens that can survive and replicate in the macrophage cytosol, e.g. *S. flexneri* and *L. monocytogenes*, most likely have evolved specific virulence strategies to evade redox stress within the cytosol. Remarkably, both *S. flexneri* and *L. monocytogenes* use actin polymerization to facilitate continuous movement inside the cytosol (145) which may play a role in evasion of ROS and RNS.

In this Chapter we describe the use of roGFP2 as a biosensor to study redox dynamics in *S.* Typhimurium; however, this biosensor could easily be used in a multitude of bacteria. Thus far, roGFP2 has already been used in the intracellular pathogen *Mycobacterium tuberculosis* to investigate intracellular oxidative stress after infection of macrophages (124). ROS and RNS evasion strategies of many intracellular pathogens remain elusive and we propose that roGFP2 will have broad utility as biosensor to study redox related virulence mechanisms and will assist in further characterization of intracellular pathogenesis. Furthermore roGFP2 can be used to study bacterial redox dynamics after exposure to antimicrobial compounds or during biofilm formation and thereby may contribute to potential clinical applications.

2.5 Material and methods

2.5.1 Bacterial strains

roGFP2 from the pRSETB-roGFP2 vector was cloned into pET28a for inducible expression in the *E. coli* BL21(DE3) background. Additionally roGFP2 was cloned into the pfpv25 vector for constitutive expression of roGFP2. The pfpv25-roGFP2 vector was then transformed into *S.* Typhimurium SL1344 and 50 μg/ml carbenicillin was added to the growth medium for maintenance of the plasmid. All mutants were made in the SL1344 background. The making of the *ssaR* and *sifA* mutants is described previously (136). The clean deletion of *sseJ* was made by allele exchange in vector pRE112 as described previously (146). Deletions were confirmed by PCR and sequencing.

2.5.2 Protein purification

roGFP2 protein was expressed and purified as previously reported (147).

2.5.3 Fluorescent protein assays

For complete reduction purified roGFP2 was pre-incubated with 10 mM DTT. Excess DTT was removed from the solution using Centri-Spin 20 columns (Princeton Separations Inc.). Reactions were carried out with 10 μg of protein in 200 μL of PBS, pH 7.4 in a black, clear bottom 96 well plate (Corning). Excitation scans were carried out in a Tecan plate reader with excitation wavelengths covering 350 nm to 500 nm while emission was measured at 510 nm. Signals for fully oxidized and fully reduced roGFP2 were obtained by adding 100 mM H_2O_2 and 10 mM DTT 30 minutes prior to the experiment. Data were analyzed in Excel and all values were normalized to the values obtained for maximally oxidized and for fully reduced protein.

2.5.4 *In vitro* real-time measurement of intra-bacterial redox potential

In vitro analysis of the intra-bacterial redox potential was done at 37°C in a Tecan plate reader with excitation at 405 nm and 480 nm while emission was measured at 510 nm. Log phase bacterial cultures were resuspended in PBS or LPM (Low Phosphate Medium pH 5.8) at OD 1.0 and 200 µL per well was loaded in a black, clear bottom 96 well plate. Background signals from the non-fluorescent corresponding strain were obtained in the same experiment. Additionally the signals for fully oxidized and fully reduced bacteria were obtained by adding 50 mM H_2O_2 and 10 mM DTT to the bacteria culture at the start of the experiment. All values were normalized to the values obtained for maximally oxidized and for fully reduced bacterial cultures. Images were analyzed by ImageJ as described previously (113).

2.5.5 Fluorescence microscopy

For real-time fluorescence analysis of SL1344 by microscopy, bacteria were grown overnight and diluted in PBS. Images were taken every 20 seconds for a period of 20 minutes with an Olympus IX81 microscope at a multitude of magnification of 600. Infected cells were fixed with 3% PFA after incubation with 50 mM NEM. Coverslips were mounted on slides using anti-fade reagent and analyzed by microscopy. In every experiment fully oxidized and fully reduced ratio values were obtained and all data were normalized to fully oxidized and fully reduced ratios. Images were analyzed by ImageJ as was described previously (113).

2.5.6 Culturing bone marrow derived macrophages

Bone marrow was collected from the tibias and femurs of 6-8 week old wild type C57BL/6J, iNOS-/- (B6.129P2-Nos2tm1Lau/J) and gp91phox-/- (B6.129S6-Cybbtm1Din/J) male mice (all

purchased from Jackson Laboratory). Each well of a 6-well plate was seeded with 1x106(RPMI 1640 containing L-Glutamine; Life Technologies, supplemented with 10% heat-inactivated FBS; Life Technologies, 100 U/ml Penicillin and 100 μg/ml Streptomycin; Life Technologies and 20 ng/ml M-CSF; Peprotech. Cells were incubated at 37°C with 5% CO2. On days 4 and 6 of culture, 2 ml medium were removed from each well and replaced with 2 ml fresh medium. On day 7 of culture, culture supernatant containing non-adherent cells were removed prior to performing assays. The purity of adherent cells was confirmed by flow cytometry for all genotypes on day 7 of culture, and >97% of cells were CD45+CD11b+F4/80+.

2.5.7 Infection experiments

HeLa cells were grown in DMEM containing 10% heat-inactivated FBS, 1% GlutaMAX, and 1% non-essential amino acids. Cells were seeded at $3.0*10^5$ in 6-well plates 48 h prior to infection. THP-1 cells were grown in RPMI supplemented with 10% inactivated FBS, 1% Glutamax and 1 % non-essential amino acids. 72 hours prior to infection, THP-1 cells were seeded at $3.6*10^6$ in 6-well plates and for the first 24 hours 100 nM PMA was added for differentiation into macrophage-like cells. After 24 hours the medium was replaced and the cells were incubated for another 48 hours before infection was started. ON cultures of *Salmonella* were used for infection (stationary phase bacteria) or diluted 1:33 in LB and sub-cultured for 3 h at 37 °C to obtain log phase bacteria. The bacteria were resuspended in PBS and used at a multiplicity of infection of 50. THP-1 cells were span down at 1000 rpm for 10 minutes to synchronize infection. Inhibitors Diphenyleneiodonium chloride (Sigma) and L-NMMA (Cedarlane) were added at concentrations of 5μM and 2mM respectively throughout the duration of the infection experiment. At 30 min post infection, cells were washed with PBS and further incubated in medium supplemented with 50

μg/ml gentamicin. At 2 hours post infection cells were washed with PBS and incubated in medium supplemented with 12 μg/ml gentamicin. For CFU counts: cells were lysed in PBS supplemented with 1% Triton X100 and 0.1% SDS. After a serial dilution the samples were plated on 50 μg/ml streptomycin plates after which colony forming units were counted manually. For AMNIS analysis: 5 minutes prior to sampling time 50 mM NEM was added to the media. The cells were washed and detached from the surface with Cell Dissociation Buffer enzyme-free Hanks' based (Gibco). Immediately after detachment 3% PFA was added to fix the infected cells. Cells were stained the next day.

2.5.8 Staining before AMNIS analysis

After fixation the cells were permeabilized with 0.1% Triton X100 in PBS. The cells were then incubated with a primary antibody against the *Salmonella* O antigen (RbαSalm O Lot2098504) for 3 hours and subsequently incubated with a secondary Alexa660 goat-α-rabbit antibody (Invitrogen).

2.5.9 AMNIS ImageStream and IDEAS/ImageJ analysis

Samples were analyzed by the AMNIS ImageStream. The laser intensities for 405 nm, 488 nm, 658 nm and 785 nm were 100, 120, 20, 3.8 respectively. The data files were further analyzed with the IDEAS software version 6.0.129.0 that is supplied by AMNIS. Infected cells were selected based on fluorescence at 660 nm. Every image of an infected cell was then analyzed by the program to bacteria cased on fluorescent intensity at 660 nm. Based on this selection, a mask was created called "bacteria" that was used for further analysis of the 405/480nm ratio of intracellular bacteria. The background fluorescence of each individual cell was obtained by a separate mask that

excluded the bacterial mask but encapsulated the rest of the cell. This mask was named "background" and the 405nm and 480nm fluorescent background intensities for each individual image were subtracted from the 405nm and 480nm fluorescent signal of the bacterial mask. The resulting 405/480 ratio signals were plotted in a histogram. Reduced and oxidized controls were obtained within each experiment and all values were normalized to oxidized and reduced ratio values. Pseudo-colored ratio images were made through analysis by ImageJ as was described previously (113).

2.5.10 Griess assay and Amplex red assay

The Griess assay (SIGMA) and the Amplex Red Hydrogen peroxide Assay (Molecular probes #A22188) were done according to the manufacturer's instructions. Samples were analyzed immediately after the samples were obtained.

2.5.11 Calculation of E_{roGFP2}

To calculate the E_{roGFP2} of *S.* Typhimurium we used the method as described by Gutscher *et al.* (117). In short, we measured the R (ratio 405/480 nm) of *S.* Typhimurium in LPM pH5.8. Additionally we obtained the R_{red} (ratio 405/480 nm of reduced control), the R_{ox} (ratio 405/480 nm of oxidized control) and the fluorescence intensity at 480 nm under reduced or oxidized conditions (*I*480*max* and *I*480*min* respectively). With these values we calculated the degree of roGFP2 oxidation (OxD_{roGFP2}) given by formula:

$$OxD_{roGFP2} = \frac{R - R_{red}}{(I480min/I480max)(R_{ox} - R) + (R - R_{red})}$$

The degree of oxidation could then be used to calculate the intracellular sensor redox potential E_{roGFP2} by using the Nernst equation:

$$E_{roGFP2} = E^{O\prime}_{roGFP2} - \left(\frac{RT}{zF}\right) * \ln\left(\frac{(1 - OxD_{roGFP2})}{OxD_{roGFP2}}\right)$$

In which R is the gas constant (8.315 J K-1 mol-1), T is the absolute temperature (310.15 K), z is the number of transferred electrons (2) and F is the Faraday constant (96,485 C mol-1). The midpoint potential of roGFP2 ($E^{0'}_{roGFP2}$) is -280 mV (125).

Chapter 3: A novel stress response mechanism-how *Salmonella* regulates the influx of reactive oxygen species.

3.1 Summary

The outer membrane (OM) of Gram-negative bacteria provides protection against toxic molecules including reactive oxygen species (ROS) that are generated by specific immune cells during infection. A decrease in OM permeability is strongly associated with multi-drug resistance and the formation of persisters making the OM a promising potential target for new antimicrobial therapies. To better understand regulation of OM permeability, we studied the real-time influx of hydrogen peroxide in *Salmonella* Typhimurium and discovered a new mechanism by which Gram-negative bacteria rapidly decrease their OM permeability upon encountering reactive oxygen species (ROS). We found that outer membrane protein A (OmpA) and outer membrane protein C (OmpC) are the main pores that facilitate OM transport of hydrogen peroxide. The pore in OmpC was rapidly closed upon encountering ROS due to binding of a periplasmic "plug" protein whereas the much smaller OmpA pore was opened after encountering ROS. Regulation of pore-opening of OmpA was mediated by the formation of a reversible disulfide bond in the periplasmic domain of OmpA. We tested persister formation after infection of macrophages using mutant strains of *Salmonella* with increased permeability. Interestingly, we found that increased OM permeability dramatically decreased persister formation. Taken together, these results reveal how Gram-negative bacteria regulate the influx of ROS over their OM to defend themselves against oxidative stress and how this mechanism contribute to the formation of persisters during infection.

3.2 Introduction

The outer membrane (OM) of Gram-negative bacterial pathogens provides protection from environmental stresses as well as from antimicrobial reactive oxygen species (ROS) (148). ROS can permeate through the membrane to cause damage to bacterial proteins, DNA and other intra-bacterial molecules (106, 149), however, not much is known about if or how bacteria regulate the influx of ROS. The influx of antibiotics is more extensively studied (148, 150). Typically, hydrophobic compounds diffuse through the OM while hydrophilic molecules mostly permeate into bacteria through pores in outer membrane proteins (OMPs) (148). Many antibiotics enter through pores in the OM and because of this, accurate regulation of OMP expression lies at the core of antibiotic resistance which is clearly illustrated by decreased OM permeability in the majority of multi-drug resistant bacteria that are isolated from patients in the clinic (151, 152). Decrease in OM permeability not only leads to antibiotic resistance but also contributes to the formation of persistent bacteria. Persisters are non-replicating antibiotic-tolerant cells that limit OM permeability and often re-initiate a full-blown infection after the antibiotic treatment is terminated (140). Because of this, it has been suggested that targeting bacterial membrane functioning is an underexploited strategy to reduce persistent infections (153). There are several distinct strategies by which Gram-negative bacteria can reduce permeability for hydrophilic antibiotics. “Slow” strategies rely on differential expression of OMPs in the OM or genetic alterations in individual OMPs rendering them less permeable for specific molecules (154). “Rapid” closure of certain pores can occur depending on transmembrane voltage, acidic pH and binding of polyamines (148). Because of analytical limitations and challenging experimental set ups, there has been no research done on rapid OM permeability changes in living bacteria. In Chapter 2, we described the use of roGFP2 to measure real-time redox changes in *Salmonella* (89).

In this Chapter we used this method to measure the influx of hydrogen peroxide in order to determine the OM permeability in living *Salmonella enterica* Typhimurium bacteria during an encounter with ROS.

3.3 Results

3.3.1 Outer membrane proteins rapidly alter OM permeability

To measure rapid real-time fluctuations across the bacterial membrane we used roGFP2 expressed inside *S.* Typhimurium (89). In order to measure the influx without rapid detoxification of H_2O_2, the HpxF(-) mutant was used which is devoid of catalases and peroxidases (133). The detoxifying power of the HpxF(-) mutant is 90-fold lower than that of WT *S.* Typhimurium and exposure to increasing amounts of H_2O_2 leads to a dose dependent response (Fig. 3-2A to 3-2C). All measurements were done with bacteria grown in medium that mimics the intracellular environment that *Salmonella* encounters during infection of macrophages (155). By measuring the H_2O_2 influx in live bacteria after challenges with varying amounts of H_2O_2, we identified a very rapid reduction of the OM permeability coinciding with an intra-bacterial redox potential of ~ -0.29V (Fig 3-1A). A rapid alteration of the OM permeability had not been reported before and we named this moment the "switching point". The sudden drop in the H_2O_2 influx during the "switching point" correlates with a sudden reduction in the membrane permeability (P). The relationship is derived as:

$$\mathbf{Influx} = \mathbf{P} * \mathbf{A} * \mathbf{\Delta C}$$

In which P is the membrane permeability coefficient, A is the surface area of the bacterial membrane and ΔC is the difference between the H_2O_2 concentrations on either side of the membrane.

We determined the influx in relation to ΔC, before and after the "switching point" and found that H_2O_2 influx follows the rules of passive diffusion (Fig 3-1B and 3-1C). However, the calculations show that the membrane permeability was reduced by ~12 fold after the "switching point" compared to before the "switching point". (For calculations see the Material and Methods section of this Chapter). Since the surface area of the bacterial membrane (A) remained constant throughout the experiment and the ΔC changed <30% over this short time period, the 12-fold reduction could only be explained by rapid alterations in membrane permeability. We performed a similar analysis in stationary phase bacteria and found that the sudden reduction in permeability after the "switching point" was even more dramatic at <30 fold (Fig 3-2D to 3-2F). To determine that the OM was driving the sudden reduction in permeability, we measured the influx in spheroblasts (bacteria without an OM). In spheroblasts, we did not observe a "switching point" indicating that changes in the OM are responsible for the rapid reduction of membrane permeability (Fig 3-2G).

Since outer membrane proteins (OMPs) facilitate diffusion of hydrophilic molecules over the OM, we first determined which OMPs were involved in the rapid alteration of OM permeability. To do this, we created single deletion mutants (*ompA*, *ompC*, *ompD* and *ompF*) and calculated the H_2O_2 influx before and after the "switching point". Each OMP that is studied in this Chapter forms a beta-barrel in the outer membrane (Fig 3-1D). By measuring the H_2O_2 influx in these mutants we found that OmpC facilitated the majority of H_2O_2 influx before the "switching point" (Fig 3-1E and Fig 3-1F) whereas the OmpA pore facilitated H_2O_2 diffusion after the "switching point" (Fig 3-1G). OmpD and OmpF did not contribute to the transport of H_2O_2 in live bacteria under the conditions used in this study.

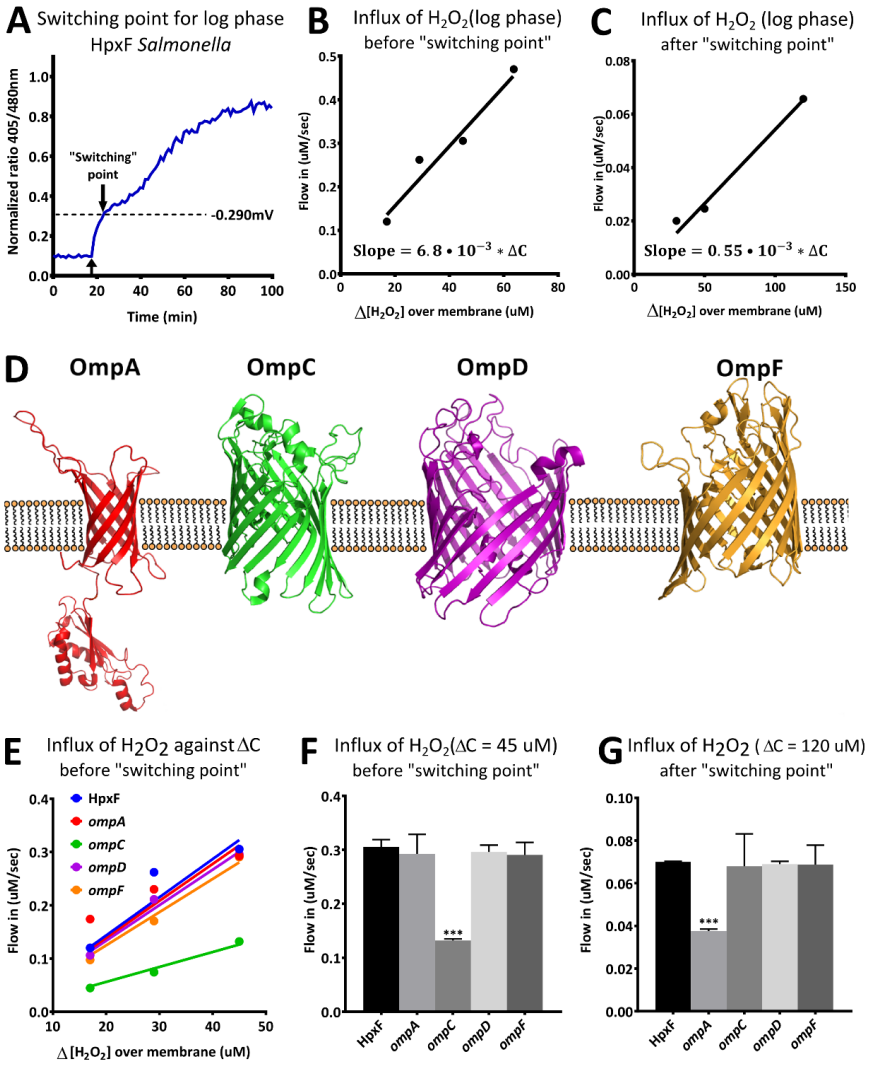

Figure 3-1: *Salmonella* rapidly reduces OM permeability during "switching point"

(A) Real-time analysis of changes to the intra-bacterial H_2O_2 concentration after a challenge with 150 μM H_2O_2. The upward arrow indicates injection of H_2O_2. The downward arrow indicates the moment after which the H_2O_2 influx is suddenly reduced. We named this moment the "switching point". (B, C) We found a linear correlation between the H_2O_2 influx and the ΔC which corresponds with the constraints for passive diffusion. More details about how calculations were done is given in the supplementary material. (D) Schematic illustration of four OMPs in the OM. The protein structures of OmpA, OmpC, OmpF and the periplasmic domain of OmpA were taken from pdb.org. The structural prediction of OmpD was done by using the iTasser server at http://zhanglab.ccmb.med.umich.edu/I-TASSER/. (E) For each of the single OMP deletions mutants a correlation between the H_2O_2 influx and the ΔC was obtained before the "switching point". (F, G) For the sake of simplicity the H_2O_2 influx was obtained before and after the "switching point" at ΔC=45μM and ΔC=120μM respectively. The *ompC* mutant has lower membrane permeability before the "switching point" whereas the *ompA* mutant has lower membrane permeability after the "switching point". Error bars represent the standard deviation and significance was obtained by a student's t-test (*** p <0.001).

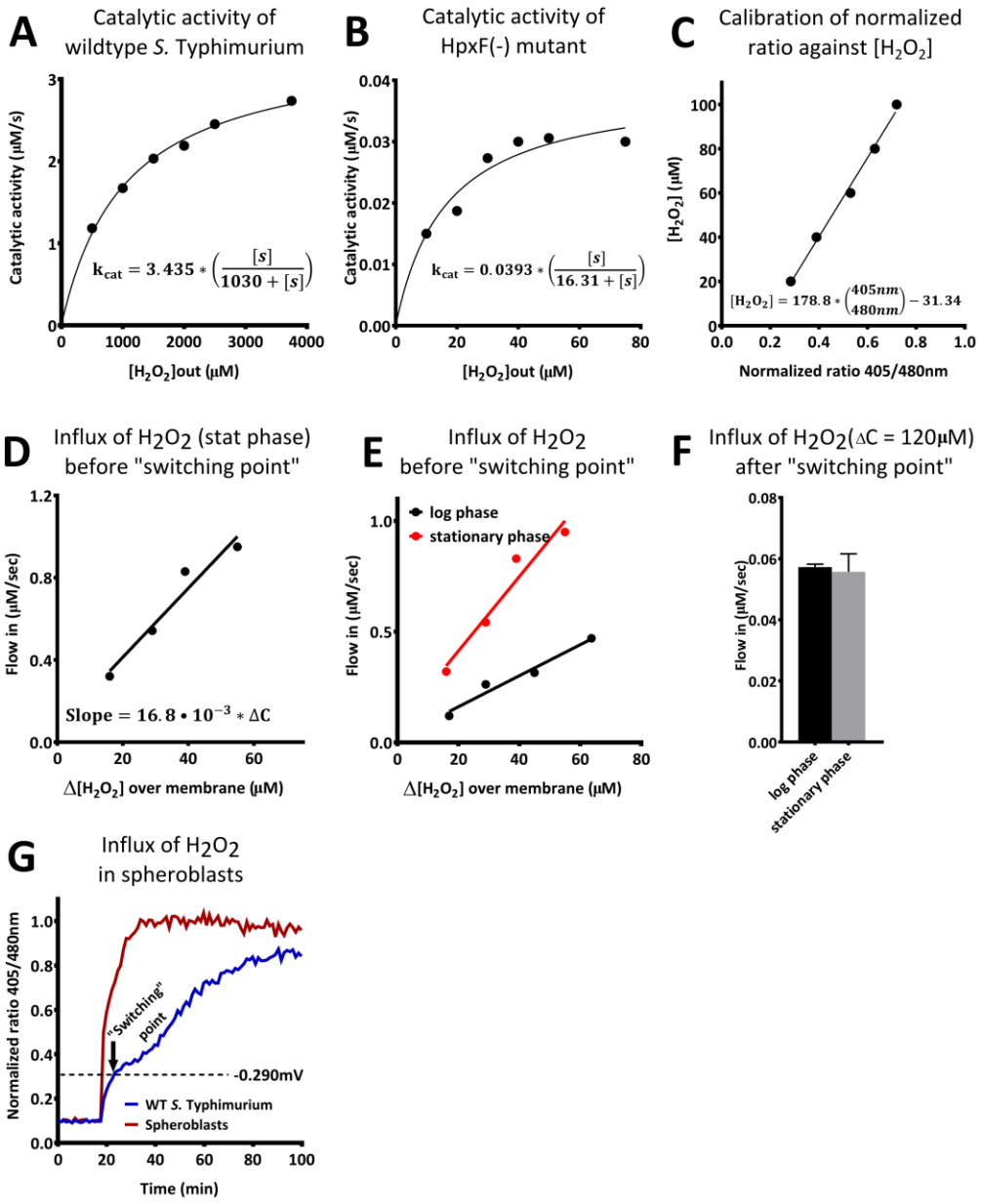

Figure 3-2: Experimental values for the calculation of membrane permeability values

(A, B) The catalytic activity of WT and HpxF(-) *S.* Typhimurium towards hydrogen peroxide. Catalytic activity was calculated by dividing the time it takes to completely eradicate the H_2O_2 challenge by the average $[H_2O_2]$ (C) Correlation between the intra-bacterial $[H_2O_2]$ and the normalized 405/480 ratio. (D) H_2O_2 influx in stationary *S.* Typhimurium before the switching point. (E) Comparison between the H_2O_2 influx in stationary and log phase bacteria before the switching point. (F) Comparison between the H_2O_2 influx in stationary and log phase bacteria after the switching point. Error bars represent the standard deviation and significance was obtained by a student's t-test. (G) Real-time H_2O_2 influx in spheroblasts (*S.* Typhimurium that lack an OM). No rapid alteration in the membrane permeability was observed.

From our results, it appears that the pore in OmpC was open before the "switching point" (under non-hazardous conditions) whereas it was closed after bacteria encountered ROS. In contrast, the much smaller OmpA pore was closed under non-hazardous conditions but opened after encountering ROS. This is the first report of OMPs being rapidly opened or closed in living bacteria. To further analyze the mechanisms resulting in the rapid closing and opening of pores in the OM we continued to investigate the changes in OmpC during the "switching point".

3.3.2 Opening and closing of OmpC

Conductivity of OMPs is mainly studied in isolation during *in vitro* experiments without biological context or potential protein binding partners. Therefore, no "plug" proteins have been identified that close pores in OMPs. However, in mitochondria the voltage-dependent anion channel, which facilitates the transport of ions and molecules between mitochondria and cytosol, binds a tubulin dimer that "plugs" the pore. Binding of this dimer closes the channel and stops respiration (156). As the OmpC pore was open before the "switching point" and closed afterwards, we hypothesized that perhaps a "plug" protein closed the pore. Previous studies have shown that OmpC binds small heat shock protein A (IbpA) (157) which, in *Salmonella*, is the homologue HslT with 98% sequence similarity. To elucidate whether HslT could function as a "plug" protein we measured the H_2O_2 influx in the single deletion mutant (*hslT*) and found that without HslT, the pore in OmpC was permanently open (Fig 3-3A). In the double mutant (*hslTompC*), OM permeability was restored to similar levels as in the *ompC* single mutant. After the "switching point" only the *hslT* single deletion mutant is more permeable than WT bacteria. These results indicate that HslT functions as the "plug" protein for OmpC that closes the pore after the "switching point". A

prediction of the OmpC-HslT binding was done showing the effective closure of the OmpC pore by its interaction with HslT (Fig 3-4).

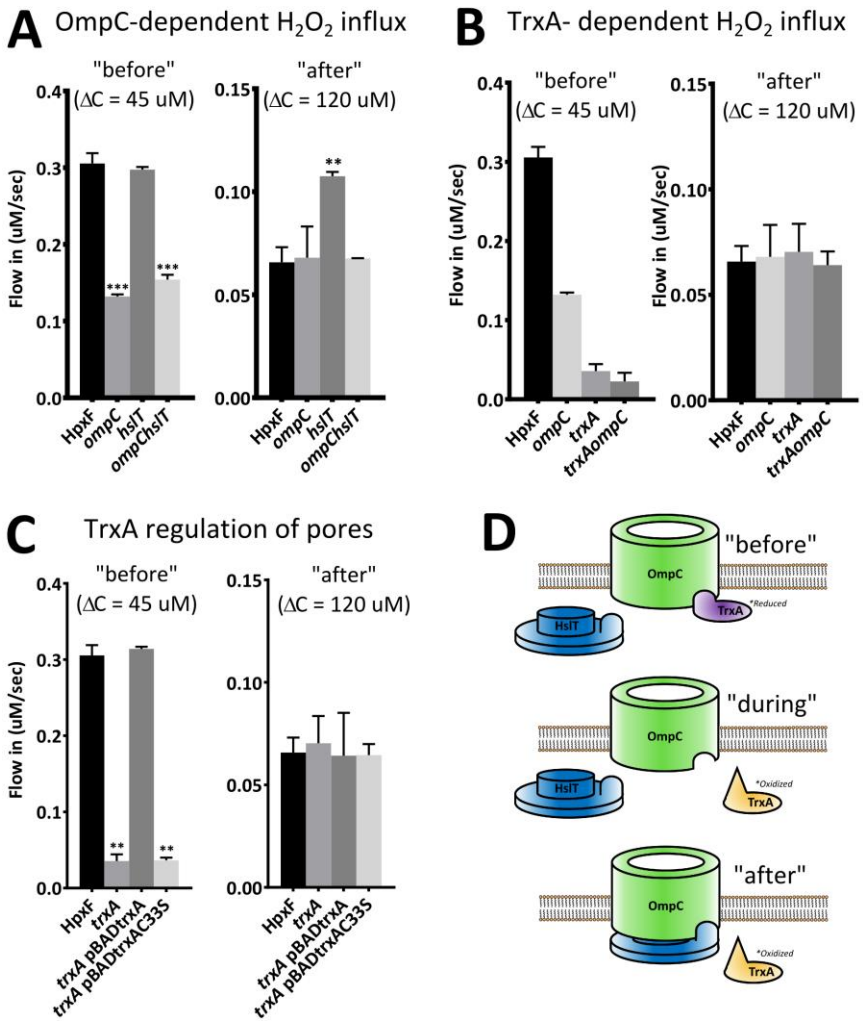

Figure 3-3: OmpC facilitates influx before the "switching point".

(A) Influx of H_2O_2 into *Salmonella*. OmpC is the main pore that facilitates H_2O_2 transport before the "switching point" whereas after the "switching point" the OmpC pore is closed. The closing of the OmpC pore is dependent on the HslT protein. Deletion of *hslT* opened the pore permanently. (B) The opening of pores before the switching point was found to be dependent on thioredoxin. After the "switching point" the presence or absence of thioredoxin had no effect on the OM permeability. The OM permeability in the *trxAompC* double mutant before the "switching point" was not significantly further reduced compared to OM permeability in the *trxA* single mutant (C) Complementation of the *trxA* mutant with a plasmid carrying the trxA gene restores normal OM permeability. Addition of a plasmid carrying the $trxA^{C33S}$ mutant does not restore OM permeability. (D) A schematic representation of a proposed model that explains the opening and closing of the OmpC pore. Potential binding of TrxA blocks interaction with HslT thereby opening the pore. The redox-sensitive disulfide in thioredoxin is essential for binding to OmpC. Error bars represent the standard deviation and significance was obtained by a student's t-test (** $p<0.01$; *** $p<0.001$).

In order to determine if another protein regulated binding of the HslT "plug" protein to OmpC, we searched if there were additional known binding partners for OmpC. In this search we found a study in which the authors describe binding of OmpC to the small redox protein thioredoxin (TrxA) (158). This small redox sensor is known to change conformation due to a reversible internal disulfide bond between CYS33 and CYS36. We measured the H_2O_2 influx in the *trxA* single mutant and the double mutant (*trxAompC*) to investigate if thioredoxin was involved in regulation of OmpC pore-closing. These measurements showed that without thioredoxin the OmpC pore was permanently closed (Fig 3-3B). Since the OM permeability after "the switching point" was unaffected by deletion of *trxA* it appears that thioredoxin plays no role in controlling OmpA closing and opening after "the switching point". Complementation of *trxA* with a plasmid carrying the trxA gene reversed the OM permeability defect (Fig. 3-3C). Complementation with a $trxA^{C33S}$ mutant gene did not reverse the OM permeability to WT levels. These results indicate that thioredoxin-mediated opening/closing of OmpC is dependent on the reversible disulfide bond in TrxA. A schematic representation of a proposed model is shown in Fig. 3-3D.

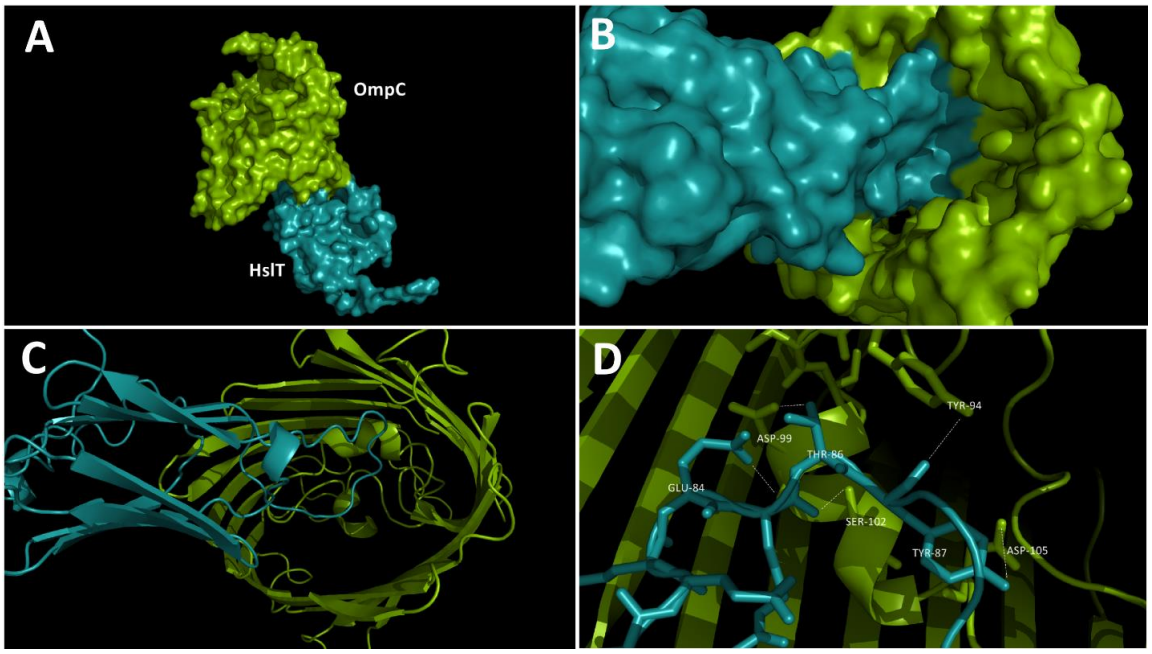

Figure 3-4: Prediction of interaction between OmpC and its "plug" protein HslT.

(A) The OmpC barrel is predicted to interact with the HslT "plug" protein effectively closing the pore within the barrel. The HslT protein structure is predicted by the iTasser webserver http://zhanglab.ccmb.med.umich.edu/I-TASSER/ (159) and protein-protein interaction was predicted by the pyDockWeb server at http://life.bsc.es/servlet/pydock/home/ using restrains on binding sites (160). (B) View from the periplasmic site of the OmpC barrel showing effective closure of the pore. (C, D) The HslT protein is predicted to interact with the internal loop4 of OmpC (161). This interaction is facilitated by hydrogen bonds between GLU-84(HslT) and ASP-99(OmpC), THR-86(HslT) and ASP-99(Omp-C), THR-86(HslT) and SER-102(OmpC), THR-87(HslT) and TYR-94(OmpC), THR-87(HslT) and ASP-105(OmpC).

3.3.3 Opening and closing of OmpA

Under harmful oxidizing conditions, the much smaller OmpA pore appeared to be the more important facilitator of H_2O_2 diffusion across the OM (Fig 3-1G). Thioredoxin was not involved in the opening of the OmpA pore (Fig 3-3A) and it appeared that the opening/closing of OmpA was regulated by a separate mechanism. Previously several studies have reported a reversible disulfide bond inside the periplasmic domain of OmpA similar to the one found in thioredoxin (158, 162). To investigate if OmpA did indeed contain a reversible disulfide bond in its periplasmic domain, a mass spectrometry screen was done using Stable Isotope Labeling by Amino Acids

(SILAC) (Fig 3-5A). In this screen we confirmed the internal reversible disulfide bond that forms inside the periplasmic domain of OmpA between CYS315 and CYS327. We hypothesized that formation/disruption of this reversible disulfide bond could regulate opening of the OmpA pore after "the switching point". First, we determined the involvement of the periplasmic domain of OmpA by deletion of the OmpA C-terminus (ompA198-350) which resulted in permanent opening of the OmpA pore (Fig. 3-5B). In addition, an ompA^{C327S} point mutant (which is unable to form an internal disulfide bond) was created and this point mutant was found to be in permanently closed conformation. Based on these results we created a representation of the mechanisms that open and close the OmpA pore (Fig. 3-5C). Interestingly, the two cysteines that regulate pore-opening of OmpA are conserved among many Gram-negative bacteria (Fig. 3-5D).

A prediction of the binding between the OmpA barrel and its periplasmic domain showed that amino acids ARG-321 and LYS-319 interact with a region rich in ASP in the OmpA barrel. It appears that only under reducing conditions ARG-321 and LYS-319 line up with their respective aspartic acid residues (Fig. 3-6). These results suggest that formation of an internal disulfide bond between cysteine-315 and cysteine-327 in the periplasmic domain prevents interaction between this periplasmic domain and the OmpA barrel.

These results reveal a novel stress mechanism by which *Salmonella* regulates OM permeability through opening and closing of specific pores. The formation and disruption of reversible disulfide bonds in thioredoxin and the periplasmic domain of OmpA drive the changes in OM permeability. These mechanisms appear to be widely conserved among Gram-negative bacteria and protect bacteria from dangerous levels of ROS.

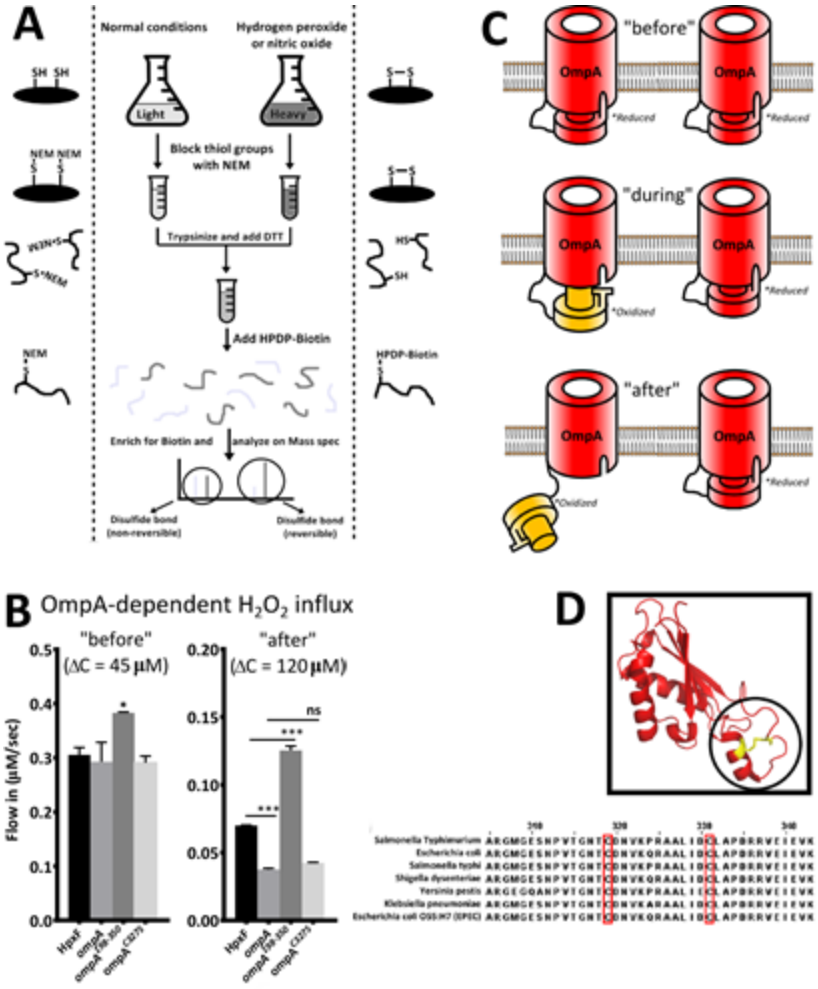

Figure 3-5: OmpA facilitates influx after the switching point.
(A) Schematic overview of SILAC-based proteomics procedure aimed at identifying reversible disulfide bonds in bacterial proteins. The screen was repeated three times with 10mM H_2O_2 and three times with addition of 10 mM SpermineNONOate. The OmpA periplasmic domain was found to form a reversible disulfide bond upon oxidative and nitrosative stress. (B) The OmpA-dependent H_2O_2 influx is dependent on its periplasmic domain (c-term). The *ompA* mutant has lower OM permeability after the "switching point" but has no effect on OM permeability before the "switching point. Deletion of the periplasmic domain leads to a permanently opened pore in OmpA. An $ompA^{C327S}$ point mutation abrogates the ability to form an internal disulfide bond inside the periplasmic domain. This point mutation renders the OmpA pore permanently closed. (C) A schematic representation of the mechanisms that lead to opening and closing of the OmpA pore by its periplasmic domain. Oxidation of the periplasmic domain leads to formation of the disulfide bond between CYS315 and CYS327 after which the periplasmic domain releases the barrel and opens the OmpA pore. (D) The two cysteines that form a disulfide bond in the periplasmic domain of OmpA are widely conserved among many Gram-negative bacteria. Error bars represent the standard deviation and significance was obtained by a student's t-test (*p <0.05; *** p <0.001).

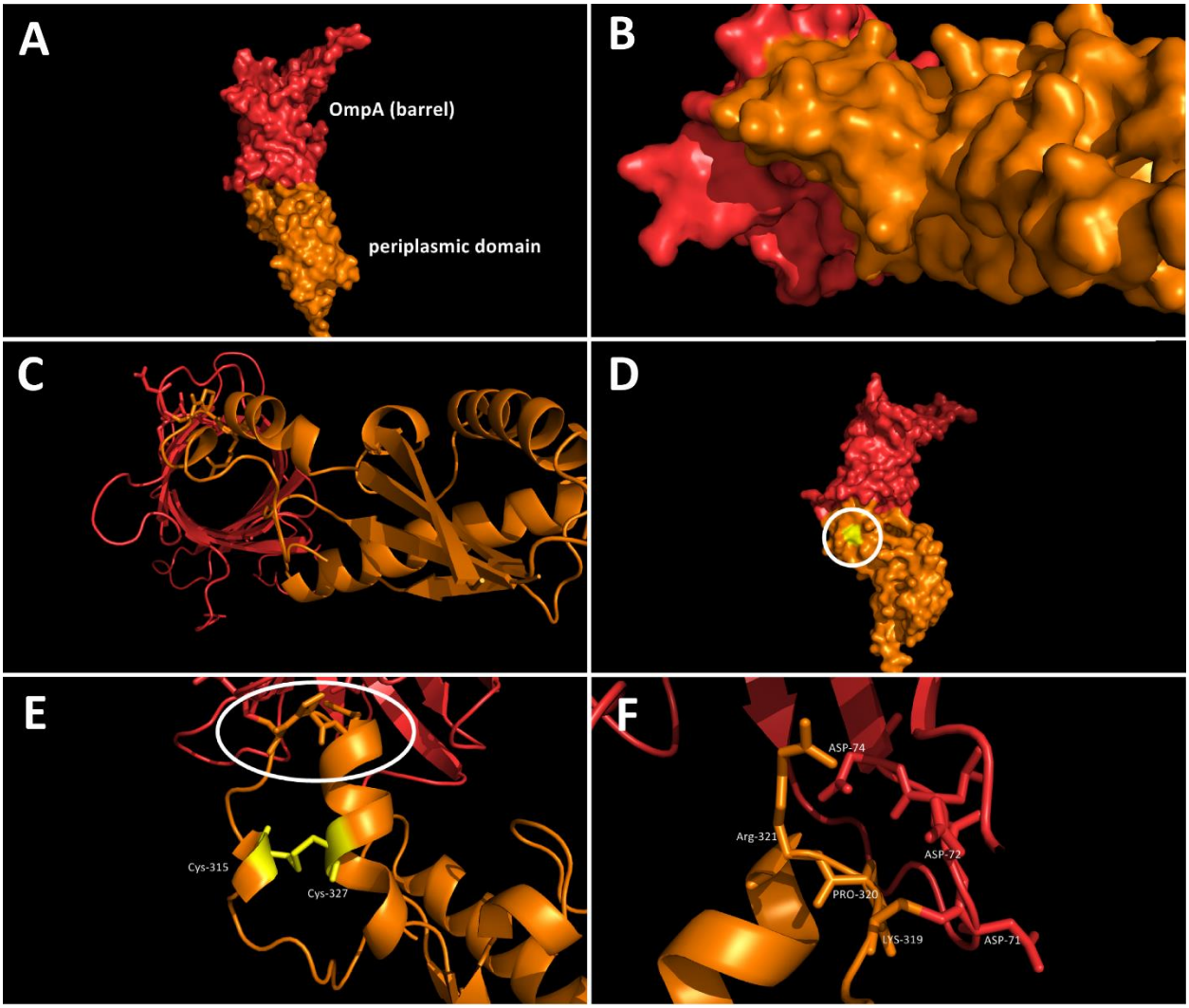

Figure 3-6: Prediction of interaction between OmpA barrel and its periplasmic domain.

(A) The OmpA barrel is predicted to interact with its periplasmic domain effectively closing the pore within the barrel. The OmpA barrel and the periplasmic domain are both obtained from the protein data bank. Protein-protein interaction was predicted by the pyDockWeb server at http://life.bsc.es/servlet/pydock/home/ using restrains on binding sites (160). (B) View from the periplasmic site into the OmpA barrel showing effective closure of the pore due to the binding of the periplasmic domain. (C, D, E) The periplasmic domain is predicted to bind the barrel through its loop that contains two cysteines. These cysteines are marked in yellow in panel D and E. The binding site is indicated by the circle in panel E. (F) Two positive residues in the periplasmic loop (ARG-321, LYS-319) are interacting with ASP-74, ASP72 and ASP-71 in the barrel. The exact position of the residues in the periplasmic loop is dependent on formation of the disulfide bond between CYS315 and CYS327. It appears that the periplasmic domain can therefore only bind the barrel if the disulfide bond is disrupted (under reducing conditions).

3.3.4 Increased OM permeability inhibits formation of persisters

It is well established that decreased OM permeability is central for bacterial persistence (153, 163). Recently it was shown that *S.* Typhimurium induce a non-replicating persister-phenotype immediately after internalization by macrophages (140). These persisters survive antibiotic treatment for 24 hours whereas genetically identical non-persisters are eradicated. In a mouse-model it was found that persisters can trigger a full-blown infection following the completion of an appropriate course of antibiotic therapy (164). Because of the strong correlation between OM permeability and bacterial persisters, we tested *Salmonella* mutants with increased OM permeability (due to being unable to close OmpC) for their ability to form macrophage-induced persisters. We focused on permeability through OmpC since the pore in OmpA is too narrow for many antibiotics and thus unlikely to play a role in persistence. We first established that internalization of bacteria by bone-marrow derived macrophages (BMDM) for 30 minutes induced formation of macrophage-induced persisters. To do this, we infected BMDM for 30 minutes and recovered internalized bacteria. After recovery, the bacteria were washed with PBS and inoculated in LB containing 100 μg/ml of the antibiotic cefotaxime and incubated overnight with shaking. In a separate experiment, bacteria were incubated in LB containing 100 μg/ml cefotaxime without prior internalization of macrophages. After 24 hours of incubation, bacteria that had survived the antibiotic incubation were plated and counted (Fig. 3-7A). The surviving bacteria were called persisters. Our results confirm previous results (140).

After validation of the concept of macrophage-induced persister formation, we tested the ability to form persisters with the *hslT* mutant that has increased OM permeability. WT *Salmonella*, the less-permeable *ompC* mutant, and the less permeable *ompChslT* double mutant were used as controls. Interestingly, we found that increased OM permeability led to a dramatic reduction in

persister formation. These results indicate that the rapid reduction of OM permeability is important for the formation of macrophage-induced persisters that have been linked to recurrent bacterial infections.

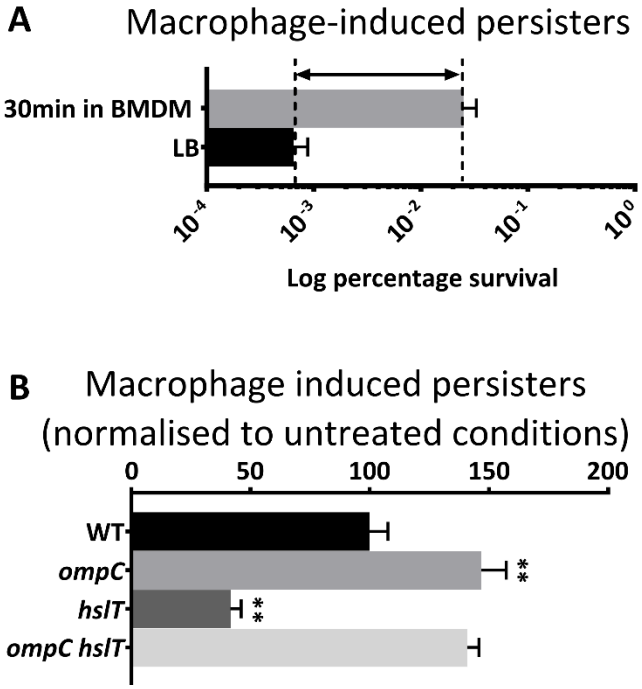

Figure 3-7: Rapid alteration of OM permeability is required for persister formation.

(A) Persistent bacteria were analyzed by CFU counts after treatment with 100 µg cefotaxime for 24 hours in LB. The grey bar represents bacteria that prior to treatment did internalize BMDM for 30 minutes. This interaction with BMDM significantly increased their ability to form persisters. The arrow indicates the macrophage-induced persisters. (B) The amount of macrophage-induced persisters was analyzed for the *ompC*, *hslT* and *ompChslT* mutants after 24 hours in LB media supplemented with 100 µg cefotaxime. The *ompC* mutant that has lower OM permeability is more likely to form persisters whereas the *hslT* mutant has significantly decreased ability in persister formation. The *ompChslT* double mutant restores persister formation to *ompC* mutant levels. Error bars represent the standard deviation and significance was obtained by a student's t-test (**p <0.01).

3.4 Discussion

Until recently the lack of adequate analytic tools has prevented the measurement of real-time influx of substances across the OM which limited our ability to study the dynamic nature of the bacterial outer membrane. Bacteria are known for their ability to rapidly adapt to environmental changes and the results of these studies outline a new mechanism for responding to oxidative stress. In

Chapter 3 we used the method that was developed for measurements in Chapter 2, to follow the real-time influx of H_2O_2 into *Salmonella*. Studying purified OMPs *in vitro* has generated a wealth of knowledge about the characteristics of individual OMPs, however; these techniques do not provide insight into the interaction between OMPs and periplasmic binding partners in living bacteria. Using our approach we were able to study changes in the OM permeability thereby exploring new stress mechanisms that allow Gram-negative bacteria to survive encounters with ROS.

Interestingly, not all OMPs were involved in the transport of H_2O_2. This is partly due to differential expression of OMPs under the conditions that were used in the analysis. We specifically selected these conditions since they mimic the intracellular environment in which ROS are encountered during the oxidative burst. However, presumably OmpF and OmpD bind unidentified "plug" proteins that close their respective pores. In previous studies OmpD has been found to bind YdeI which could function as the "plug" protein for the OmpD pore (165). Additional studies are required to determine the mechanisms that regulates OmpF and OmpD closing/opening.

Of note, we found that post-translational modification (PTM) of cysteines is the underlying mechanism for closing and opening of OmpC and OmpA. Especially in eukaryotic cells, PTMs regulate a plethora of processes. In bacteria the number of PTMs is more limited and particularly in the periplasm where no ATP is present, very few protein undergo PTM. It is surprising that such sophisticated regulatory processes can occur within the physical bounds of the bacterial periplasm to modulate OM permeability. There will presumably be other processes in the bacterial periplasm that are regulated by redox-sensitive thiol oxidation and/or disulfide bond formation.

Conventionally, it is thought that bacterial pathogens are only negatively affected by host antimicrobial systems such as the oxidative burst. However, more recent findings illustrate that

bacterial pathogens have acquired mechanisms by which they can benefit from ROS and RNS (91, 101). The results presented in this study, indicate that ROS and RNS trigger mechanisms to close and open pores in the OM which eventually enhanced bacterial persistence. Using our understanding of these mechanisms to combat multi-drug resistance, and persister formation in recurrent infections is an exciting new approach to develop new antimicrobial therapies. Our results show great promise for the concept of new pharmaceuticals that "force" pores to stay open during antibiotic treatment in order to eliminate persistent/recurrent infections.

Taken together these results expose a novel mechanism by which Gram-negative bacteria alter OM permeability to regulate the influx of oxidizing substances. It is intriguing that rapid alterations in membrane permeability can have dramatic consequences but have not been studied in living systems. Many additional hydrophilic toxic molecules are transported through pores in the OM and it is fascinating to find that bacteria have evolved mechanisms to "sense" these molecules in order to regulate OM permeability depending on their environment.

3.5 Material and methods

3.5.1 Bacterial strains

roGFP2 was cloned into the pfpv25 vector for constitutive expression of roGFP2 and transformed into *S.* Typhimurium. After transformation 50ug/ml carbenicillin was added to the growth media to maintain the plasmid. The HpxF(-) strain was kindly donated to us by Dr. Laurent Aussel (133). The genes for "plug" protein hslt, the C-terminal domain (AA198-AA350) of ompA and trxA were cloned into vector pet28a for inducible overexpression in BL21 (DE3). Point mutations ompAC327S and trxAC33S were made using the QuikChange® II Site-Directed Mutagenesis Kit (Stratagene). The WT trxA or trxAC33S were cloned into the pBAD33 vector under control of an

arabinose inducible promotor and transformed into the *trxA* deletion mutant or subsequent target strain.

3.5.2 Gene deletions

Clean deletions in the HpxF(-) background and in the WT background were made using allelic exchange as previously described (146). In short, 500 base pair flanking regions surrounding the gene of interest were amplified by PCR and cloned into the PRE112 vector. After verification by sequencing, this vector was transformed into the SM10λpir strain while growth media was supplemented with 50μg/ml DAP (Diaminopimelic acid) and conjugated into recipient *S.* Typhimurium HpxF(-) or subsequent target strains. Plasmid integration was driven by antibiotic selection, and subsequent plasmid excision was driven by sucrose counter selection and verified by antibiotic sensitivity. Gene deletion was verified by PCR and sequencing (166).

3.5.3 Protein purification

Proteins were expressed by IPTG-inducible expression as was previously described (166). In short, BL21(DE3) cultures carrying the plasmid were grown at 37C until OD ~0.8 and induced overnight with 0.1 mM IPTG while temperature was set at 16°C. After induction, cells were harvested and resuspended in lysis buffer (PBS, pH 7.4, 1 mM EDTA, 1 mM DTT, 10 μg/ml DNase, 10 μg/ml RNase, and complete protease inhibitor mixture (Roche Applied Science)). Cells were lysed by three times passage through a French pressure cell at 10,000 psi. The lysate was separated in a soluble and insoluble fraction by centrifugation at 30,000 × *g* for 30 min. The insoluble fraction was used for the purification of outer membrane proteins. Soluble proteins were purified through binding on a Ni-sepharose (GE healthcare). After washing the column with 5 times the column

volume with washing buffer (PBS7.4, 20mM imidazole), the protein was eluted in elution buffer (20mM Tris-HCl 7.4, 300mM imidazole).

3.5.4 Fluorescence measurement of fluctuations in the intra-bacterial redox potential

Real-time fluctuations of the intra-bacterial hydrogen peroxide concentration were analyzed in a Tecan fluorescent plate reader with excitation at 405 nm and 480 nm while emission was measured at 510 nm (89). Prior to analysis, bacteria were grown in Low Phosphate Medium pH 5.8 (which is used to mimic intracellular conditions) to OD ~1.0 Bacteria were washed and resuspended in saline at OD = 2. 100 uL of this bacterial culture was loaded in a black, clear bottom 96 well plate. Bacteria were challenged with 0µM, 20µM, 40µM, 60µM, 80µM, 100µM, 150µM, 200µM of hydrogen peroxide and the H_2O_2 influx was analyzed. Background signals from non-fluorescent bacteria were obtained in the same experiment. Additionally the signals for fully oxidized and fully reduced bacteria were obtained by adding 50 mM H_2O_2 and 10 mM DTT to the bacterial culture at the start of the experiment. The 405/480 ratio values were normalized to the 405/480 ratio values for maximum oxidized and reduced conditions. The increase in 405/480 ratio values from endogenous bacterial ROS formation that we obtained from the 0µM control experiment were subtracted from our measurements.

3.5.5 Calculation of H_2O_2 influx

To determine $\Delta\mathbf{C}$, which is given by:

$$\Delta\mathbf{C} = \mathbf{C_{out}} - \mathbf{C_{in}}$$

We obtained the intra-bacterial [H_2O_2] ($\mathbf{C_{in}}$) by using the correlation between R and the intra-bacterial [H_2O_2] that we obtained in Fig 3-2C. Additionally, by using $\mathbf{k_{cat}}$ (Fig 3-2B), we calculated the $\mathbf{C_{out}}$ by:

$$\mathbf{C_{out}} = \mathbf{C_{start}} - (\mathbf{k_{cat}} * \boldsymbol{dt})$$

For most of the analysis in this Chapter we chose to calculate the influx before the "switching point" at $\Delta\mathbf{C}$=45μM and after the "switching point" at $\Delta\mathbf{C}$=120μM. At these given moments in our data analysis we obtained the H_2O_2 influx by:

$$\mathbf{Influx} = \frac{\Delta \mathbf{C_{in}}}{\boldsymbol{dt}}$$

3.5.6 Bioinformatics analysis

The structures of OmpA (2JMM), OmpC (3UU2), OmpF (4KRA), OmpA-periplasmic domain (4ERH) were obtained from the protein database http://www.rcsb.org/pdb. Structural prediction of OmpD and HslT was done using the iTASSER webserver server at http://zhanglab.ccmb.med.umich.edu/I-TASSER/ (159). Predictions for protein-protein interactions were done using the pyDockWeb server at http://life.bsc.es/servlet/pydock/home/ using restrains on binding sites (160). The obtained structures were further analyzed and visualized using Pymol.

3.5.7 SILAC proteomics

A strain carrying deletions in *lysA* and *argH* was grown in LPM. In this growth media, casamino acids were replaced by addition of individual amino acids at the following concentrations: Ala, 2.8%; Asp, 6.3%; Cys, 0.3%; Glu, 21.1%; Gly, 2.2%; His, 2.7%; Ile, 5.6%; Leu, 8.4%; Met, 2.7%;

Phe, 4.6%; Pro, 9.9%; Ser, 5.6%; Thr, 4.2%; Trp, 1.1%; Tyr, 6.1%; Val, 5.0%; Arg, 3.6%; and Lys, 7.5%). In order to label bacterial proteins with heavy amino acids, the Lys and Arg residues were replaced by [4,4,5,5-D4]lysine and [U-13C6]arginine instead of natural abundance, isotopically labeled arginine and lysine.

Light and heavy labelled cultures were grown for 5 hours at 37°C. Only 5 ml of the heavy labelled culture was then subjected to a challenge with either 2 x 5 mM H_2O_2 (separated by a 10 minute interval) or a challenge with 5mg/ml of SpermineNONOate whereas 5 ml of the light labelled bacterial culture was left untouched. After 20 minutes the cultures were spun down, resuspended in Guanidine/MOPS buffer (6M Guanidine HCL pH7.5, 150mM NaCl, 5mM EDTA, 25mM MOPS) and lysed by sonication. Alkylation of free thiol groups was done by adding 40mM N-ethyl maleimide for two hours at room temperature. After this, 4 volumes of ice cold methanol were added and the protein fraction was incubated ON at -20C. The next morning protein fractions were spun down for 45min at 15 000 x g at 4°C, and the protein pellet was washed twice with ice cold methanol. The protein pellets were dissolved in 100 µL of the Guanidine/MOPS buffer and protein fractions were pooled. 10mM DTT was added at 37 °C for 30 min prior to addition of 0.4mM HPDP-biotin (Proteochem). Samples were mixed and incubate for 2 hours at room temperature. After labelling with HPDP-biotin, LysC was added and protein fractions were incubated for 3 hours at 37°C followed by 4x dilution with 50mM ammonium bicarbonate and then add trypsin to incubate overnight. After tryptic digest is complete we enriched for HPDP-biotin peptides by using Neutravidin beads (Fisher Scientific) previously equilibrated with 20 mM ABC and left on rotation for 1 h at room temperature to allow binding of the biotinylated peptides to NeutrAvidin. After centrifugation at 200 × *g* for 10 s, the supernatant was discarded and the beads were washed 4 times with 20 mM ammonium bicarbonate, 0.5 M NaCl. Two additional

washings with 5 mM ammonium bicarbonate /20% acetonitrile were done to remove nonspecifically bound peptides. Peptides were eluted by incubating the beads for 10 min with 2 volumes of 100 mM mercaptoethanol. The samples were then dried in a speedvac and resuspended in 20 uL of 5% formic acid and cleaned using C18 Zip Tips prior to mass spectrometric analysis.

3.5.8 NanoLC-MS/MS analysis

NanoLC-MS/MS analysis was conducted using an LTQ-Orbitrap Velos mass spectrometer (Thermo Fisher Scientific) equipped with an 1100 series nanoflow HPLC system (Agilent) as described (167). An in-house analytical column (200 mm length x 75 µm inner diameter) was prepared with ReproSil-Pur C18-AQ materials (3 µm, Dr. Maisch). Prior to analytical separation peptides were loaded for 10 min onto a fused 5 silica trap column (20 mm length x 100 µm inner diameter), which was packed with 5 µm Aqua C18 beads (Phenomenex). Analytical separation was performed at a flow rate of 5 µL/min. A 90 min gradient from 100% buffer A (0.5% acetic acid) to 40% buffer B (0.5% acetic acid, 80% acetonitrile) was performed at a flow rate of 250 nL/min to elute the peptides. Following settings for MS analysis were chosen: one full scan (resolution 60,000; m/z 300–1,500) followed by top 10 MS/MS scans using CID in the linear ion trap (min. signal required, 200; isolation width, 3; normalized collision energy, 35; activation Q, 0.25; activation time, 10 ms) using dynamic exclusion (repeat count, 1; repeat duration, 30 s; exclusion list size, 500; exclusion duration, 60 s).

3.5.9 Data analysis

MaxQuant (v1.3.0.5) (168) was used to analyze all raw data. For the search following parameters were included: two missed cleavage sites, cysteine carbamidomethyl fixed modification, as well

as variable modifications, such as methionine oxidation and N-terminal protein acetylation. MS/MS tolerance was set to 0.5 Da. Peptide mass tolerance was 6 ppm. Andromeda (169) was used to search against the UniProt/Swiss-Prot *Salmonella* Typhimurium database (downloaded on July 2011) including common serum contaminants and enzyme sequences. 1% was set as false discovery rate (FDR) at peptide and at protein level.

3.5.10 Persister assays

Quantification of persisters was done as previously described (140). In short; bacteria were grown overnight in LB medium and were inoculated in fresh LB medium (1/400 dilution) containing cefotaxime (100 μg/ml). Prior to treatment a sample was taken and dilutions were plated to determine the inoculum size. Bacteria were incubated for 24 hours at 37°C while shaking before being washed 2 times in PBS and plated for CFU counting. Macrophage-induced persisters were first incubated with BMDM for 30 minutes. After 30 minutes cells were washed with PBS 3 times and cells were lysed with lysis buffer (1% TritonX100, 0.1% SDS in PBS). Inoculum size was determined by plating. Inoculum was incubated in fresh LB medium containing cefotaxime (100 μg/ml) for 24 hours t 37°C while shaking before being washed 2 times in PBS and plated for CFU counting. The total number of macrophage-induced persisters was normalized to the inoculum size.

3.5.11 Culturing bone marrow derived macrophages

Bone marrow was collected from the tibias and femurs of 6-8 week old wildtype C57BL/6J, iNOS-/- (B6.129P2-Nos2tm1Lau/J) and gp91phox-/- (B6.129S6-Cybbtm1Din/J) male mice (all purchased from Jackson Laboratory). In each well of a 6-well plate, $1x10^6$ cells were seeded in

growth media (RPMI 1640 containing L-Glutamine; Life Technologies, supplemented with 10% heat-inactivated FBS; Life Technologies, 100 U/ml Penicillin and 100 μg/ml Streptomycin; Life Technologies and 20 ng/ml M-CSF; Peprotech). Cells were incubated at 37°C with 5% CO2 for 7 days. On days 4 and 6, media was removed and replaced with 2 ml fresh medium. On day 7, culture supernatant containing non-adherent cells were removed prior to performing assays. The purity of adherent cells was confirmed by flow cytometry for all genotypes on day 7 of culture, and >97% of cells were CD45+CD11b+F4/80+.

Chapter 4: Oxidation of a cysteine residue in *Salmonella* effector SteB regulates tubulin-mediated bacterial translocation to the juxtanuclear position.

4.1 Summary

The Gram-negative bacterium, *Salmonella enterica* Typhimurium, uses two distinct type III secretion systems to deliver greater than 35 effectors directly into host cells to facilitate bacterial survival and replication. Following translocation into the host cell, many *Salmonella* effectors undergo post translational modifications (PTMs). These PTMs allow *Salmonella* to respond to changes in the host environment and direct effectors to specific cellular compartments. Although more than 35 *Salmonella* effectors have been identified, the functions of many effectors, and how PTMs may play a role in regulating their activities, remains unclear. In this manuscript we describe a mass spectrometry screen to identify *Salmonella* effectors that undergo PTMs in response to reactive oxygen species (ROS) encountered during infection. For the first time, we showed redox-sensitive thiol oxidation of a bacterial effector during oxidative stress and found that SteB undergoes thiol oxidation at cysteine 103 (CYS103). In addition, we found that SteB bound to tubulin and that deletion of *steB* resulted in deficient microtubule-dependent trafficking of the *Salmonella* containing vacuole (SCV) to the juxtanuclear position. Proper positioning was dependent on CYS103 thiol oxidation since a *steB*^{C103S} point mutant displayed improper SCV positioning. Based on these results we concluded that redox-sensitive thiol oxidation of CYS103 regulates SteB-mediated trafficking of the SCV along microtubules.

4.2 Introduction

One of the most prevalent agents of infectious diarrhea is the Gram-negative bacterium, *Salmonella enterica* Typhimurium. This pathogen colonizes the human gut by orchestrating the activities of greater than 35 effectors that are secreted by two type III secretion systems (T3SS). T3SS-1 and T3SS-2 are located on two *Salmonella* Pathogenicity Islands (SPI-1 and SPI-2, respectively) and each secretes a distinct set of effector proteins (170). T3SS-1 associated effectors are secreted first and are involved in internalization of *Salmonella* by non-phagocytic cells, while T3SS-2-secreted effectors are generally associated with intracellular survival and replication (170). Inside the host cell, *Salmonella* bacteria survive inside a *Salmonella* containing vacuole (SCV) from where effectors are secreted (171). The SCV is strongly associated with the microtubule network of the cell and tubulin-mediated transport allows trafficking of the SCV to the juxtanuclear position in close proximity to the Golgi apparatus. It is thought that *Salmonella* favors this position due to convenient access to nutrients (171). The positioning of the SCV at the juxtanuclear position is, at least in part, dependent on the SPI-2 effectors SseF and SseG, since *sseF*, *sseG* and *sseFsseG* mutants are unable to maintain this position (66, 172). How the SCV travels along microtubules to this position is currently unknown, and thus far, no *Salmonella* effector has been described that directly interacts with tubulin.

Salmonella effectors not only manipulate SCV trafficking along microtubules but also impact the host endocytic (11) and secretory pathways (173). Microtubules form an extensive network that facilitate transport of nutrient-carrying vesicles and antimicrobials throughout the cell. It is therefore not surprising that several bacterial pathogens hijack tubulin-mediated cellular trafficking to gain access to nutrients and evade immune responses (174).

After translocation into the cytosol, effectors are often modified by host proteins or by changes in the local environment. These post translational modifications (PTMs) alter effector localization (175-177) and stability (95) and often have profound effects on the outcome of infection. Changes in the local environment of effectors strongly depend on which cellular compartment is targeted and what cell type is infected. In particular, infection of immune cells can generate an oxidative burst where secreted effectors most likely encounter reactive oxygen species (ROS) and reactive nitrogen species (RNS). Since the local environment can have a profound impact on effector functioning, we were interested in potential interactions between ROS/RNS and effectors. At a transcriptional level, *Salmonella* has already been found to alter its virulence program through RNS-mediated modifications of regulator SsrB (91). In this case, a cysteine residue in SsrB undergoes S-Nitrosylation after which transcription of SPI-2 effectors is switched off (91). We hypothesized that effectors could also be directly affected by ROS/RNS and therefore we performed a mass spectrometry screen with 35 *Salmonella* effectors to identify redox-sensitive PTM after interaction with hydrogen peroxide. Since cysteine residues are especially likely to interact with ROS/RNS we focused on cysteine thiol oxidation. In this screen we found that effector SteB underwent thiol oxidation on a specific cysteine residue that impacts its activity. In addition to this modification, we found that SteB interacted with tubulin and that SteB-mediated trafficking along microtubules was regulated by thiol oxidation. This is the first report of redox-sensitive thiol oxidation of bacterial effectors that alters effector-mediated processes during infection.

4.3 Results

4.3.1 Identification of *Salmonella* effectors that undergo thiol modifications

Redox-sensitive thiol modifications are known to affect protein function and have been particularly well-characterized for some bacterial transcription factors (91, 178, 179). These modifications involve direct interaction between cysteine residues and ROS or RNS after which a disulfide bond is formed or cysteines become S-Nitrosylated or glutathionylated (180). In order to identify potential redox-sensitive thiol modifications in *Salmonella* effectors, we cloned, expressed, purified and pooled 35 *Salmonella* effectors at a concentration of 10 µg per effector. A schematic representation of this approach is shown in Fig. 4-1A. The total effector pool was split into two separate tubes, one of which was used to analyze reducing conditions and the other to analyze oxidizing conditions. 1 mM dithiothreitol (DTT) was added to the "reduced" tube and 1 mM hydrogen peroxide was added to the "oxidized" tube. The peptides were enriched for redox-sensitive thiols and the only modified *Salmonella* effector identified by mass spectrometry was SteB. SteB contains five cysteine residues in total and, in our analysis, only CYS103 was found to undergo thiol oxidation. To confirm thiol oxidation of CYS103 and to test if other cysteines were involved in disulfide bond formation after thiol oxidation, individual point mutations were made in which each cysteine was replaced by a serine residue. The mutant proteins $SteB^{C6S}$, $SteB^{C49S}$, $SteB^{C56S}$, $SteB^{C103S}$ and $SteB^{C126S}$ were expressed and purified. Similar to the initial mass spectrometry approach, the mutant proteins were divided into two tubes. For each mutant, one tube was oxidized while the other was reduced by addition of hydrogen peroxide or DTT, respectively. After alkylation and reduction, oxidized thiol groups were labelled with 5-iodoacetamidefluorescein (5-IAF). The labelled proteins were separated by SDS-PAGE and fluorescence of oxidized proteins was compared to fluorescence of reduced proteins. After

determination of fluorescence intensity, Western blot analysis and densitometry was done to quantify total protein concentration. Fluorescence intensity was normalized to the protein concentration and the fold increase in fluorescence intensity between oxidized and reduced protein was calculated (Fig. 4-1B). These results confirmed that only CYS103 undergoes a redox-sensitive thiol modification. To test dimerization potential, all purified mutant proteins were analyzed by Western blot under reducing or non-reducing conditions (Fig. 4-1C). These results suggest that the $SteB^{C103S}$ mutant is less likely to exist in monomeric conformation than any of the other mutant proteins.

4.3.2 Identification of SteB host binding partners

SteB has been shown to be secreted through T3SS-1 and consists of 133 amino acids (181). Thus far, no known phenotype has been associated with *steB* deletion. To gain a better idea of the role of SteB during infection, we performed a mass spectrometry screen using Stable Isotope Labelling by Amino Acids (SILAC) to identify potential SteB host binding partners. Previously in our lab, several host binding partners for *Salmonella* effectors were identified by using GST-tagged effectors to pull down binding partners from cell lysates (166). For this screen we collected lysates from RAW264.7 cells, labelled with "light", "medium" or "heavy" arginine and lysine residues, and incubated with immobilized GST, GST-tagged SteB and GST-tagged $SteB^{C103S}$. Host proteins that precipitated with SteB or $SteB^{C103S}$ were identified by mass spectrometry. A schematic representation of this approach is shown in Fig. 4-2A. The assay was repeated 3x and in each experiment, peptides corresponding to tubulin were specifically precipitated with SteB and $SteB^{C103S}$.

Table 4-1. Primers used in Chapter 4.

Plasmids		
pET28a - Salmonella effectors		
AvrA	TCGTCGGATCCATGATATTTTCGGTGCAGGAGC	ACGACGAATTCTTACGGTTTAAGTAAAGACTTATATTC
GogB	TCGTCGGATCCATGAAAATAGGATTCCAACCAGCC	ACGACGAATTCTCAACGATTTCTATTTTTAGGCTTA
PibB	TCGTCGGATCCATGCCAATAACTAACGCGTCCC	ACGACGAATTCCTAAAATATCGGATGGGGGAAAAG
PibB2	TCGTCGGATCCATGGAGCGTTCACTCGATAGTC	ACGACGAATTCCTAAATATTTTCACTATAAAATTCGTTA
SifA	GTCGAATTCATGCCGATTACTATAGGGAATGG	GACCTCGAGTTATAAAAAACAACATAAACAGCCGC
SifB	TCGTCGGATCCATGCCAATTACTATCGGGAGAGG	ACGACGAATTCTCAACTCTGGTGATGAGCCTC
SipA	TCGTCGGATCCATGGTTACAAGTGTAAGGACTCA	ACGACGAATTCTTAACGCTGCATGTGCAAGCC
SipB	TCGTCGGATCCATGGTAAATGACGCAAGTAGCA	ACGACCTCGAGTTATGCGCGACTCTGGCGC
SipC	TCGTCGGATCCATGTTAATTAGTAATGTGGGAATAAATC	ACGACGAATTCTTAAGCGCGAATATTGCCTGCG
SipD	TCGTCGAATTCATGCTTAATATTCAAAATTATTCCGC	ACGACCTCGAGTTATCCTTGCAGGAAGCTTTTG
SlrP	TCGTCGGATCCATGTTTAATATTACTAATATACAATCTACG	ACGACGAATTCCTATCGCCAGTAGGCGCTC
SopA	TCGTCGGATCCATGAAGATATCATCAGGCGCAAT	ACGACGAATTCCTACGCCCAGGCCAGTGG
SopB	TCGTCGGATCCATGCAAATACAGAGCTTCTATCAC	ACGACGAATTCTCAAGATGTGATTAATGAAGAAATGC
SopD	TCGTCGGATCCATGCCAGTCACTTTAAGCTTCG	ACGACGAATTCTTATGTCAGTAATATATTACGACTGC
SopD2	TCGTCGGATCCATGCCAGTTACGTTAAGTTTTGG	ACGACGAATTCTTATATAAGCATATTGCGACAACTC
SopE	TCGTCGGATCCGTGACAAAAATAACTTTATCTCCCC	ACGACGAATTCTCAGGGAGTGTTTTGTATATATTTA
SopE2	TCGTCGGATCCGTGACTAACATAACACTATCCACC	ACGACGAATTCTCAGGAGGCATTCTGAAGATACT
SptP	TCGTCGGATCCATGCTAAAGTATGAGGAGAGAAAAT	ACGACGAATTCTCAGCTTGCCGTCGTCATAAG
SpvB	GTCGAATTCATGTTGATACTAAATGGTTTTTCATCTGC	GACCTCGAGCTATGAGTTGAGTACCCTCATGTTTA
SpvC	TCGTCGGATCCATGCCCATAAATAGGCCTAATC	ACGACGAATTCTTACTCTGTCATCAAACGATAAAAC
SsaB	TCGTCGGATCCATGTCTGAGGAGGGATTCATG	ACGACGAATTCTTATACCCCACCCGAATAAAGTTT
SseC	TCGTCGGATCCATGAATCGAATTCACAGTAATAGCG	ACGACCTCGAGTTAAGCGCGATAGCCAGCTATTC
SseD	TCGTCGGATCCATGGAAGCGAGTAACGTAGCAC	ACGACGAATTCTTACCTCGTTAATGCCCGGAG
SseF	GTCGGATCCATGAAAATTCATATTCCGTCAGCGG	GACGAATTCTCATGGTTCTCCCCGAGATGTATG
SseG	GTCGGATCCATGAAACCTGTTAGCCCAAATGC	GACGAATTCTTACTCCGGCGCACGTTGTTC
SseI	TCGTCGGATCCATGCCCTTTCATATTGGAAGCG	ACGACGAATTCTTACATTTTACCTATTAAGGAATA
SseJ	GTCGGATCCATGCCATTGAGTGTTGGACAGGG	GACGAATTCTTATTCAGTGGAATAATGATGAGCTATAAAAC
SseK1	TCGTCGGATCCATGATCCCACCATTAAATAGATATG	ACGACGAATTCCTACTGCACATGCCTCGCC
SseK2	TCGTCGGATCCATGGCACGTTTTAATGCCGCT	ACGACGAATTCTTACCTCCAAGAACTGGCAGT
SseL	GTCGGATCCGTGAGCGATGAGGCGCTTACATTG	GACGAATTCTTACTGGAGACTGTATTCATATATTTGCC
SspH1	TCGTCGGATCCATGTTTAATATCCGCAATACACAAC	ACGACCTCGAGTCAGTTAAGACGCCACCGG
SspH2	TCGTCGGATCCATGCCCTTTCATATTGGAAGCG	ACGACGAATTCTCAGTTACGACGCCACTGAAC
SteA	TCGTCGGATCCATGCCATATACATCAGTTTCTACC	ACGACGAATTCCTAACAAAACTGGCTAAACATAAACGC
SteB	TCGTCGGATCCATGCCTATTTCGATTTGTAAACATG	ACGACGAATTCTTATCTGACATTACCATTTGAGTG
SteC	TCGTCGGATCCATGCCGTTTACATTTCAGATCGG	ACGACGAATTCCTATTTTTTTAATTCATCCTTTAATACC

Plasmids		
pET28a - SteB mutants		
SteBC6S	TCGTCGGATCCATGCCTATTTCGATTAGTAAACATGGTG CTCCTTTTGTTGTTCAACATG	ACGACGAATTCTTATCTGACATTACCATTTGAGTG
SteBC49S	CTCTCATGAGGAAATAAAATTTATAAGTAGCTATAGTG CAAATGGAGCCTGTTTTTCC	GGAAAAACAGGCTCCATTTGCACTATAGCTACT TATAAATTTTATTTCCTCATGAGAG
SteBC56S	ATTTATAAGTTGCTATAGTGCAAATGGAGCCAGTTTTT CCAATGCACAGATGCTAGCCAATGCC	GGCATTGGCTAGCATCTGTGCATTGGAAAAACTG GCTCCATTTGCACTATAGCAACTTATAAAT
SteBC103S	CAGCATAAGCTTGCGGCCAATATTTCTTATGTAGGTA ATCGGCTTCTGAGC	GCTCAGAAGCCGATTACCTACATAAGAAATATTG GCCGCAAGCTTATGCTG
SteBC126S	TCGTCGGATCCATGCCTATTTCGATTTGTAAACATG	ACGAC GAATTC TTATCTGACATTACCATTTGAGTG ACTGGTTAGCAGATGTTTCAGGCCAAACCCAAG
pCMV2B - SteB mutants		
SteB	TCGTCGGATCCATGCCTATTTCGATTTGTAAACATG	ACGACGAATTCTTATCTGACATTACCATTTGAGTG
SteBC6S	TCGTC GGATCC ATGCCTATTTCGATTAGTAAACATG GTGCTCCTTTTGTTGTTCAACATG	ACGACGAATTCTTATCTGACATTACCATTTGAGTG
SteBC49S	CTCTCATGAGGAAATAAAATTTATAAGTAGCTATAG TGCAAATGGAGCCTGTTTTTCC	GGAAAAACAGGCTCCATTTGCACTATAGCTACTT ATAAATTTTATTTCCTCATGAGAG
SteBC56S	ATTTATAAGTTGCTATAGTGCAAATGGAGCCAGTTT TTCCAATGCACAGATGCTAGCCAATGCC	GGCATTGGCTAGCATCTGTGCATTGGAAAAACTGG CTCCATTTGCACTATAGCAACTTATAAAT
SteBC103S	CAGCATAAGCTTGCGGCCAATATTTCTTATGTAGGT AATCGGCTTCTGAGC	GCTCAGAAGCCGATTACCTACATAAGAAATATTGG CCGCAAGCTTATGCTG
SteBC126S	TCGTCGGATCCATGCCTATTTCGATTTGTAAACATG	ACGAC GAATTC TTATCTGACATTACCATTTGAGT GACTGGTTAGCAGATGTTTCAGGCCAAACCCAAG
pWSK129		
SteB	GGAAAGGGTAAAAGCATCGGTATG	TCTGACATTACCATTTGAGTG
SteBC103S	CAGCATAAGCTTGCGGCCAATATTTCTTATGTAG GTAATCGGCTTCTGAGC	GCTCAGAAGCCGATTACCTACATAAGAAATATTGG CCGCAAGCTTATGCTG
pGEX6P1		
SteB	TCGTCGGATCCATGCCTATTTCGATTTGTAAACATG	ACGACGAATTCTTATCTGACATTACCATTTGAGTG
SteBC103S	CAGCATAAGCTTGCGGCCAATATTTCTTATGTAGG TAATCGGCTTCTGAGC	GCTCAGAAGCCGATTACCTACATAAGAAATATTG GCCGCAAGCTTATGCTG
pRE112		
Δ*steB*	ATGAT GGTACC TACGTTTTTTATCTTCAGGTGAATGCGG	GGAAGGACATGGCATGACACTTTACATGGATTA TTACCTGAGATTGATTTCAAAC
	GTTTGAAATCAATCTCAGGTAATAATCCATGTAAAGTGT CATGCCATGTCCTTCC	ATGAT GAGCTC CTTTTTACGTCTTTTTTTGGCAGCGG

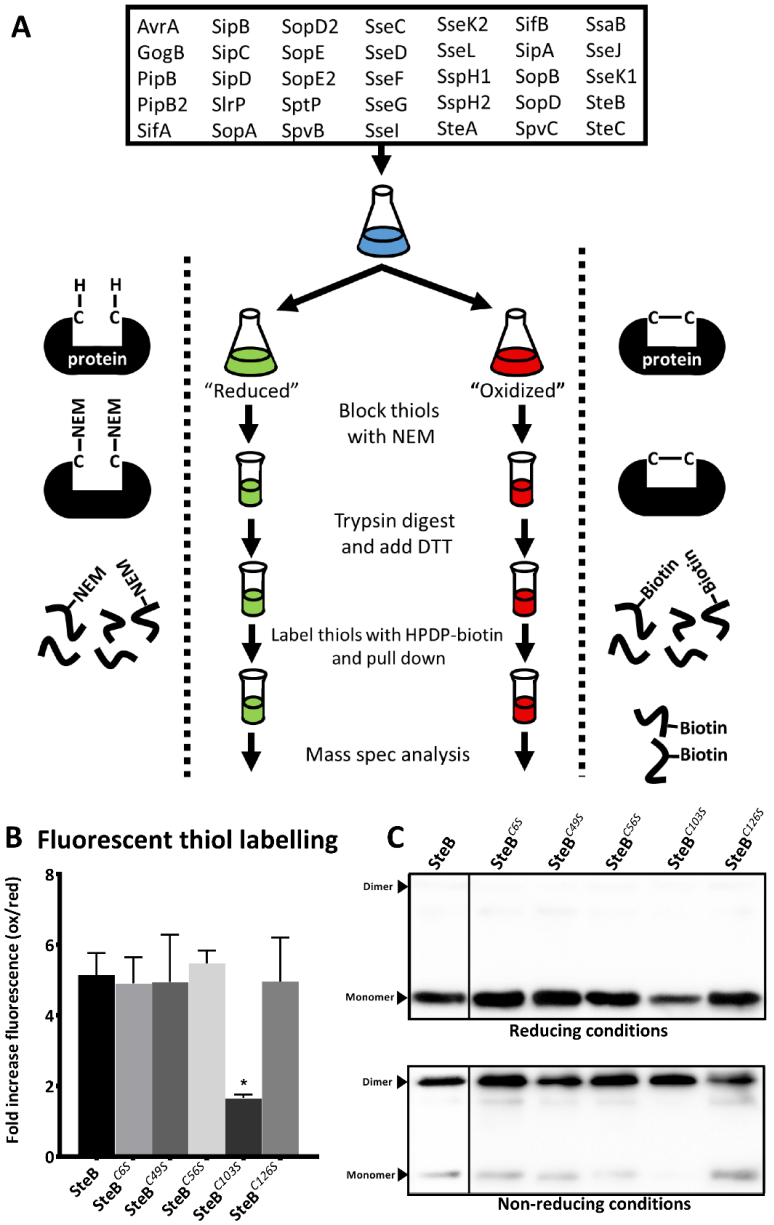

Figure 4-1: Identification and confirmation of thiol oxidation in Salmonella effector SteB.

(A) Experimental set up for the identification of redox-sensitive thiols in 35 *Salmonella* effectors. 35 effectors were cloned in pET28a carrying a HIS tag, expressed in BL21(DE3), purified and pooled together at a concentration of 10 µg per effector. The total effector pool of HIS-tagged effectors was split over two separate tubes, one of which was used to analyze reducing conditions and the other to analyze oxidizing conditions. 1 mM dithiothreitol (DTT) was added to the "reduced" tube and 1 mM hydrogen peroxide was added to the "oxidized tube". The peptides were enriched for redox-sensitive thiols and the only modified *Salmonella* effector identified by mass spectrometry was SteB. (B) The fold increase of normalized fluorescence intensity for each cysteine mutation in SteB. (C) Dimerization of SteB and SteB cysteine mutants under reducing and non-reducing conditions analyzed by Western blot. Error bars represent the standard deviation and significance was analyzed by a student's t-test (* $p < 0.05$).

The direct interaction between SteB and tubulin was confirmed by co-immunoprecipitation in which HIS-tagged SteB or SteB^{C103S} was used to pull down tubulin (Fig. 4-2B). This interaction was independent of CYS103 thiol modification as indicated by equal binding of tubulin to SteB or SteB^{C103S} and independent of the addition of DTT or hydrogen peroxide. A structural prediction of SteB was made using a computational algorithm (Fig. 4-2C) (159). Subsequently, the binding pocket of SteB and tubulin was predicted by the pyDockWeb algorithm (160). Similar binding pockets were predicted for monomeric tubulin and microtubules. This pocket appeared to overlap with the binding of stathmin, a tubulin destabilizing protein.

4.3.3 SteB does not affect tubulin polymerization or destabilization

Only two other bacterial effectors have been described to bind tubulin directly and both effectors inhibit formation of microtubule networks (182, 183). To investigate whether SteB was involved in tubulin polymerization or microtubule destabilization, the microtubule networks of HeLa cells infected with *Salmonella* were analyzed by immunofluorescence of a β-tubulin antibody. Microtubules were visualized 22 hours post infection with wild type (WT) *Salmonella*, Δ*steB*, Δ*steB* psteB or Δ*steB* psteB^{C103S} bacteria (Fig 4-3A). No visual differences to the microtubule networks were observed and all Δ*steB* mutants were associated with microtubules similar to WT bacteria. To explore whether SteB enables the formation of tubulin dimers, α/β tubulin was incubated for three hours with or without addition of HIS-SteB or HIS-SteB^{C103S}. The assay was done under reducing, native or oxidizing conditions by addition of DTT, water or hydrogen peroxide, respectively and analyzed by Western blot (Fig. 4-3B). No tubulin dimers were observed. Lastly, we investigated whether tubulin polymerization dynamics were affected in the presence of SteB (Fig. 4-3C). No inhibition or induction of tubulin polymerization was observed. These results

suggest that the interaction between SteB and tubulin does not affect tubulin polymerization or destabilization of microtubules *in vitro* or structure of the microtubule network *in vivo*.

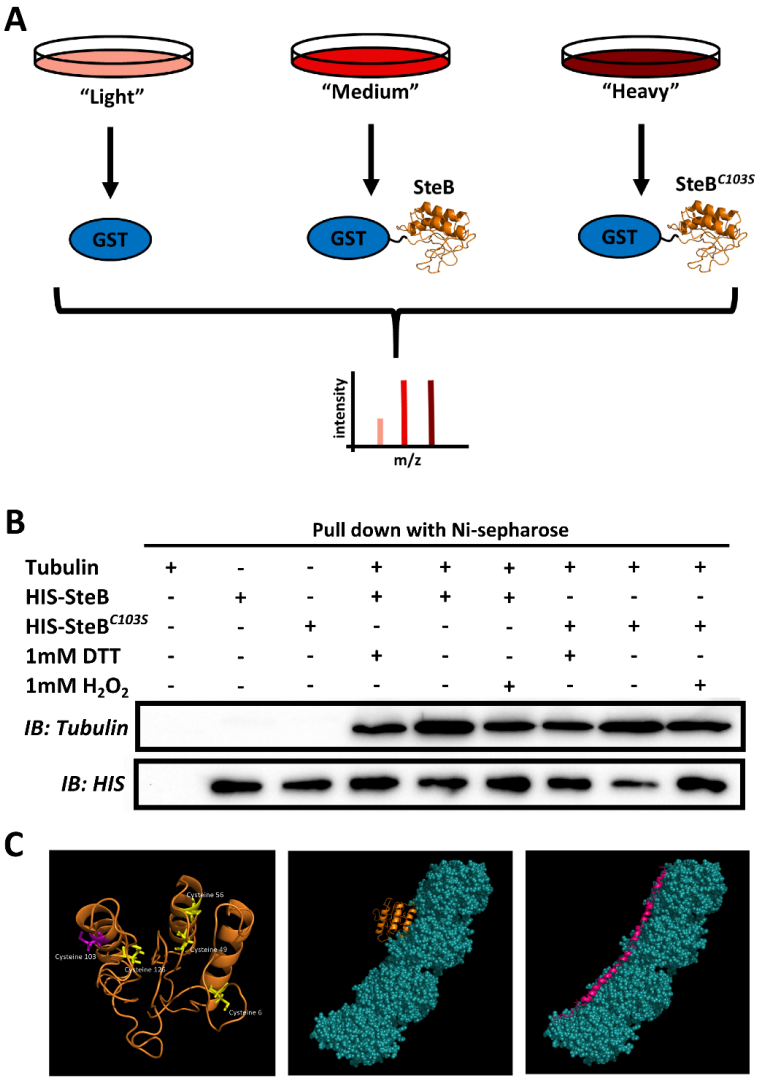

Figure 4-2: *Salmonella* effector SteB binds tubulin.

(A) Experimental set up for the identification of SteB host binding partners in a SILAC mass spectrometry approach. Lysates from RAW264.7 cells, labelled with "light", "medium" or "heavy" arginine and lysine residues were collected and incubated with GST, GST-tagged SteB and GST-tagged SteB^{C103S} immobilized on glutathione agarose. After incubation, the bait proteins and binding host proteins were eluted by 8M Urea. Host proteins that precipitated with GST, SteB or SteB^{C103S} were identified by mass spectrometry. (B) Confirmation of direct SteB-tubulin binding by pull down with HIS-tagged SteB or HIS-tagged SteB^{C103S}. Binding is independent of reducing/oxidizing conditions and thiol oxidation. (C) The SteB protein structure (orange) as predicted by the iTasser webserver http://zhanglab.ccmb.med.umich.edu/I-TASSER/ (159) (left). Cysteine residues are shown in yellow and the CYS103 residue is shown in pink. Prediction of binding pocket of SteB on microtubules (middle) is similar to the known binding pocket of stathmin (right). The SteB-tubulin interaction was predicted by the pyDockWeb server at http://life.bsc.es/servlet/pydock/home/ (160).

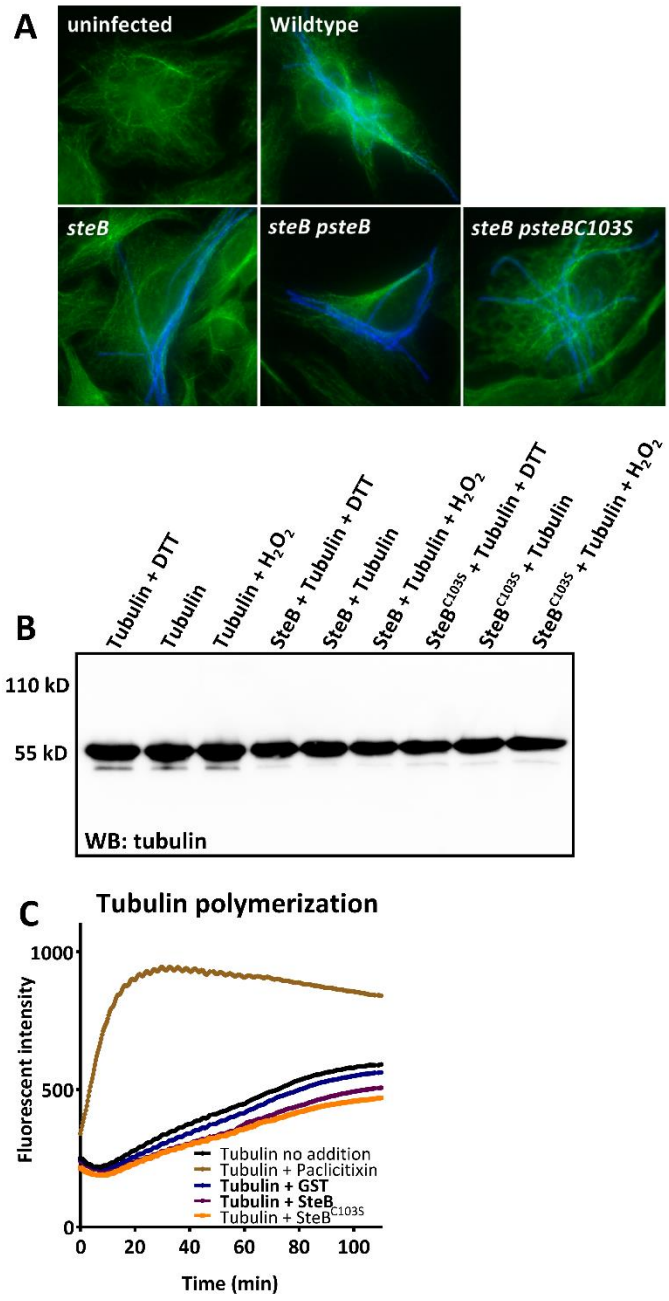

Figure 4-3: Effects of SteB on tubulin polymerization.

(A) Immunofluorescence analysis of *Salmonella*-infected HeLa cells. HeLa cells were infected with WT, Δ*steB*, Δ*steB* psteB or Δ*steB* psteB^{C103S} and fixed at 22 hours post infection. *Salmonella* is shown in blue and tubulin is shown in green. No differences to the microtubule network were observed. (B) Formation of potential tubulin dimers after incubation of α/β tubulin with HIS-SteB or HIS-SteB^{C103S} for 3 hours under reducing, native or oxidizing conditions by addition of DTT, water or hydrogen peroxide, respectively. The assay did not show dimerization of tubulin (C) *In vitro* tubulin polymerization assay under conditions that promote microtubule formation. The assay was performed with the addition of GST, GST-SteB or GST-SteB^{C103S}. Addition of paclicitixin was used as a positive control to show enhanced polymerization. WB: western blot; DTT: dithiothreitol; H_2O_2: hydrogen peroxide.

4.3.4 SteB is cytoplasmic and does not affect the mitochondrial VDAC pore.

Inside the host cell, mitochondria provide the most reduced cellular compartment in which redox fluctuations play a significant role (184). We explored the possibility that SteB may be activated in close proximity to mitochondria. Tubulin and mitochondria have an intimate relationship and recently it was found that tubulin dimers regulate mitochondrial respiration through binding with the voltage-dependent anion channel (VDAC) (156). Binding of tubulin dimers effectively blocked the VDAC pore and lowered ADP/ATP permeability over the mitochondrial outer membrane thereby lowering the rate of respiration (156). To determine whether SteB was localized to the mitochondria, we transfected HeLa cells with FLAG-SteB or FLAG-SteB^{C103S} vectors, and analyzed cells by immunofluorescence of a α-FLAG antibody (Fig. 4-4A). Additionally, we visualized the nucleus, actin and mitochondria and found cytoplasmic localization of SteB and SteB^{C103S} with no co-localization to mitochondria or actin.

To rule out any effect SteB may have on mitochondrial respiration, the production of hydrogen peroxide was analyzed to quantify the rate of respiration. We measured hydrogen peroxide production after transfection of bone-marrow derived macrophages (BMDM) with pCMV2B, pCMV2B-steB or pCMV2B-steB^{C103S} (Fig. 4-4B) and after infection of BMDM with WT *Salmonella*, Δ*steB*, Δ*steB* psteB or Δ*steB* psteB^{C103S} (Fig. 4-4C). However, no significant reduction in the rate of hydrogen peroxide production was observed in BMDM, suggesting that SteB most likely does not affect the rate of mitochondrial respiration.

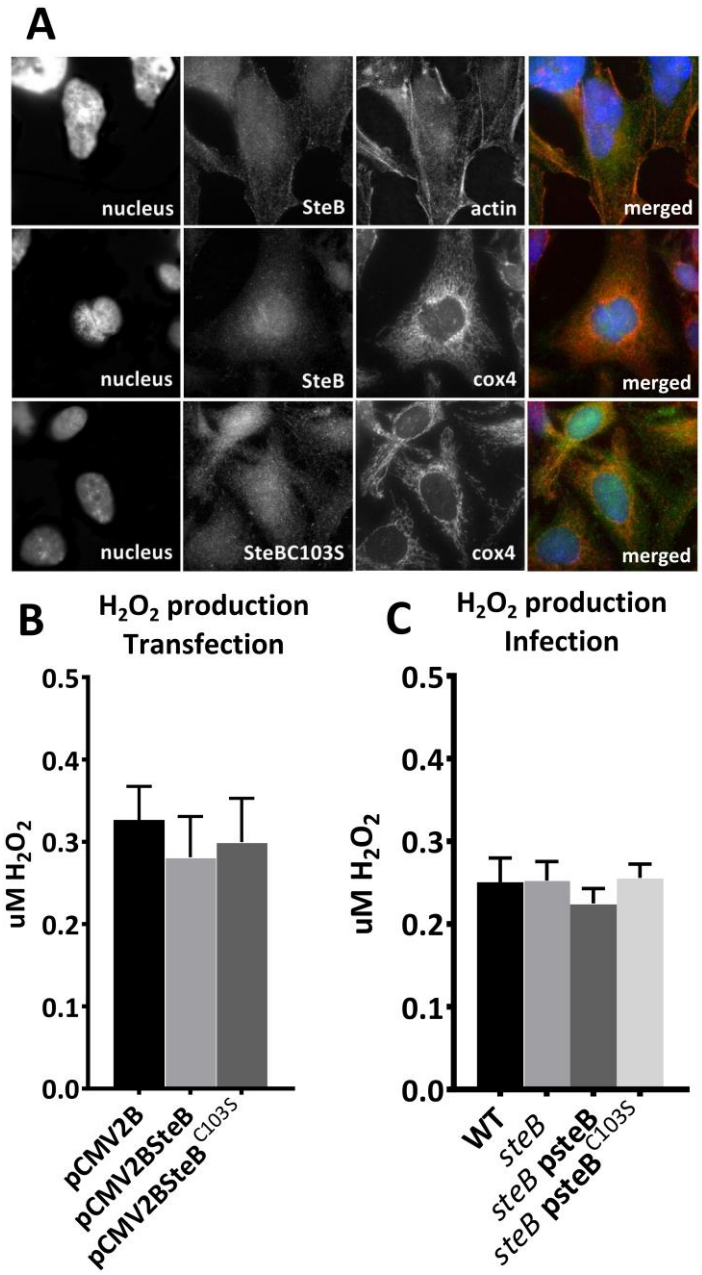

Figure 4-4: SteB is cytoplasmic and does not regulate mitochondrial respiration.

(A) Immunofluorescence analysis of HeLa cells transfected with pCMV2B-steB or pCMV2B-SteB^{C103S}. The photos in the top row show actin (red), whereas the middle row and bottom row show mitochondria (red). SteB or SteB^{C103S} are shown in green and DNA is stained with DAPI in blue. No co-localization of SteB or SteB^{C103S} with actin or mitochondria was observed and SteB appeared to be localized to the cytoplasm. (B) H_2O_2 production of BMDM after transfection with pCMV2B, pCMV2B-steB or pCMV2B-SteB^{C103S} analyzed by the Amplex red assay. (C) H_2O_2 production of BMDM 16 hours post infection of WT, Δ*steB*, Δ*steB* psteB or Δ*steB* psteB^{C103S} analyzed by the Amplex red assay. H_2O_2: hydrogen peroxide. Each bar represents 6 replicates. Error bars represent the standard deviation.

4.3.5 SteB does not affect tubulin-mediated inflammasome activation.

Microtubules are involved in assembly of the NLRP3 inflammasome which is activated upon infection with *Salmonella* (185). The NLRP3 inflammasome is assembled after recognition of bacterial elements by the NOD-like receptor, NLRP3, after which caspase-1 activation leads to processing of pro-interleukin 1β to bioactive IL-1β (186). Assembly involves microtubule-mediated co-localization of NLRP3, ASC and mitochondria, leading to pro-inflammatory cytokine release (186). Inside the cell, cytokine trafficking can also be mediated by microtubules (187). To investigate if SteB impacted NLRP3 assembly or cytokine trafficking, we measured cytokine secretion from BMDM of C57BL/6 mice after transfection with pCMV2B, pCMV2B-steB or pCMV2B-steB^{C103S} and stimulation with 1 ng/ml *Salmonella* lipopolysaccharide (LPS) (Fig. 4-5A). No significant differences in IL-6, MCP1 or TNFα cytokine secretion were observed. In order to investigate if the host's oxidative or nitrosative burst had any effect on SteB-functioning, BMDM from WT, *gp91phox-/-* and *iNOS-/-* mice were transfected with pCMV2B or pCMV2B-steB and cytokine secretion was measured (Fig. 4-5B). No significant differences in IL-6, MCP1 or TNFα cytokine secretion were observed. Recently, it was found that some antimicrobial peptides are only active under anoxic or anaerobic conditions (188). To test whether the conditions used in our previous experiments were too oxidized to observe effects of SteB on cytokine secretion we added 0, 0.25, 0.5, 0.75 or 1 mM DTT immediately after macrophage stimulation with 1 ng/ml *Salmonella* LPS (Fig. 4-5C). Again, no differences in IL-6, MCP1 or TNFα cytokine secretion were observed. Based on these results, it is unlikely that SteB is involved in NLRP3 inflammasome assembly or cytokine secretion.

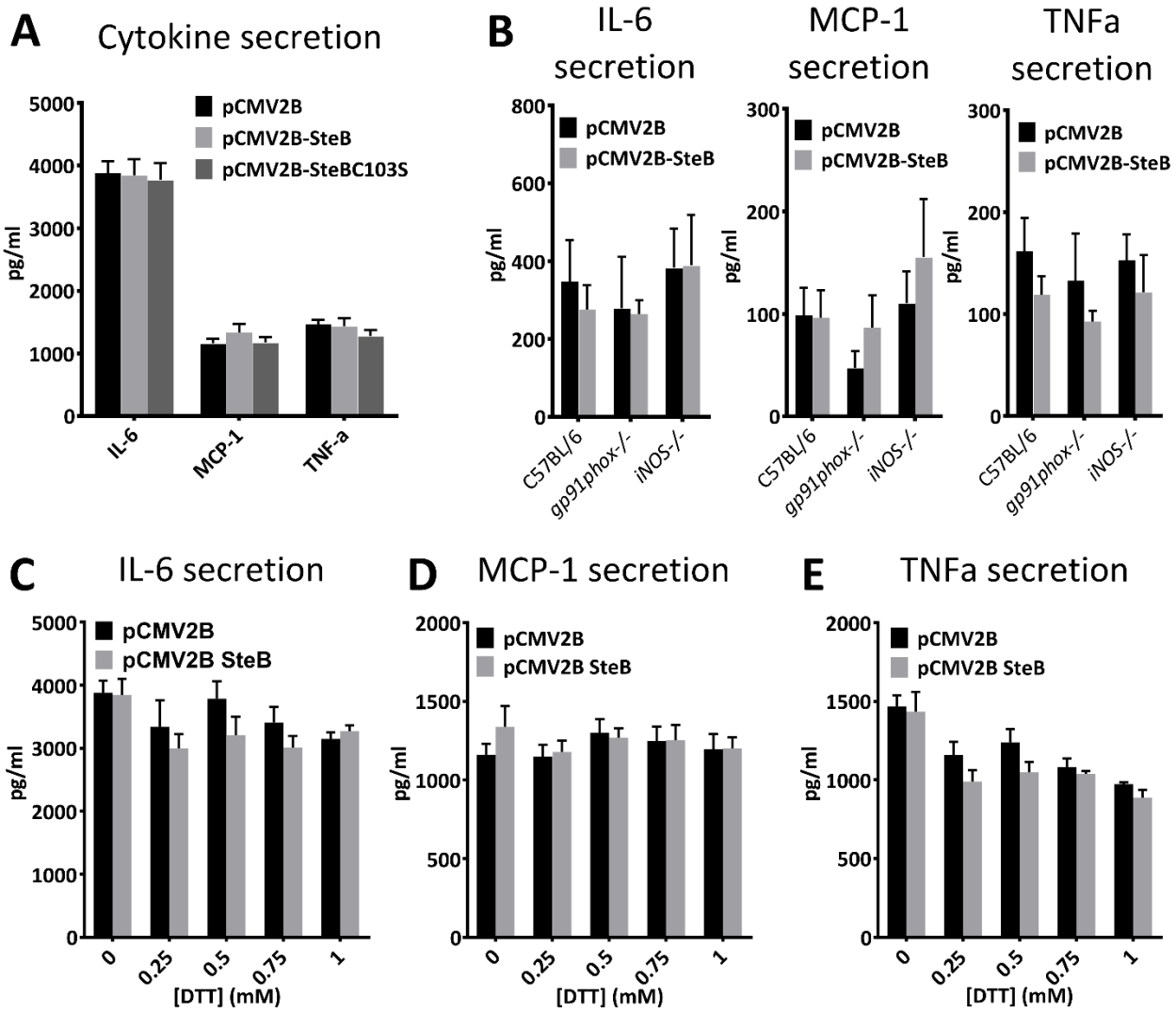

Figure 4-5: Cytokine secretion by BMDM after transfection with SteB.

(A) Cytokine secretion of IL-6, MCP-1 and TNFα as obtained by cytometric bead array after transfection of BMDM of C57BL/6 mice with pCMV2B, pCMV2B-steB or pCMV2B-SteB^{C103S} and subsequent stimulation with 1 ng/ml *Salmonella* LPS. (B) Cytokine secretion after transfection of BMDM derived from C57BL/6, *gp91phox-/-* or *iNOS-/-* mice with pCMV2B or pCMV2B-steB and analysis by cytometric bead array. (C) Cytokine secretion after transfection of BMDM and addition of 0, 0.25, 0.5, 0.75 or 1 mM DTT immediately after stimulation with LPS. DTT: dithiothreitol; LPS: lipopolysaccharide. Each bar represents 6 replicates. Error bars represent the standard deviation and significance was determined using a student's t-test.

4.3.6 SteB facilitates *Salmonella*-mediated trafficking to juxtanuclear position.

Although a distinct association between intracellular *Salmonella* and microtubules has been observed (189, 190), the mechanisms underlying microtubule-mediated trafficking of the SCV to the juxtanuclear position are unclear. Both *Salmonella* effectors SseF and SseG have been implicated in maintaining this positioning, however, no effector has been identified that facilitates initial trafficking to this position. In order to explore the involvement of SteB in SCV trafficking to the juxtanuclear position, intracellular *Salmonella* were analyzed during HeLa cell infection (Fig. 4-6A). At 6 hours post infection, most WT bacteria were found localized at the juxtanuclear position while Δ*steB* bacteria were deficient in their ability to properly position in the juxtanuclear region. Complementation with a plasmid carrying *steB* restored proper positioning of the SCV while complementation with a plasmid carrying the *steB*^{C103S} mutant did not restore juxtanuclear positioning. We quantified this difference by microscopic analysis of at least 100 infected cells per experiment (Fig. 4-6B).

Deletion of *steB* has not been found to affect bacterial survival and replication in a macrophage (191). It is therefore challenging to establish a role for CYS103 thiol oxidation during infection. However, during SteB protein purification and cloning practices in previous experiments, we observed that the replacement of cysteine residue 103 for a serine residue to form SteB^{C103S}, resulted in a protein that was significantly more toxic for bacteria. Based on these observations we hypothesized that the SteB^{C103S} mutant was not inactive but instead was deficient in controlling its activity. If this hypothesis was correct, co-transfection of THP-1 cells with pCMV2B-steB^{C103S} and Δ*steB Salmonella* would affect survival and replication of intracellular *Salmonella* differently than co-transfection with pCMV2B or pCMV2B-steB. To test this hypothesis, we measured survival of intracellular bacteria by CFU counts at 2 and 16 hours post infection. The 16h/2h fold

change was used as a measure for bacterial survival. As previously reported (191), we did not observe any attenuation in bacterial replication/survival for the Δ*steB* mutant (Fig. 4-6C). Infection with Δ*steB* and co-transfection with pCMV2B-SteB did not affect survival however co-transfection with pCMV2B-steB^{C103S} significantly decreased bacterial survival inside THP-1 cells (Fig. 4-6C). These results indicate that SteB^{C103S} is not inactive and suggest that thiol oxidation is crucial for regulation of proper effector activity leading to a model in which SteB-mediated trafficking of the SCV is regulated by oxidation of CYS103.

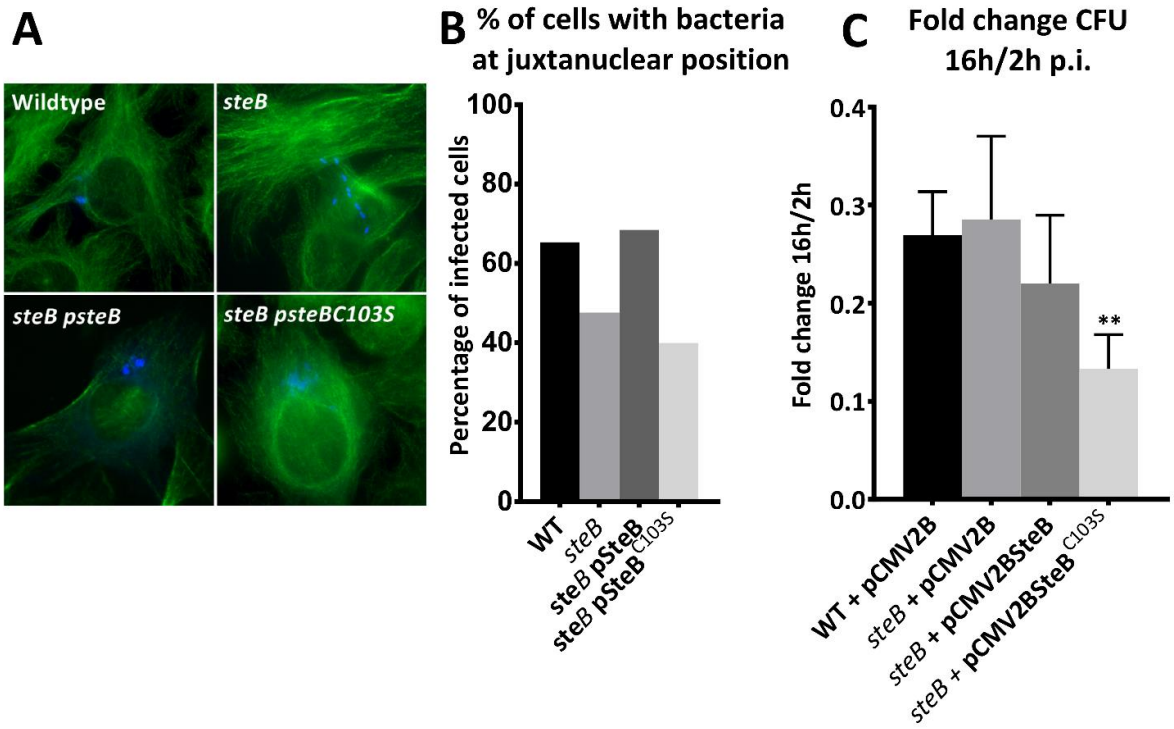

Figure 4-6: SteB affects trafficking to juxtanuclear position.

(A) Immunofluorescence analysis of *Salmonella*-infected HeLa cells at 6 hours post infection. *Salmonella* is shown in blue and microtubules are shown in green. No differences were observed in microtubule network formation. The juxtanuclear position is close to the nucleus as shown for WT bacteria. (B) Quantification of infected cells that contain bacteria at the juxtanuclear position. For each bar more than 100 infected cells were analyzed. (C) Bacterial replication/survival by measuring fold decrease in colony forming units at 16h/2h after infection with WT and Δ*steB* bacteria and co-transfection with pCMV2B, pCMV2B-steB or pCMV2B-SteB^{C103S} in THP-1 cells. Each bar represents six replicates. Error bars represent the standard deviation and significance was analyzed by a student's t-test (** $p < 0.01$).

4.4 Discussion

Modifications of effectors after translocation into the host cell have been found to alter effector localization, stability and interactions with host binding partners (95, 175, 177). In this study, we identify the first redox-sensitive thiol modification in a bacterial effector and show that this modification has regulatory properties. These findings highlight the utilization of redox chemistry and, in particular, the direct use of ROS and RNS by *Salmonella* to regulate effector functions during infection. *Salmonella* has already been found to utilizes redox-sensitive PTM to regulate expression of SPI-2 effectors by S-Nitrosylation of transcriptional regulator SsrB (91). Thus far, redox-sensitive PTMs have been mostly associated with transcriptional regulators and it is intriguing that in Chapter 3 and in Chapter 4, we found two examples of redox-sensitive PTMs that affect protein functions directly. These findings are encouraging and motivate a search for several unexplored redox-sensitive PTMs on bacterial proteins that affect virulence directly.

The role of many effectors has not been established yet since characterization of effector function in the host cell is incredibly challenging. The absence of obvious phenotypes in certain single deletion mutants makes characterization of effector function even more complicated. Redundancy of effector functions is thought to be the reason for the absence of phenotypes after deletion of certain *Salmonella* effectors (191, 192). Arguably effectors that do not show attenuated virulence upon deletion, are less important for infection and therefore less interesting for researchers. A counterargument can easily be made, based on results obtained in this study. Since deletion of *steB* alone did not show attenuation of bacterial survival and replication inside macrophages, the abolition of effector regulation by site directed mutagenesis of cysteine 103 resulted in significant attenuation of bacterial survival/replication. These results show that even effectors that do not

show attenuation after deletion, perform functions during infection that can be vital or detrimental if not regulated properly.

The association between microtubules and *Salmonella* has been known for many years, however, we still do not know all of the players involved in tubulin-mediated trafficking of the SCV (189, 190). SteB was found to be one of the missing players that could explain juxtanuclear positioning of the SCV. Other bacterial pathogens that secrete tubulin-binding effectors include *Pseudomonas syringae*, which secretes effector HopZ1a (182). This effector acetylates tubulin which leads to disruption of plant microtubule networks and secretory pathways while suppressing cell wall-mediated defense (182). *Chlamydia* species secrete the effector CopN, which binds to tubulin and inhibits its polymerization by sequestering free αβ-tubulin dimers, similar to one of the mechanisms utilized by stathmin. Both HopZ1a and CopN affect tubulin polymerization/destabilization which is different from SteB. SteB does not appear to have any effect on microtubule formation or stability however since *Salmonella* utilizes microtubules during infection it is not surprising that it does not disrupt microtubule networks. How exactly SteB mediates trafficking remains to be elucidated. One interesting possibility involves the potential interplay between SseF, SseG and SteB in proper trafficking and positioning of the SCV during infection. A potential functional or physical interaction between these effectors awaits further investigation.

Interestingly, *Salmonella typhi* lacks the *steB* gene. No data has been reported on juxtanuclear positioning of the SCV during *S. typhi* infections, however, it is worthwhile to note that *S.* Typhimurium infection is generally much more acute than *S. typhi* infection. *S.* Typhimurium could therefore require more rapid positioning to the juxtanuclear position compared to *S. typhi* in order to quickly establish acute infection.

Taken together, the results in this chapter reveal for the first time a direct redox-sensitive PTM in a bacterial effector that regulates effector activity. Thiol oxidation of cysteine 103 in SteB appears to regulate tubulin-mediated trafficking of the SCV to the juxtanuclear position during infection. These findings fit seamlessly with recent publications that describe more examples of redox chemistry that benefit bacterial pathogenesis and allow *Salmonella* to exploit immune responses (91, 100, 101).

4.5 Materials and methods

4.5.1 Cloning

All effectors were PCR amplified from *Salmonella* (SL1344) genomic DNA except the sequence of SspH1 which was amplified from *Salmonella* (LT2) genomic DNA. An extensive list of all primers used is described in Table 1. Effector genes were cloned into expression vector pET28a and transformed into expression strain BL21(DE3) for IPTG inducible expression. Cysteine to serine mutations were made in vectors pET28a, pGEX6P1, pCMV2B and pWSK129 by site-directed mutagenesis with the Quickchange pfuULTRA kit. The *steB* deletion mutant was made in the SL1344 background by allele exchange using vector pRE112 as described previously (146). Deletion was confirmed by PCR and sequencing.

4.5.2 Protein purification

Effectors were individually expressed in BL21(DE3) as described previously (166). In short, 50 ml of bacteria (per effector) were grown at 37°C until an OD_{600} of 0.8 was reached after which 0.1 mM IPTG was added. At this time, the bacteria were transferred to 16°C and incubated overnight while shaking. The next morning, bacteria were pelleted by centrifugation at 3000 x g for 30

minutes and washed with saline before re-suspension in bacterial lysis buffer (20 mM HEPES pH 7.5, 20 mM Imidazole, 120 mM Potassium acetate, 0.1% Triton X-100, 10 µg/ml DNAse, 10 µg/ml RNAse). Bacteria were lysed by sonication and lysates were incubated with Ni-sepharose for 3 hours. Each lysate/Ni-sepharose suspension was poured onto a separate column and columns were washed with 20x the column volume of washing buffer (PBS, 20 mM Imidazole). Proteins were eluted in elution buffer (Tris-HCl pH 7.5, 300 mM Imidazole) and protein concentrations were determined using Bradford Reagent.

4.5.3 Sample preparation for detection of oxidized thiols

10 µg of each purified effector protein was pooled and the total effector pool was divided over two tubes. To one tube, 1 mM DTT was added to create reducing conditions, whereas in the other tube, 1 mM hydrogen peroxide was added to create oxidizing conditions and both tubes were incubated for 30 minutes. After 30 minutes, the cultures were spun down, resuspended in Guanidine/MOPS buffer (6M Guanidine HCL pH 7.5, 150 mM NaCl, 5 mM EDTA, 25 mM MOPS) and lysed by sonication. Alkylation of free thiol groups was done by adding 40 mM N-ethyl maleimide for 2 hours at room temperature. After this, 4 volumes of ice cold methanol were added and the protein fraction was incubated overnight (ON) at -20°C. The next morning, protein fractions were spun down for 45 minutes at 15 000 x g at 4°C, and the protein pellet was washed twice with ice cold methanol. The protein pellets were dissolved in 100 µL of Guanidine/MOPS buffer and protein fractions were pooled. 10 mM DTT was added at 37°C for 30 minutes prior to addition of 0.4 mM HPDP-biotin (Proteochem). Samples were mixed and incubated for 2 hours at room temperature. After labelling with HPDP-biotin, LysC was added and protein fractions were incubated for 3 hours at 37°C followed by 4x dilution with 50 mM ammonium bicarbonate and then trypsin was

added to incubate overnight. After tryptic digest was complete, HPDP-biotin peptides were enriched using Neutravidin beads (Fisher Scientific) previously equilibrated with 20 mM ABC and left on rotation for 1 h at room temperature to allow binding of the biotinylated peptides to NeutrAvidin. After centrifugation at 200 × *g* for 10 s, the supernatant was discarded and the beads were washed 4x with 20 mM ammonium bicarbonate, 0.5 M NaCl. Two additional washings with 5 mM ammonium bicarbonate /20% acetonitrile were done to remove nonspecifically bound peptides. Peptides were eluted by incubating the beads for 10 minutes with 2 volumes of 100 mM mercaptoethanol. The samples were then dried in a speedvac and resuspended in 20 uL of 5% formic acid and cleaned using C18 Zip Tips prior to mass spectrometric analysis.

4.5.4 Sample preparation for detection of SteB binding partners

Samples were prepared as described previously (166). In short, 50 µg of purified GST, GST-SteB or GST-SteB^{C103S} were incubated with light, medium or heavy labelled protein lysates from RAW264.7 cells, respectively (15 mg of protein lysate per sample). 40 µl of glutathione agarose in lysis buffer was added and the mixture was incubated for 3 hours. Glutathione agarose was washed 5x with washing buffer (Tris-HCl pH 7.5) and eluted with 8 M Urea buffer and samples were pooled. 4 volumes of Tris-HCl pH 7.5 were added and protein fractions were incubated with LysC for 3 hours at 37°C followed by 4x dilution with 50 mM ammonium bicarbonate and trypsin was added overnight. After tryptic digest, peptide samples were cleaned using C18 Zip Tips prior to mass spectrometric analysis.

4.5.5 NanoLC-MS/MS analysis

NanoLC-MS/MS analysis was conducted using an LTQ-Orbitrap Velos mass spectrometer (Thermo Fisher Scientific) equipped with an 1100 series nanoflow HPLC system (Agilent) as described (167). An in-house analytical column (200 mm length x 75 μm i.d.) was prepared with ReproSil-Pur C18-AQ materials (3 μm, Dr. Maisch). Samples were loaded onto a 2 cm long, 100 μm inner diameter fused 5 silica trap column containing 5 μm Aqua C18 beads (Phenomenex) for 10 minutes prior to analytical separation at a flow rate of 5 μL/minute. Peptides were eluted at a flow rate of 250 nL/minute from the analytical column by altering the gradient from 100% buffer A (0.5% acetic acid) to 40% buffer B (0.5% acetic acid, 80% acetonitrile) over 90 minutes. Settings for MS analysis were as follows: one full scan (resolution 60,000; m/z 300–1,500) followed by top 10 MS/MS scans using CID in the linear ion trap (min. signal required, 200; isolation width, 3; normalized collision energy, 35; activation Q, 0.25; activation time, 10 ms) using dynamic exclusion (repeat count, 1; repeat duration, 30 s; exclusion list size, 500; exclusion duration, 60 1s). All raw data were analyzed and processed by MaxQuant (v1.3.0.5) (168). Search parameters included two missed cleavage sites, cysteine carbamidymethyl fixed modification, and variable modifications including methionine oxidation and protein N-terminal acetylation. The peptide mass tolerance was 6 ppm and the MS/MS tolerance was 0.5 Da. Database search was performed by Andromeda (169) against UniProt/Swiss-Prot *Salmonella* Typhimurium (downloaded on July 2011) with common serum contaminants and enzyme sequences. False discovery rate (FDR) was set to 1% at peptide and at protein level.

4.5.6 Thiol labelling with 5-iodoacetamidofluorescein

Confirmation of thiol oxidation was done by labelling of thiols with 5-iodofluorescein (5-IAF) and visualization on 15% polyacrylamide gels. 50 μg of purified HIS-tagged effector was split over two tubes. For each effector protein, one tube was reduced and one tube was oxidized with 1 mM DTT or 1 mM hydrogen peroxide, respectively. After 30 minutes 4 volumes of Guanidine/MOPS buffer (6 M Guanidine HCL pH 7.5, 150 mM NaCl, 5 mM EDTA, 25 mM MOPS) was added and thiols were alkylated by addition of 40 mM N-ethyl maleimide. Samples were incubated for 30 minutes after which 4 volumes of ice cold methanol were added and samples were left overnight at -20°C. The next morning, protein pellets were washed 3x with ice cold methanol prior to addition of 10 mM DTT and 200 μM 5-IAF. After incubation for 2 hours, 4 volumes of ice cold methanol were added and samples were left overnight at -20°C. Again, protein pellets were washed 3x with ice cold methanol and protein was resuspended in 3 x SDS Laemmli loading buffer. The protein samples were run on 15% SDS polyacrylamide gels and fluorescence was analyzed using a Biorad Gel Imaging System. Total fluorescence was determined by ImageLab 4.0 and normalized to total protein as determined by Western blot and densitometry analysis with ImageLab 4.0. The fold increase in normalized fluorescence between oxidized versus reduced protein was then used to determine thiol oxidation.

4.5.7 Western blot analysis

Western blot analysis was done as previously described (166). In short: Proteins were separated on 12–15% SDS acrylamide gels and transferred to PVDF membranes (Bio-Rad). Membranes were blocked with 5% w/v skim milk powder, 0.1% v/v Tween in PBS and incubated in the same buffer with primary or secondary antibodies as follows: beta-tubulin (Abcam) 1:2000, penta-his

(Life Technologies) 1:1000, goat α-mouse HRP (Jackson ImmunoResearch Laboratories) 1:10,000. Proteins were detected with Biorad detection reagent in the Biorad Gel Imaging System.

4.5.8 Confirmation of SteB-tubulin binding

20 µg of purified tubulin (Cytoskeleton, Inc.) was incubated with 40 µl Ni-sepharose (GE Healthcare) coated with empty control, 50 µg purified SteB or 50 µg $SteB^{C103S}$ proteins for 2 hours. Each scenario was repeated in reducing, normal and oxidizing conditions. Ni-sepharose was washed 3x with washing buffer (PBS pH 7.4, 20 mM Imidazole). Proteins were eluted in 100 µl elution buffer (Tris-HCl pH 7.5, 500 mM Imidazole) and 50 µl 3 x SDS Laemmli loading buffer was added. Protein solutions were analyzed by Western blot analysis.

4.5.9 Tubulin dimerization assay

20 µg of purified tubulin was incubated with SteB, $SteB^{C103S}$, or alone, under reducing conditions, normal conditions or oxidizing conditions to analyze dimerization. After incubation of 3 hours at room temperature, samples were analyzed by Western blot analysis.

4.5.10 Tubulin polymerization assay

The tubulin polymerization assay (Cytoskeleton Inc, Tubulin Polymerization Assay Kit Cat. # BK006P) was done according to the manufacturer's instructions. Samples were analyzed in a Tecan fluorescence plate reader.

4.5.11 Culturing bone marrow derived macrophages

Bone marrow was collected from the tibias and femurs of 6-8 week old wild type C57BL/6J, iNOS-/- (B6.129P2-Nos2tm1Lau/J) and gp91phox-/- (B6.129S6-Cybbtm1Din/J) male mice (all purchased from Jackson Laboratory). Each well of a 6-well plate was seeded with $1x10^6$ cells in buffer (RPMI 1640 containing L-Glutamine; Life Technologies, supplemented with 10% heat-inactivated FBS; Life Technologies, 100 U/ml Penicillin and 100 µg/ml Streptomycin; Life Technologies and 20 ng/ml M-CSF; Peprotech). Cells were incubated at 37°C with 5% CO_2. On days 4 and 6 of culture, 2 ml medium were removed from each well and replaced with 2 ml fresh medium. On day 7 of culture, culture supernatant containing non-adherent cells were removed prior to performing assays. The purity of adherent cells was confirmed by flow cytometry for all genotypes on day 7 of culture and >97% of cells were CD45+CD11b+F4/80+.

4.5.12 Determination of cytokine secretion

Secretion of cytokines was determined using a BD cytometric Bead Array Mouse inflammation kit according to the manufacturer's instructions (Cat 552364 from BD Biosciences).

4.5.13 Amplex Red assay

The Amplex Red Hydrogen peroxide Assay (Molecular probes #A22188) was done according to the manufacturer's instructions. Samples were analyzed immediately after the samples were obtained.

4.5.14 Infection and transfection experiments

HeLa cells were grown in DMEM (Gibco) containing 10% heat-inactivated FBS, 1% GlutaMAX, and 1% non-essential amino acids. Cells were seeded at $3.0x10^5$ in 6-well plates 48 hours prior to infection. BMDM and THP-1 cells were grown in RPMI supplemented with 10% inactivated FBS, 1% Glutamax and 1 % non-essential amino acids. 72 hours prior to infection, THP-1 cells were seeded at $3.6x10^6$ in 6-well plates and for the first 24 hours 100 nM phorbol 12-myristate 13-acetate (PMA) was added for differentiation into macrophage-like cells. After 24 hours, the medium was replaced and the cells were incubated for another 48 hours before infection was started. BMDM were prepared as described previously (89). Transfection of HeLa cells was done with JetPrime (Polyplus Transfection) and transfection of BMDM and THP-1 cells was done with JetPEI-Macrophage (Polyplus Transfection) according to manufacturer's instructions. For infection experiments, ON cultures of *Salmonella* were used for infection (stationary phase bacteria) or diluted 1:33 in LB and sub-cultured for 3 hours at 37°C to obtain log phase bacteria. The bacteria were resuspended in PBS and used at a multiplicity of infection of 10. THP-1 cells and BMDM were spun down at 1000 rpm for 10 minutes to synchronize infection. At 30 minutes post infection, cells were washed with PBS and further incubated in media supplemented with 50 μg/ml gentamicin. At 2 hours post infection, cells were washed with PBS and incubated in media supplemented with 12 μg/ml gentamicin. For CFU counts, cells were lysed in PBS supplemented with 1% Triton X-100 and 0.1% SDS. After serial dilution, the samples were plated on LB agar plates after which colony forming units were counted manually. For cytokine determination, 100 μl of cell media were frozen down at -80°C and used for analysis at a later time point. For immunofluorescence microscopy, cells were fixed with 3% paraformaldehyde for 30 minutes or by methanol fixation if tubulin was stained.

4.5.15 Immunofluorescence microscopy

HeLa cells were grown on coverslips in 12 well plates. Cells were transfected 24 hours prior to fixation or infected with *Salmonella* and fixed at specific time intervals. For visualization of SteB localization, cells were fixed with 4% paraformaldehyde followed by permeabilization with 0.2% Triton X-100. For visualization of microtubules, cells were fixed with ice cold methanol. Cells were blocked with BSA buffer (PBS -/- pH 7.4, 1% bovine serum albumin, 0.01% tween) and incubated with α-FLAG M2 mouse monoclonal antibody (Sigma-Aldrich) (1/200), α-COX4 rabbit antibody (Abcam) (1/200) or α-beta-tubulin mouse monoclonal antibody (1/200) followed by secondary antibodies, Alexa 488-conjugated goat α-mouse (Life Technologies) 1/200) and Alexa 568-conjugated goat α-rabbit (Life Technologies) 1/200). Coverslips were mounted using ProLong Gold Antifade Reagent with DAPI (Life Technologies). Images were obtained with an Olympus IX81 microscope at a multitude of magnification of 600. Images were analysed and edited with ImageJ.

Bioinformatic analysis and prediction of protein structures

The structure of SteB was predicted by the iTasser webserver http://zhanglab.ccmb.med.umich.edu/I-TASSER/ (159) and protein-protein interactions were predicted by the pyDockWeb server at http://life.bsc.es/servlet/pydock/home/ using restrains on binding sites (160). Protein structures were edited and visualized with pyMOL.

Chapter 5: Conclusions

5.1 The changing dogma

The findings presented in this dissertation fit seamlessly into the renewed perspective that combines the beneficial aspects of ROS and RNS to the pathogen alongside their antimicrobial activities. It would appear that the effects of ROS and RNS are in balance between help and harm to the bacteria. In the relationship between *Salmonella* and oxidative/nitrosative stress, the antimicrobial effects of ROS and RNS do not necessarily exclude additional roles for ROS/RNS in regulatory processes that affect pathogenesis. Previous studies have reported the reversible disulfide bond in the periplasmic domain of OmpA (162, 193, 194); however, thus far no data has been published on potential regulatory mechanisms mediated by this disulfide bond. The findings presented in this thesis show a crucial regulatory role for this redox-sensitive disulfide in controlling protein function of OmpA. The concept that there are beneficiary roles for oxidative/nitrosative stress to bacterial pathogenesis may extend to other interactions between *Salmonella* and the immune system. Only very recently some of these ideas were compiled in an elegant review article showing how *Salmonella* exploits activated immune defenses to promote its replication in the host (100). Further research and investigation is needed to fully appreciate and define the complexity of the relationship between Salmonella and host defense systems.

5.2 Need for adequate analytical tools

One major difficulty faced by researchers was the lack of adequate analytical tools available to measure real-time fluctuations in ROS/RNS levels. The instability and short-lived nature of ROS and RNS make accurate measurements challenging and often lead to confusing results. The

roGFP2 biosensor described in Chapter 2, proved to be indispensable for further investigations of which the data is presented in this thesis (89). Other groups have recently reported other novel analytical tools for measuring redox potential in bacteria (124, 195) and there is great potential for their shared use to gain even better and more sophisticated understanding of oxidative/nitrosative stress in bacteria.

5.3 Stress responses and new therapies

Despite great interest in increasing fundamental understanding of bacterial infections, the ultimate goal behind much of pathogenesis research is to improve existing antimicrobial therapies or develop novel therapies which will decrease human infections. The findings described in this thesis reveal new bacterial stress responses and adaptations that allow *Salmonella* to exploit the host's immune responses. In the next paragraphs we will discuss our results in the context of finding new antibiotics and explore how a better understanding of bacterial stress responses can lead to novel targets for antimicrobial therapies.

5.4 The need for new antimicrobial therapies

Ever since the discovery of penicillin in 1927 and subsequent development and mass production of antibiotics, bacterial infections have often been thought of as treatable conditions in the developed world. However, in the developing world, due to lack of access to antimicrobial therapies, many people still die every day due to curable infections. Additionally, in recent years due to misuse of antibiotics, new multidrug resistant bacteria are evolving which have no known therapy. Even in the developed world patients are dying of these infections because none of the available therapies are effective. According to the Center of Disease Control, each year in the

United States alone, at least 2 million people become infected with bacteria that are resistant to antibiotics resulting in at least 23,000 people that die as a direct result of these infections (196). It is distressing that in the past thirty years essentially no new antibiotics have been developed due to economic and regulatory challenges. In the war against multi-drug resistance, small victories include the very recent discovery of a new antibiotic target (197) and the recent development of CRISPR-based approaches that allow for more flexibility in combating antibiotic resistance (198). Despite these new developments, additional discoveries will be required to combat the further progression of multidrug resistance and to ensure that bacterial infections continue to be curable entities for generations in the future.

5.5 Understanding heterogeneity

To minimize harmful effects, most antibiotics exploit intrinsic differences between bacterial cells and eukaryotic cells to arrest growth and kill bacteria. When given enough time in the presence of antibiotics, bacteria can develop resistance to the antibiotic by acquisition of genetic elements or point mutations. Bacterial stress responses often lay the foundation for developing antibiotic resistance and persistence as was shown in Chapter 3 when describing the decrease in OM permeability after encountering ROS and RNS. Targeting or inhibiting fundamental bacterial stress responses in combination with antibiotics has been suggested to enhance the clinical efficacy of antibiotics (199) (200). Bacterial stress responses also lead to heterogeneity in bacterial populations (140, 141). Heterogeneity allows bacteria to have a diverse response to antimicrobial stresses emplaced by the host immune system. In Chapter 2 the concept of heterogeneity was exemplified by the different responses to redox stress by intracellular bacteria. Only recently have the appropriate tools become available to analyze heterogeneity within a bacterial population and

gain a better understanding of the differences between sub-populations which would be essential for designing novel antimicrobial approaches that are effective against all of the sub-populations.

5.6 Oxidative stress and heterogeneity

The exact mechanism of how heterogeneity is established within a bacterial population is unclear. Specific signals likely exist that act on certain bacteria more than others which then stimulates a cascade of transcriptional/translational events resulting in multiple distinct subpopulations. It is possible that ROS and RNS fuel heterogeneity through the redox-sensitive modification in transcriptional regulator SsrB (91). S-Nitrosylation of SsrB inhibits transcription of SPI-2 effectors allowing for fusion between the SCV and lysosomes. Fusion of the SCV with lysosomes increases exposure of bacteria to RNS which in turn further inhibits transcription of SPI-2 effectors. This concept extrapolates differences in redox stress among bacteria that reside in separate SCV. As such, diversification of SPI-2 expression by SsrB S-Nitrosylation could lead to the concept of heterogeneity to the extent that some intracellular bacteria "take the hit", thereby taking away pressure on other intracellular bacteria that can replicate rapidly. This idea is further supported by the observation that during infection with *ssaR* mutants no heterogeneity was observed. Although more research is required to validate this concept, it is already evident that bacterial stress responses are at least in part responsible for heterogeneous bacterial populations.

5.7 Combatting persistence

Heterogeneity results in subsets of bacteria that are non-replicating, have decreased metabolic activity, limited OM permeability and are often not eliminated by the immune system or by antibiotics. After termination of antibiotic therapy these bacteria can then re-activate and cause

recurrent infections (164). This makes antibiotics treatment difficult and prolonged while also allowing bacteria significantly more time to gain antibiotic resistance in the presence of these antibiotics. In particular when treating infections with *Mycobacterium tuberculosis* and *Pseudomonas aeruginosa*, combatting persistence is of significant clinical importance and is essential in order to cure patients of infection. In Chapter 3, alteration of OM permeability was shown to affect persister formation. The concept of targeting membrane permeability as a way of killing bacteria more effectively has been explored previously (153). In this report, the increase in OM permeability was accomplished by targeting the OM directly. Although successful in increasing OM permeability, this approach gives bacteria the chance to gain resistance by changing the consistency of their OM. The discovery of innate mechanisms that alter OM permeability in Chapter 3 reveals new targets for accomplishing higher OM permeability during antibiotic treatment. The benefit to targeting innate mechanisms that are essential for bacterial fitness versus those which effect the OM directly, is that bacteria cannot easily change these mechanisms to acquire resistance. Increased OM permeability could be accomplished by targeting "plug" proteins or by designing molecules or small peptides that occupy the binding spot of "plug" proteins thereby forcing pores to stay open or closed. By targeting "plug" proteins or OMPs to increase OM permeability during antibiotic therapy, persister-formation would likely be reduced while enhancing the clinical efficacy of antibiotics. This would also be beneficial as it would be an adjunct to previously developed antibiotics that are known to be safe in humans instead of needing to develop entirely new therapies.

5.8 Targeting regulation of virulence

An alternate approach for combatting bacterial infections is targeting virulence regulation instead of killing bacterial pathogens. It is still unclear why certain bacteria cause infection while others live with us symbiotically as part of our microbiota. Over the past decade, the human microbiome project revealed that many of the microbes inside of us aid our immune system in fighting infections and are essential to staying healthy. Interestingly, several of these commensal bacteria are completely harmless in most people but can become opportunistic pathogens and cause disease under specific circumstances. A more thorough understanding of what stimulates bacteria to "switch on" virulence mechanisms could lead to the development of ways to prevent this from happening and stop commensal bacteria from converting to pathogens that cause disease. Since it is *Salmonella* effectors that drive the process of infection (170), we studied how these effectors are directly regulated by ROS/RNS and, in Chapter 4, we describe the identification of a redox-sensitive regulatory switch in effector SteB. Remarkably, abolition of regulatory properties by site-directed mutagenesis significantly attenuates Salmonella's ability to survive and replicate intracellularly whereas deletion of *steB* from WT *Salmonella* does not have the same effect. These results suggest that targeting regulatory mechanisms of effectors has potential for counteracting virulence and transform pathogens into commensals. It may be that the transformation of bacterial pathogens into non-harmful microbiota could be the most promising approach to deal with infections in the future.

5.9 Final conclusion

The host pathogen relationship has been explored since the germ theory identified the potential for microscopic creatures to cause disease in humans. The intricacies of this relationship however, are

only just beginning to be appreciated. In this thesis the example of reactive oxygen and nitrogen species has been used to outline the balance between bacterial and host mechanisms for survival. This is not as simple of a picture as may once have been imagined. Is oxidative/nitrosative stress good or bad for *Salmonella*? Clearly most intracellular *Salmonella* bacteria die from exposure to ROS and/or RNS but, at the same time, some *Salmonella* bacteria benefit tremendously from ROS/RNS-mediated stress responses and ROS/RNS-mediated regulation of virulence. The results in this thesis show that *S.* Typhimurium actively evades oxidative stress through SPI-2 effector-mediated processes while also utilizing ROS and RNS as signaling moieties to regulate stress responses and virulence. It is still unclear exactly how ROS and RNS contribute to heterogeneity and persister formation but the results presented in this thesis do point to potential avenues for targeting bacterial redox stress responses as novel antimicrobial therapies. Understanding of the relationship between human and microbe is only in its infancy and the future has many exciting frontiers.

Bibliography

1. McGhie EJ, Brawn LC, Hume PJ, Humphreys D, & Koronakis V (2009) Salmonella takes control: effector-driven manipulation of the host. *Curr Opin Microbiol* 12(1):117-124.
2. Valdez Y, Ferreira RBR, & Finlay BB (2009) Molecular Mechanisms of Salmonella Virulence and Host Resistance. *Curr Top Microbiol* 337:93-127.
3. Ekperigin HE & Nagaraja KV (1998) Microbial food borne pathogens. Salmonella. *Vet Clin North Am Food Anim Pract* 14(1):17-29.
4. Sansonetti PJ (2004) War and peace at mucosal surfaces. *Nat Rev Immunol* 4(12):953-964.
5. Lee CA, *et al.* (2000) A secreted Salmonella protein induces a proinflammatory response in epithelial cells, which promotes neutrophil migration. *P Natl Acad Sci USA* 97(22):12283-12288.
6. Wall DM, *et al.* (2007) Identification of the *Salmonella enterica* serotype Typhimurium SipA domain responsible for inducing neutrophil recruitment across the intestinal epithelium. *Cellular Microbiology* 9(9):2299-2313.
7. Drecktrah D, Knodler LA, Ireland R, & Steele-Mortimer O (2006) The mechanism of Salmonella entry determines the vacuolar environment and intracellular gene expression. *Traffic* 7(1):39-51.
8. Bakowski MA, Braun V, & Brumell JH (2008) Salmonella-containing vacuoles: directing traffic and nesting to grow. *Traffic* 9(12):2022-2031.
9. Steele-Mortimer O (2008) The Salmonella-containing vacuole - Moving with the times. *Current Opinion in Microbiology* 11(1):38-45.

10. Brumell JH, Goosney DL, & Finlay BB (2002) SifA, a type III secreted effector of *Salmonella* Typhimurium, directs Salmonella-induced filament (Sif) formation along microtubules. *Traffic* 3(6):407-415.

11. Brumell JH, Tang P, Mills SD, & Finlay BB (2001) Characterization of Salmonella-induced filaments (Sifs) reveals a delayed interaction between Salmonella-containing vacuoles and late endocytic compartments. *Traffic* 2(9):643-653.

12. Catron DM, *et al.* (2004) *Salmonella enterica* serovar Typhimurium requires nonsterol precursors of the cholesterol biosynthetic pathway for intracellular proliferation. *Infect Immun* 72(2):1036-1042.

13. Knodler LA & Steele-Mortimer O (2003) Taking possession: biogenesis of the Salmonella-containing vacuole. *Traffic* 4(9):587-599.

14. Malik Kale P, *et al.* (2011) Salmonella - at home in the host cell. *Frontiers in Microbiology* 2.

15. Marcus SL, Brumell JH, Pfeifer CG, & Finlay BB (2000) Salmonella pathogenicity islands: big virulence in small packages. *Microbes Infect* 2(2):145-156.

16. Brown NF & Finlay BB (2011) Potential origins and horizontal transfer of type III secretion systems and effectors. *Mob Genet Elements* 1(2):118-121.

17. Cirillo DM, Valdivia RH, Monack DM, & Falkow S (1998) Macrophage-dependent induction of the Salmonella pathogenicity island 2 type III secretion system and its role in intracellular survival. *Mol Microbiol* 30(1):175-188.

18. Waterman SR & Holden DW (2003) Functions and effectors of the Salmonella pathogenicity island 2 type III secretion system. *Cell Microbiol* 5(8):501-511.

19. Brown NF, *et al.* (2005) Salmonella pathogenicity island 2 is expressed prior to penetrating the intestine. *Plos Pathogens* 1(3):252-258.

20. Agbor TA & McCormick BA (2011) Salmonella effectors: important players modulating host cell function during infection. *Cell Microbiol* 13(12):1858-1869.

21. Coburn B, Li YL, Owen D, Vallance BA, & Finlay BB (2005) *Salmonella enterica* serovar Typhimurium pathogenicity island 2 is necessary for complete virulence in a mouse model of infectious enterocolitis. *Infection and Immunity* 73(6):3219-3227.

22. Brawn LC, Hayward RD, & Koronakis V (2007) Salmonella SPI1 effector SipA persists after entry and cooperates with a SPI2 effector to regulate phagosome maturation and intracellular replication. *Cell Host Microbe* 1(1):63-75.

23. Bajaj V, Lucas RL, Hwang C, & Lee CA (1996) Co-ordinate regulation of *Salmonella* Typhimurium invasion genes by environmental and regulatory factors is mediated by control of hilA expression. *Mol Microbiol* 22(4):703-714.

24. Eichelberg K & Galan JE (1999) Differential regulation of *Salmonella* Typhimurium type III secreted proteins by pathogenicity island 1 (SPI-1)-encoded transcriptional activators InvF and HilA. *Infect Immun* 67(8):4099-4105.

25. Lara-Tejero M & Galan JE (2009) *Salmonella enterica* serovar Typhimurium Pathogenicity Island 1-Encoded Type III Secretion System Translocases Mediate Intimate Attachment to Nonphagocytic Cells. *Infect Immun* 77(7):2635-2642.

26. Hayward RD, *et al.* (2005) Cholesterol binding by the bacterial type III translocon is essential for virulence effector delivery into mammalian cells. *Mol Microbiol* 56(3):590-603.

27. Nichols CD & Casanova JE (2010) Salmonella-directed recruitment of new membrane to invasion foci via the host exocyst complex. *Curr Biol* 20(14):1316-1320.

28. Haraga A, Ohlson MB, & Miller SI (2008) Salmonellae interplay with host cells. *Nat Rev Microbiol* 6(1):53-66.

29. Hapfelmeier S, *et al.* (2004) Role of the Salmonella pathogenicity island 1 effector proteins SipA, SopB, SopE, and SopE2 in *Salmonella enterica* subspecies 1 serovar Typhimurium colitis in streptomycin-pretreated mice. *Infect Immun* 72(2):795-809.

30. Boyle EC, Brown NF, & Finlay BB (2006) *Salmonella enterica* serovar Typhimurium effectors SopB, SopE, SopE2 and SipA disrupt tight junction structure and function. *Cell Microbiol* 8(12):1946-1957.

31. Raffatellu M, *et al.* (2005) SipA, SopA, SopB, SopD, and SopE2 contribute to *Salmonella enterica* serotype Typhimurium invasion of epithelial cells. *Infect Immun* 73(1):146-154.

32. Patel JC & Galan JE (2005) Manipulation of the host actin cytoskeleton by Salmonella - all in the name of entry. *Current Opinion in Microbiology* 8(1):10-15.

33. Friebel A, *et al.* (2001) SopE and SopE2 from *Salmonella* Typhimurium activate different sets of RhoGTPases of the host cell. *J Biol Chem* 276(36):34035-34040.

34. Patel JC & Galan JE (2006) Differential activation and function of Rho GTPases during Salmonella-host cell interactions. *Journal of Cell Biology* 175(3):453-463.

35. Zhou D, Chen LM, Hernandez L, Shears SB, & Galan JE (2001) A Salmonella inositol polyphosphatase acts in conjunction with other bacterial effectors to promote host cell actin cytoskeleton rearrangements and bacterial internalization. *Mol Microbiol* 39(2):248-259.

36. McGhie EJ, Hayward RD, & Koronakis V (2001) Cooperation between actin-binding proteins of invasive Salmonella: SipA potentiates SipC nucleation and bundling of actin. *Embo J* 20(9):2131-2139.

37. Zhou DG, Mooseker MS, & Galan JE (1999) An invasion-associated Salmonella protein modulates the actin-bundling activity of plastin. *P Natl Acad Sci USA* 96(18):10176-10181.

38. Myeni SK & Zhou D (2010) The C terminus of SipC binds and bundles F-actin to promote Salmonella invasion. *J Biol Chem* 285(18):13357-13363.

39. Humphreys D, Hume PJ, & Koronakis V (2009) The Salmonella effector SptP dephosphorylates host AAA+ ATPase VCP to promote development of its intracellular replicative niche. *Cell Host Microbe* 5(3):225-233.

40. Stender S, *et al.* (2000) Identification of SopE2 from *Salmonella* Typhimurium, a conserved guanine nucleotide exchange factor for Cdc42 of the host cell. *Mol Microbiol* 36(6):1206-1221.

41. Rogers LD, *et al.* (2008) Identification of cognate host targets and specific ubiquitylation sites on the Salmonella SPI-1 effector SopB/SigD. *J Proteomics* 71(1):97-108.

42. Rogers LD, Brown NF, Fang Y, Pelech S, & Foster LJ (2011) Phosphoproteomic analysis of Salmonella-infected cells identifies key kinase regulators and SopB-dependent host phosphorylation events. *Science Signaling* 4(191):rs9.

43. Srikanth CV, *et al.* (2010) Salmonella Pathogenesis and Processing of Secreted Effectors by Caspase-3. *Science* 330(6002):390-393.

44. Zhang Y, Higashide WM, McCormick BA, Chen J, & Zhou DG (2006) The inflammation-associated Salmonella SopA is a HECT-like E3 ubiquitin ligase. *Mol Microbiol* 62(3):786-793.

45. Raupach B, Peuschel SK, Monack DM, & Zychlinsky A (2006) Caspase-1-mediated activation of interleukin-1beta (IL-1beta) and IL-18 contributes to innate immune defenses against *Salmonella enterica* serovar Typhimurium infection. *Infect Immun* 74(8):4922-4926.

46. Guiney DG (2005) The role of host cell death in Salmonella infections. *Role of Apoptosis in Infection* 289:131-150.

47. Haraga A & Miller SI (2006) A Salmonella type III secretion effector interacts with the mammalian serine/threonine protein kinase PKN1. *Cell Microbiol* 8(5):837-846.

48. Wu H, Jones RM, & Neish AS (2012) The Salmonella effector AvrA mediates bacterial intracellular survival during infection in vivo. *Cell Microbiol* 14(1):28-39.

49. Lin SL, Le TX, & Cowen DS (2003) SptP, a *Salmonella* Typhimurium type III-secreted protein, inhibits the mitogen-activated protein kinase pathway by inhibiting Raf activation. *Cell Microbiol* 5(4):267-275.

50. Knodler LA, Finlay BB, & Steele-Mortimer O (2005) The Salmonella effector protein SopB protects epithelial cells from apoptosis by sustained activation of Akt. *J Biol Chem* 280(10):9058-9064.

51. Kuijl C, *et al.* (2007) Intracellular bacterial growth is controlled by a kinase network around PKB/AKT1. *Nature* 450(7170):725-U710.

52. Haneda T, *et al.* (2011) Salmonella type III effector SpvC, a phosphothreonine lyase, contributes to reduction in inflammatory response during intestinal phase of infection. *Cell Microbiol*.

53. Le Negrate G, *et al.* (2008) Salmonella secreted factor L deubiquitinase of *Salmonella* Typhimurium inhibits NF-kappaB, suppresses IkappaBalpha ubiquitination and modulates innate immune responses. *J Immunol* 180(7):5045-5056.

54. Bernal-Bayard J & Ramos-Morales F (2009) Salmonella Type III Secretion Effector SlrP Is an E3 Ubiquitin Ligase for Mammalian Thioredoxin. *J Biol Chem* 284(40):27587-27595.

55. Bernal-Bayard J, Cardenal-Munoz E, & Ramos-Morales F (2010) The Salmonella type III secretion effector, salmonella leucine-rich repeat protein (SlrP), targets the human chaperone ERdj3. *J Biol Chem* 285(21):16360-16368.

56. Guiney DG & Fierer J (2011) The Role of the spv Genes in Salmonella Pathogenesis. *Front Microbiol* 2:129.

57. Buckner MMC, Croxen MA, Arena ET, & Finlay BB (2011) A comprehensive study of the contribution of *Salmonella enterica* serovar Typhimurium SPI2 effectors to bacterial colonization, survival and replication in typhoid fever, macrophage and epithelial cell infection models. *Virulence* 2(3):208-216.

58. Dai S, Zhang Y, Weimbs T, Yaffe MB, & Zhou D (2007) Bacteria-generated PtdIns(3)P recruits VAMP8 to facilitate phagocytosis. *Traffic* 8(10):1365-1374.

59. Hernandez LD, Hueffer K, Wenk MR, & Galan JE (2004) Salmonella modulates vesicular traffic by altering phosphoinositide metabolism. *Science* 304(5678):1805-1807.

60. Cain RJ, Hayward RD, & Koronakis V (2008) Deciphering interplay between Salmonella invasion effectors. *Plos Pathog* 4(4).

61. Bakowski MA, Cirulis JT, Brown NF, Finlay BB, & Brumell JH (2007) SopD acts cooperatively with SopB during *Salmonella enterica* serovar Typhimurium invasion. *Cell Microbiol* 9(12):2839-2855.

62. Ibarra JA & Steele-Mortimer O (2009) Salmonella- the ultimate insider. Salmonella virulence factors that modulate intracellular survival. *Cell Microbiol* 11(11):1579-1586.

63. Arpaia N, *et al.* (2011) TLR Signaling Is Required for *Salmonella* Typhimurium Virulence. *Cell* 144(5):675-688.

64. Walthers D, *et al.* (2007) The response regulator SsrB activates expression of diverse Salmonella pathogenicity island 2 promoters and counters silencing by the nucleoid-associated protein H-NS. *Mol Microbiol* 65(2):477-493.

65. Nikolaus T, *et al.* (2001) SseBCD proteins are secreted by the type III secretion system of Salmonella pathogenicity island 2 and function as a translocon. *Journal of Bacteriology* 183(20):6036-6045.

66. Abrahams GL, Muller P, & Hensel M (2006) Functional dissection of SseF, a type III effector protein involved in positioning the Salmonella-containing vacuole. *Traffic* 7(8):950-965.

67. Shotland Y, Kramer H, & Groisman EA (2003) The Salmonella SpiC protein targets the mammalian Hook3 protein function to alter cellular trafficking. *Mol Microbiol* 49(6):1565-1576.

68. Dumont A, *et al.* (2010) SKIP, the host target of the Salmonella virulence factor SifA, promotes kinesin-1-dependent vacuolar membrane exchanges. *Traffic* 11(7):899-911.

69. Jackson LK, Nawabi P, Hentea C, Roark EA, & Haldar K (2008) The Salmonella virulence protein SifA is a G protein antagonist. *P Natl Acad Sci USA* 105(37):14141-14146.

70. Brown NF, *et al.* (2006) Mutational analysis of Salmonella translocated effector members SifA and SopD2 reveals domains implicated in translocation, subcellular localization and function. *Microbiol-Sgm* 152:2323-2343.

71. Ohlson MB, Fluhr K, Birmingham CL, Brumell JH, & Miller SI (2005) SseJ deacylase activity by *Salmonella enterica* serovar Typhimurium promotes virulence in mice. *Infect Immun* 73(10):6249-6259.

72. Christen M, *et al.* (2009) Activation of a bacterial virulence protein by the GTPase RhoA. *Science Signaling* 2(95):ra71.

73. Ruiz-Albert J, *et al.* (2002) Complementary activities of SseJ and SifA regulate dynamics of the *Salmonella* typhimurium vacuolar membrane. *Mol Microbiol* 44(3):645-661.

74. Schroeder N, *et al.* (2010) The virulence protein SopD2 regulates membrane dynamics of Salmonella-containing vacuoles. *Plos Pathog* 6(7):e1001002.

75. Mota LJ, Ramsden AE, Liu M, Castle JD, & Holden DW (2009) SCAMP3 is a component of the Salmonella-induced tubular network and reveals an interaction between bacterial effectors and post-Golgi trafficking. *Cell Microbiol* 11(8):1236-1253.

76. Poh J, *et al.* (2008) SteC is a Salmonella kinase required for SPI-2-dependent F-actin remodelling. *Cell Microbiol* 10(1):20-30.

77. Srikanth CV, Mercado-Lubo R, Hallstrom K, & McCormick BA (2011) Salmonella effector proteins and host-cell responses. *Cellular and Molecular Life Sciences* 68(22):3687-3697.

78. Miao EA, *et al.* (2003) Salmonella effectors translocated across the vacuolar membrane interact with the actin cytoskeleton. *Mol Microbiol* 48(2):401-415.

79. Nawabi P, Catron DM, & Haldar K (2008) Esterification of cholesterol by a type III secretion effector during intracellular Salmonella infection. *Mol Microbiol* 68(1):173-185.

80. Arena ET, *et al.* (2011) The deubiquitinase activity of the Salmonella pathogenicity island 2 effector, SseL, prevents accumulation of cellular lipid droplets. *Infect Immun* 79(11):4392-4400.

81. Auweter SD, Yu HB, Arena ET, Guttman JA, & Finlay BB (2011) Oxysterol-binding protein (OSBP) enhances replication of intracellular Salmonella and binds the Salmonella SPI-2 effector SseL via its N-terminus. *Microbes Infect*.

82. Liu JZ, *et al.* (2012) Zinc sequestration by the neutrophil protein calprotectin enhances Salmonella growth in the inflamed gut. *Cell Host Microbe* 11(3):227-239.

83. Osman D & Cavet JS (2011) Metal sensing in Salmonella: implications for pathogenesis. *Adv Microb Physiol* 58:175-232.

84. Fang FC (2004) Antimicrobial reactive oxygen and nitrogen species: concepts and controversies. *Nat Rev Microbiol* 2(10):820-832.

85. Babior BM, Lambeth JD, & Nauseef W (2002) The neutrophil NADPH oxidase. *Arch Biochem Biophys* 397(2):342-344.

86. Stuehr DJ (1999) Mammalian nitric oxide synthases. *Biochim Biophys Acta* 1411(2-3):217-230.

87. Aussel L, *et al.* (2011) Salmonella detoxifying enzymes are sufficient to cope with the host oxidative burst. *Mol Microbiol* 80(3):628-640.

88. Rushing MD & Slauch JM (2011) Either periplasmic tethering or protease resistance is sufficient to allow a SodC to protect *Salmonella enterica* serovar Typhimurium from phagocytic superoxide. *Molecular Microbiology* 82(4):952-963.

89. van der Heijden J, Bosman ES, Reynolds LA, & Finlay BB (2014) Direct measurement of oxidative and nitrosative stress dynamics in Salmonella inside macrophages. *Proc Natl Acad Sci U S A.*

90. Vazquez-Torres A (2012) Redox Active Thiol Sensors of Oxidative and Nitrosative Stress. *Antioxid Redox Sign* 17(9):1201-1214.

91. Husain M, *et al.* (2010) Redox sensor SsrB Cys203 enhances Salmonella fitness against nitric oxide generated in the host immune response to oral infection. *Proc Natl Acad Sci U S A* 107(32):14396-14401.

92. Kroger C, *et al.* (2013) An infection-relevant transcriptomic compendium for *Salmonella enterica* serovar Typhimurium. *Cell host & microbe* 14(6):683-695.

93. Mulder DT, *et al.* (2015) Multiple histidines in the periplasmic domain of the *Salmonella enterica* sensor kinase SsrA enhance signaling in response to extracellular acidification. *Molecular microbiology* 95(4):678-691.

94. Knodler LA, Winfree S, Drecktrah D, Ireland R, & Steele-Mortimer O (2009) Ubiquitination of the bacterial inositol phosphatase, SopB, regulates its biological activity at the plasma membrane. *Cell Microbiol* 11(11):1652-1670.

95. Kubori T & Galan JE (2003) Temporal regulation of salmonella virulence effector function by proteasome-dependent protein degradation. *Cell* 115(3):333-342.

96. Boucrot E, Beuzon CR, Holden DW, Gorvel JP, & Meresse S (2003) *Salmonella* Typhimurium SifA effector protein requires its membrane-anchoring C-terminal hexapeptide for its biological function. *J Biol Chem* 278(16):14196-14202.

97. Reinicke AT, *et al.* (2005) A *Salmonella* Typhimurium effector protein SifA is modified by host cell prenylation and S-acylation machinery. *J Biol Chem* 280(15):14620-14627.

98. Hicks SW, Charron G, Hang HC, & Galan JE (2011) Subcellular targeting of Salmonella virulence proteins by host-mediated S-palmitoylation. *Cell Host Microbe* 10(1):9-20.

99. Lu Y, *et al.* (2012) Identification of genes responsible for biofilm formation or virulence in *Salmonella enterica* serovar pullorum. *Avian diseases* 56(1):134-143.

100. Behnsen J, Perez-Lopez A, Nuccio SP, & Raffatellu M (2015) Exploiting host immunity: the Salmonella paradigm. *Trends in immunology* 36(2):112-120.

101. Winter SE, *et al.* (2010) Gut inflammation provides a respiratory electron acceptor for Salmonella. *Nature* 467(7314):426-429.

102. Thiennimitr P, *et al.* (2011) Intestinal inflammation allows Salmonella to use ethanolamine to compete with the microbiota. *Proc Natl Acad Sci U S A* 108(42):17480-17485.

103. Fang FC (2004) Antimicrobial reactive oxygen and nitrogen species: Concepts and controversies. *Nature Reviews Microbiology* 2(10):820-832.

104. Azenabor AA, Kennedy P, & York J (2009) Free intracellular Ca2+ regulates bacterial lipopolysaccharide induction of iNOS in human macrophages. *Immunobiology* 214(2):143-152.

105. Berger SB, *et al.* (2010) SLAM is a microbial sensor that regulates bacterial phagosome functions in macrophages. *Nat Immunol* 11(10):920-927.

106. Imlay JA (2013) The molecular mechanisms and physiological consequences of oxidative stress: lessons from a model bacterium. *Nat Rev Microbiol* 11(7):443-454.

107. Chakravortty D, Hansen-Wester I, & Hensel M (2002) Salmonella pathogenicity island 2 mediates protection of intracellular Salmonella from reactive nitrogen intermediates. *J Exp Med* 195(9):1155-1166.

108. Vazquez-Torres A, *et al.* (2000) Salmonella pathogenicity island 2-dependent evasion of the phagocyte NADPH oxidase. *Science* 287(5458):1655-1658.

109. Slauch JM (2011) How does the oxidative burst of macrophages kill bacteria? Still an open question. *Molecular Microbiology* 80(3):580-583.

110. Fang FC (2011) Antimicrobial actions of reactive oxygen species. *MBio* 2(5).

111. Imlay JA (2015) Diagnosing oxidative stress in bacteria: not as easy as you might think. *Current opinion in microbiology* 24:124-131.

112. Hanson GT, *et al.* (2004) Investigating mitochondrial redox potential with redox-sensitive green fluorescent protein indicators. *J Biol Chem* 279(13):13044-13053.

113. Morgan B, Sobotta MC, & Dick TP (2011) Measuring E(GSH) and H2O2 with roGFP2-based redox probes. *Free Radic Biol Med* 51(11):1943-1951.

114. Cannon MB & Remington SJ (2008) Redox-sensitive green fluorescent protein: probes for dynamic intracellular redox responses. A review. *Methods in molecular biology* 476:51-65.

115. Lohman JR & Remington SJ (2008) Development of a family of redox-sensitive green fluorescent protein indicators for use in relatively oxidizing subcellular environments. *Biochemistry* 47(33):8678-8688.

116. Cannon MB & Remington SJ (2006) Re-engineering redox-sensitive green fluorescent protein for improved response rate. *Protein science : a publication of the Protein Society* 15(1):45-57.

117. Gutscher M, *et al.* (2008) Real-time imaging of the intracellular glutathione redox potential. *Nature methods* 5(6):553-559.

118. Fahey RC (2013) Glutathione analogs in prokaryotes. *Biochim Biophys Acta* 1830(5):3182-3198.

119. Gutscher M, *et al.* (2009) Proximity-based protein thiol oxidation by H2O2-scavenging peroxidases. *J Biol Chem* 284(46):31532-31540.

120. Meyer AJ & Dick TP (2010) Fluorescent protein-based redox probes. *Antioxid Redox Signal* 13(5):621-650.

121. Jubany-Mari T, Alegre-Batlle L, Jiang K, & Feldman LJ (2010) Use of a redox-sensing GFP (c-roGFP1) for real-time monitoring of cytosol redox status in *Arabidopsis thaliana* water-stressed plants. *FEBS letters* 584(5):889-897.

122. Back P, *et al.* (2012) Exploring real-time in vivo redox biology of developing and aging *Caenorhabditis elegans*. *Free radical biology & medicine* 52(5):850-859.

123. Breckwoldt MO, *et al.* (2014) Multiparametric optical analysis of mitochondrial redox signals during neuronal physiology and pathology in vivo. *Nature medicine* 20(5):555-560.

124. Bhaskar A, *et al.* (2014) Reengineering redox sensitive GFP to measure mycothiol redox potential of *Mycobacterium tuberculosis* during infection. *PLoS pathogens* 10(1):e1003902.

125. Hanson GT, *et al.* (2004) Investigating mitochondrial redox potential with redox-sensitive green fluorescent protein indicators. *J Biol Chem* 279(13):13044-13053.

126. Valdivia RH & Falkow S (1996) Bacterial genetics by flow cytometry: rapid isolation of *Salmonella* Typhimurium acid-inducible promoters by differential fluorescence induction. *Molecular microbiology* 22(2):367-378.

127. Song M, *et al.* (2013) Low-molecular-weight thiol-dependent antioxidant and antinitrosative defences in Salmonella pathogenesis. *Molecular microbiology* 87(3):609-622.

128. Albrecht SC, Barata AG, Grosshans J, Teleman AA, & Dick TP (2011) In vivo mapping of hydrogen peroxide and oxidized glutathione reveals chemical and regional specificity of redox homeostasis. *Cell Metab* 14(6):819-829.

129. Lipton SA, *et al.* (2002) Cysteine regulation of protein function--as exemplified by NMDA-receptor modulation. *Trends Neurosci* 25(9):474-480.

130. Gutscher M, *et al.* (2009) Proximity-based protein thiol oxidation by H2O2-scavenging peroxidases. *J Biol Chem* 284(46):31532-31540.

131. Winterbourn CC, Hampton MB, Livesey JH, & Kettle AJ (2006) Modeling the reactions of superoxide and myeloperoxidase in the neutrophil phagosome: implications for microbial killing. *J Biol Chem* 281(52):39860-39869.

132. Burton NA, *et al.* (2014) Disparate impact of oxidative host defenses determines the fate of Salmonella during systemic infection in mice. *Cell Host Microbe* 15(1):72-83.

133. Hebrard M, Viala JP, Meresse S, Barras F, & Aussel L (2009) Redundant hydrogen peroxide scavengers contribute to Salmonella virulence and oxidative stress resistance. *J Bacteriol* 191(14):4605-4614.

134. Forest CG, Ferraro E, Sabbagh SC, & Daigle F (2010) Intracellular survival of *Salmonella enterica* serovar Typhi in human macrophages is independent of Salmonella pathogenicity island (SPI)-2. *Microbiology* 156(Pt 12):3689-3698.

135. Suvarnapunya AE & Stein MA (2005) DNA base excision repair potentiates the protective effect of Salmonella Pathogenicity Island 2 within macrophages. *Microbiology* 151(Pt 2):557-567.

136. Brumell JH, Rosenberger CM, Gotto GT, Marcus SL, & Finlay BB (2001) SifA permits survival and replication of *Salmonella* Typhimurium in murine macrophages. *Cell Microbiol* 3(2):75-84.

137. Gallois A, Klein JR, Allen LA, Jones BD, & Nauseef WM (2001) Salmonella pathogenicity island 2-encoded type III secretion system mediates exclusion of NADPH oxidase assembly from the phagosomal membrane. *J Immunol* 166(9):5741-5748.

138. McGourty K, *et al.* (2012) Salmonella inhibits retrograde trafficking of mannose-6-phosphate receptors and lysosome function. *Science* 338(6109):963-967.

139. Ruiz-Albert J, *et al.* (2002) Complementary activities of SseJ and SifA regulate dynamics of the *Salmonella* Typhimurium vacuolar membrane. *Mol Microbiol* 44(3):645-661.

140. Helaine S, *et al.* (2014) Internalization of Salmonella by macrophages induces formation of nonreplicating persisters. *Science* 343(6167):204-208.

141. Helaine S & Holden DW (2013) Heterogeneity of intracellular replication of bacterial pathogens. *Curr Opin Microbiol* 16(2):184-191.

142. Murray PJ & Wynn TA (2011) Protective and pathogenic functions of macrophage subsets. *Nat Rev Immunol* 11(11):723-737.

143. Aachoui Y, *et al.* (2013) Caspase-11 Protects Against Bacteria That Escape the Vacuole. *Science* 339(6122):975-978.

144. Mathur R, *et al.* (2012) A mouse model of *Salmonella* typhi infection. *Cell* 151(3):590-602.

145. Gouin E, *et al.* (1999) A comparative study of the actin-based motilities of the pathogenic bacteria *Listeria monocytogenes*, *Shigella flexneri* and *Rickettsia conorii*. *J Cell Sci* 112 (Pt 11):1697-1708.

146. Edwards RA, Keller LH, & Schifferli DM (1998) Improved allelic exchange vectors and their use to analyze 987P fimbria gene expression. *Gene* 207(2):149-157.

147. Auweter SD, *et al.* (2011) Quantitative mass spectrometry catalogues Salmonella pathogenicity island-2 effectors and identifies their cognate host binding partners. *J Biol Chem* 286(27):24023-24035.

148. Delcour AH (2009) Outer membrane permeability and antibiotic resistance. *Biochim Biophys Acta* 1794(5):808-816.

149. Seaver LC & Imlay JA (2001) Hydrogen peroxide fluxes and compartmentalization inside growing *Escherichia coli*. *J Bacteriol* 183(24):7182-7189.

150. Mahendran KR, Kreir M, Weingart H, Fertig N, & Winterhalter M (2010) Permeation of antibiotics through *Escherichia coli* OmpF and OmpC porins: screening for influx on a single-molecule level. *J Biomol Screen* 15(3):302-307.

151. Masi M & Pages JM (2013) Structure, Function and Regulation of Outer Membrane Proteins Involved in Drug Transport in Enterobactericeae: the OmpF/C - TolC Case. *Open Microbiol J* 7:22-33.

152. Lavigne JP, *et al.* (2012) Membrane permeability, a pivotal function involved in antibiotic resistance and virulence in *Enterobacter aerogenes* clinical isolates. *Clin Microbiol Infect* 18(6):539-545.

153. Hurdle JG, O'Neill AJ, Chopra I, & Lee RE (2011) Targeting bacterial membrane function: an underexploited mechanism for treating persistent infections. *Nat Rev Microbiol* 9(1):62-75.

154. Weingart H, Petrescu M, & Winterhalter M (2008) Biophysical characterization of in- and efflux in Gram-negative bacteria. *Curr Drug Targets* 9(9):789-796.

155. Coombes BK, Brown NF, Valdez Y, Brumell JH, & Finlay BB (2004) Expression and secretion of Salmonella pathogenicity island-2 virulence genes in response to acidification exhibit differential requirements of a functional type III secretion apparatus and SsaL. *J Biol Chem* 279(48):49804-49815.

156. Rostovtseva TK, *et al.* (2008) Tubulin binding blocks mitochondrial voltage-dependent anion channel and regulates respiration. *Proc Natl Acad Sci U S A* 105(48):18746-18751.

157. Butland G, *et al.* (2005) Interaction network containing conserved and essential protein complexes in *Escherichia coli*. *Nature* 433(7025):531-537.

158. Kumar JK, Tabor S, & Richardson CC (2004) Proteomic analysis of thioredoxin-targeted proteins in *Escherichia coli*. *Proc Natl Acad Sci U S A* 101(11):3759-3764.

159. Roy A, Kucukural A, & Zhang Y (2010) I-TASSER: a unified platform for automated protein structure and function prediction. *Nat Protoc* 5(4):725-738.

160. Jimenez-Garcia B, Pons C, & Fernandez-Recio J (2013) pyDockWEB: a web server for rigid-body protein-protein docking using electrostatics and desolvation scoring. *Bioinformatics* 29(13):1698-1699.

161. Basle A, Rummel G, Storici P, Rosenbusch JP, & Schirmer T (2006) Crystal structure of osmoporin OmpC from *E. coli* at 2.0 A. *J Mol Biol* 362(5):933-942.

162. Leichert LI & Jakob U (2004) Protein thiol modifications visualized in vivo. *PLoS Biol* 2(11):e333.

163. Bolla JM, *et al.* (2011) Strategies for bypassing the membrane barrier in multidrug resistant Gram-negative bacteria. *FEBS letters* 585(11):1682-1690.

164. Kaiser P, *et al.* (2014) Cecum lymph node dendritic cells harbor slow-growing bacteria phenotypically tolerant to antibiotic treatment. *PLoS Biol* 12(2):e1001793.

165. Pilonieta MC, Erickson KD, Ernst RK, & Detweiler CS (2009) A protein important for antimicrobial peptide resistance, YdeI/OmdA, is in the periplasm and interacts with OmpD/NmpC. *J Bacteriol* 191(23):7243-7252.

166. Auweter SD, *et al.* (2011) Quantitative mass spectrometry catalogues Salmonella pathogenicity island-2 effectors and identifies their cognate host binding partners. *J Biol Chem* 286(27):24023-24035.

167. Rogers LD, Brown NF, Fang Y, Pelech S, & Foster LJ (2011) Phosphoproteomic analysis of Salmonella-infected cells identifies key kinase regulators and SopB-dependent host phosphorylation events. *Science signaling* 4(191):rs9.

168. Cox J & Mann M (2008) MaxQuant enables high peptide identification rates, individualized p.p.b.-range mass accuracies and proteome-wide protein quantification. *Nature biotechnology* 26(12):1367-1372.

169. Cox J, *et al.* (2011) Andromeda: a peptide search engine integrated into the MaxQuant environment. *J Proteome Res* 10(4):1794-1805.

170. van der Heijden J & Finlay BB (2012) Type III effector-mediated processes in Salmonella infection. *Future microbiology* 7(6):685-703.

171. Steele-Mortimer O (2008) The Salmonella-containing vacuole: moving with the times. *Current opinion in microbiology* 11(1):38-45.

172. Salcedo SP & Holden DW (2003) SseG, a virulence protein that targets Salmonella to the Golgi network. *The EMBO journal* 22(19):5003-5014.

173. Mota LJ, Ramsden AE, Liu M, Castle JD, & Holden DW (2009) SCAMP3 is a component of the Salmonella-induced tubular network and reveals an interaction between bacterial effectors and post-Golgi trafficking. *Cellular microbiology* 11(8):1236-1253.

174. Radhakrishnan GK & Splitter GA (2012) Modulation of host microtubule dynamics by pathogenic bacteria. *Biomolecular concepts* 3(6):571-580.

175. Patel JC, Hueffer K, Lam TT, & Galan JE (2009) Diversification of a Salmonella virulence protein function by ubiquitin-dependent differential localization. *Cell* 137(2):283-294.

176. Quezada CM, Hicks SW, Galan JE, & Stebbins CE (2009) A family of Salmonella virulence factors functions as a distinct class of autoregulated E3 ubiquitin ligases. *Proc Natl Acad Sci U S A* 106(12):4864-4869.

177. Reinicke AT, *et al.* (2005) A *Salmonella* Typhimurium effector protein SifA is modified by host cell prenylation and S-acylation machinery. *J Biol Chem* 280(15):14620-14627.

178. Vazquez-Torres A (2012) Redox active thiol sensors of oxidative and nitrosative stress. *Antioxidants & redox signaling* 17(9):1201-1214.

179. Zheng M, Aslund F, & Storz G (1998) Activation of the OxyR transcription factor by reversible disulfide bond formation. *Science* 279(5357):1718-1721.

180. Chouchani ET, James AM, Fearnley IM, Lilley KS, & Murphy MP (2011) Proteomic approaches to the characterization of protein thiol modification. *Current opinion in chemical biology* 15(1):120-128.

181. Geddes K, Worley M, Niemann G, & Heffron F (2005) Identification of new secreted effectors in *Salmonella enterica* serovar Typhimurium. *Infection and immunity* 73(10):6260-6271.

182. Lee AH, *et al.* (2012) A bacterial acetyltransferase destroys plant microtubule networks and blocks secretion. *PLoS pathogens* 8(2):e1002523.

183. Archuleta TL, *et al.* (2011) The Chlamydia effector chlamydial outer protein N (CopN) sequesters tubulin and prevents microtubule assembly. *J Biol Chem* 286(39):33992-33998.

184. Go YM & Jones DP (2008) Redox compartmentalization in eukaryotic cells. *Biochim Biophys Acta* 1780(11):1273-1290.

185. Broz P, *et al.* (2010) Redundant roles for inflammasome receptors NLRP3 and NLRC4 in host defense against Salmonella. *The Journal of experimental medicine* 207(8):1745-1755.

186. Misawa T, *et al.* (2013) Microtubule-driven spatial arrangement of mitochondria promotes activation of the NLRP3 inflammasome. *Nature immunology* 14(5):454-460.

187. Stanley AC & Lacy P (2010) Pathways for cytokine secretion. *Physiology* 25(4):218-229.

188. Schroeder BO, *et al.* (2011) Reduction of disulphide bonds unmasks potent antimicrobial activity of human beta-defensin 1. *Nature* 469(7330):419-423.

189. Kuhle V, Jackel D, & Hensel M (2004) Effector proteins encoded by Salmonella pathogenicity island 2 interfere with the microtubule cytoskeleton after translocation into host cells. *Traffic* 5(5):356-370.

190. Guignot J, *et al.* (2004) Microtubule motors control membrane dynamics of Salmonella-containing vacuoles. *Journal of cell science* 117(Pt 7):1033-1045.

191. Figueira R, Watson KG, Holden DW, & Helaine S (2013) Identification of salmonella pathogenicity island-2 type III secretion system effectors involved in intramacrophage replication of *S. enterica* serovar typhimurium: implications for rational vaccine design. *mBio* 4(2):e00065.

192. Buckner MM, Croxen MA, Arena ET, & Finlay BB (2011) A comprehensive study of the contribution of *Salmonella enterica* serovar Typhimurium SPI2 effectors to bacterial colonization, survival, and replication in typhoid fever, macrophage, and epithelial cell infection models. *Virulence* 2(3):208-216.

193. Bardwell JC, *et al.* (1993) A pathway for disulfide bond formation in vivo. *Proc Natl Acad Sci U S A* 90(3):1038-1042.

194. Lu S, *et al.* (2015) Mapping native disulfide bonds at a proteome scale. *Nature methods*.

195. Choi H, Yang Z, & Weisshaar JC (2015) Single-cell, real-time detection of oxidative stress induced in *Escherichia coli* by the antimicrobial peptide CM15. *Proc Natl Acad Sci U S A* 112(3):E303-310.

196. CDC (2013) Antibiotic Resistance Threats in the United States, 2013.

197. Ling LL, *et al.* (2015) A new antibiotic kills pathogens without detectable resistance. *Nature* 517(7535):455-459.

198. Citorik RJ, Mimee M, & Lu TK (2014) Sequence-specific antimicrobials using efficiently delivered RNA-guided nucleases. *Nature biotechnology* 32(11):1141-1145.

199. Lee S, *et al.* (2009) Targeting a bacterial stress response to enhance antibiotic action. *Proc Natl Acad Sci U S A* 106(34):14570-14575.

200. Kohanski MA, Dwyer DJ, & Collins JJ (2010) How antibiotics kill bacteria: from targets to networks. *Nat Rev Microbiol* 8(6):423-435.

Appendix

Appendix A

Finally, besides the studies presented in this dissertation, these are publications that arise from work outside the scope of this thesis:

1. Auweter SD, Bhavsar AP, de Hoog CL, Li Y, Chan YA, **van der Heijden J**, Lowden MJ, Coombes BK, Rogers LD, Stoynov N, Foster LJ, Finlay BB. Quantitative mass spectrometry catalogues *Salmonella* pathogenicity island-2 effectors and identifies their cognate host binding partners. *J Biol Chem*. 2011 Jul 8;286(27):24023-35.
2. Robyn Law, HT Law, Joshua Scurll, Roland Scholz, Stephanie Shames, Wanyin Deng, Matthew Croxen, Yuling Li, Carmen de Hoog, **Joris van der Heijden**, Leonard Foster, Julian Guttman, and B. Brett Finlay. Pathogenic *E. coli* targets the kinesin-1 cofactor ensconsin and disrupts transferrin receptor trafficking. *MBio* Under review.